ENERGY HARVESTING AND MODELING OF

PHOTOSYNTHETIC POWER CELL

ARVIND VYAS RAMANAN

A Thesis

In

The Department

Of

Electrical and Computer Engineering

Presented in Partial Fulfillment of the Requirements for the

Degree of Master of Applied Science (Electrical Engineering and Computer Science) at

Concordia University

Montréal, Québec, Canada

April 2013

CONCORDIA UNIVERSITY
SCHOOL OF GRADUATE STUDIES

This is to certify that the thesis prepared

By: Arvind Vyas Ramanan

Entitled: "Energy harvesting and Modeling of Photosynthetic power cell"

and submitted in partial fulfillment of the requirements for the degree of

Master of Applied Science

Complies with the regulations of this University and meets the accepted standards with respect to originality and quality.

Signed by the final examining committee:

_____Chair
        Dr. Yousef R. Shayan

_____Examiner, External to the Program
        Dr. Sivakumar Narayanswamy, MIE

_____Examiner
        Dr. Pragasen Pillay

_____Supervisor
        Dr. Sheldon S. Williamson

_____Co-Supervisor
        Dr. Muthukumaran Packirisamy, MIE

Approved by: _____
                Dr. W. E. Lynch, Chair
        Department of Electrical and Computer Engineering

April, 2013   _____
                Dr. Robin A. L. Drew
        Dean, Faculty of Engineering and Computer Science

ABSTRACT

Energy Harvesting and Modeling of Photosynthetic power cell

Arvind Vyas Ramanan

The need for energy is inevitable for mankind. Climate change, depletion of natural resources, pollution and other factors have created the necessity to look for energy from renewable sources. Furthermore, there are challenges aplenty in the field of renewable energy as renewable energy sources are unpredictable, non-dependable and limited such as wind, solar photo voltaic and tidal power. Apart from these there are few unconventional renewable energy sources that have not been explored thoroughly or exploited. The photosynthetic power cell is one among them.

The photosynthetic power cell (PSC) harvests the energy produced at the lowest level of the food cycle which is "photosynthesis" in plants. The photosynthetic power cell extracts the energy produced during photosynthesis and respiration in form of electrical energy. The developed device differs from other published works in terms of improved performance, fabrication technique and material of structure. The two main types of sources used in the photosynthetic power cell are aerobic unicellular organisms (e.g. algae and cyanobacteria) and sub-cellular thylakoid photosystems / chloroplasts isolated from plant cells (e.g. spinach plant's sub-cellular thylakoid photosystems isolated from the plant cells). The photosynthetic power cell produces energy under both dark and light conditions. The developed PSC is a polymer based structure instead of silicon, integrating the conventional MEMS processes with polymers. The principle of the operation of the device is based on 'photosynthesis'. Photosynthesis and respiration both involve electron

transfer chains. The electrons are extracted with the help of electrodes and a redox agent, and a power electronic converter is designed to harvest the energy. The developed device is capable of producing an open circuit voltage of 0.9 volts and about 200 µW of peak power. The µPSC has an active area of 4.84 cm^2 which approximately translates to a power density of 400 mW/m^2. This makes it as one of the best performing µPSC. The other top performing µPSC devices report power densities between 100 to 250 mW/m^2.

In order to harvest energy from µPSC, power electronic converters are a necessity. Three different power electronic topologies are investigated to find the feasibility of energy harvesting using µPSC. Also, the cell should be operated at the maximum power point in order to get the best results. Common maximum power point tracking (MPPT) techniques as well as a novel MPPT technique is devised and tested for the energy harvesting application using µPSC.

In this thesis work, the device's working principle, fabrication of the device and testing of the developed prototype along with the design and development of the power electronic converters with MPPT algorithm for energy harvesting application with µPSC are presented. A short introduction, basic photosynthesis process, background and history of µPSC are discussed in first chapter. The cell design, construction, working and fabrication of the cell are discussed in the second chapter. The third chapter deals with the experimental set up, characterization and testing of the cell. In the fourth chapter, modeling, analysis, simulation of PSC is executed. Analysis, identification and simulation of suitable power electronic converters with MPPT are investigated in the fifth chapter. Conclusions, future work form the epilogue.

ACKNOWLEDGMENTS

CONTENTS

List of Figures

xi

List of Acronyms

PSC   Photosynthetic Power cell

μPSC   Micro Photosynthetic Power cell

MFC   Microbial Fuel Cell

PEM   Proton Exchange Membrane

PEMFC   Proton Exchange Membrane Fuel Cell

MEMS   Microelectromechanical Systems

PV   Photovoltaic

SOFC   Solid Oxide Fuel Cell

MCFC   Molten Carbonate Fuel Cell

Li-Ion   Lithium Ion

LiPo   Lithium Polymer

MPPT   Maximum Power Point Tracking

MPP   Maximum Power Point

OCV   Open Circuit Voltage

SSC   Short circuit current

ATP   Adenosine Triphosphate

ADP	Adenosine Diphosphate
NADP	Nicotinamide Adenine Dinucleotide Phosphate
NADPH	NADPH is the reduced form of NADP
UV	Ultra Violet radiation
PR	Photoresist
EMI	Electro-Magnetic Interference
ESR	Equivalent Series Resistance
MOSFET	Metal Oxide Semiconductor Field Effect Transistor
SCC	Switched capacitor Converter
P&O	Perturb and observe
CCM	Continuous conduction mode
DCM	Discontinuous conduction mode
PWM	Pulse width modulation
DDS	Digital direct synthesizer

CHAPTER 1

1 INTRODUCTION

1.1 Renewable energy, Energy harvesting and Power electronics

Our need for energy is ever increasing. Data from IEA (The International Energy Agency) suggests that from 1990 to 2008, the average energy use per person increased by 10%, while the world population increased by 27%. Also, the use of regional energy also grew worldwide, in the Middle East it increased by 170%, China by 146%, India by 91%, Africa by 70%, Latin America by 66%, the USA by 20%, the EU-27 by 7%, and world overall grew by 39% [1].

It cannot be more obvious that energy demand will continue to grow. Climate challenge, pollution, depletion of natural resources and fossil fuels are other major factors in finding and using energy. Thus it becomes vital to explore various renewable energy sources. Energy from renewable resources such as wind, solar and tidal has been religiously researched upon over the years. Energy harvesting is relatively new, and has gained a lot of potential and attention due to the revolution in small, miniature devices started by MEMS and personal and mobile electronic devices.

Energy harvesting as the name suggests extracts and stores electrical energy from renewable resources at low power levels in the range of few micro watts to a few milli watts (10μW to 4000μW). Energy harvesting devices are small scale and energize low power devices such as wireless autonomous devices, wireless sensor networks, and

wearable electronics. Typical energy harvesting sources are vibrations - kinetic energy, thermal gradient - thermal energy, light – photovoltaic – solar power, micro fuel cells (hydrogen, direct methanol, microbial fuel cell, and photosynthetic power cell are some varieties of micro fuel cells).

Micro fuel cells are quite similar to fuel cells but their power levels are very low compared to their larger counter parts. Energy harvesting can be called as renewable energy at low power levels. Irrespective of the power levels being high or low it should be consumable and be usable for devices. The power (voltage and current) produced by renewable energy sources and energy harvesting devices are not steady and is neither constant nor not readily available in usable form. Power electronics is solely responsible for being able to tap and use renewable energy.

Power electronic converters usually condition the power to more usable forms. For example, in order to charge a smartphone one would specifically need 5V and current levels of 1A. This specific voltage and current cannot be precisely derived from renewable energy sources or energy harvesting devices directly. A power electronic converter that is suitably designed for an application can process the unusable power to a usable form. Thus the role of power electronics in the field of renewable energy and energy harvesting is vital.

1.1.1 Renewable energy and energy harvesting technologies

The term renewable energy usually refers to power generated in large scale, that is generated from common renewable energy sources such as hydro, solar, tidal and wind. Renewable energy power plants usually generate power in the range of few mega watts to

a few thousand mega watts. Jiuquan wind power base, the largest wind power project in the world located at Northwest China has an installed capacity of 5.16 GW with more than 3,500 erected wind turbines, and at present the turbines are generating 1.15 GW of power [2]. Currently the world's largest photovoltaic power plant as of Aug-2012 is Agua Caliente Solar Project in Arizona, United States which has an installed capacity of 250MW [3]. However Charanka Solar Park, Gujarat, India will be the largest photovoltaic power plant when completed in 2014 with a capacity of 500 MW [4].

Energy harvesting is a paradigm shift in power levels when compared to renewable energy power plants. Energy harvesting is scavenging for power at very low levels in the range of few micro and milli watts. Energy harvesting devices convert ambient energy into electrical energy. The systems are capable of converting energy in motion, electro-magnetic induction based on Faraday's principle and piezo-electric devices are common in motion based applications. Powering wearable electronics, recharging cell phones, mobile computers, radio communication equipment from vibrations and other generated motion are some of the application examples. Energy from thermal gradient can be converted using the Seebeck or Peltier effect (difference in temperature at an alloy junction). Energy from ambient light can be harvested using photovoltaics (PV) for indoor applications.

Though renewable, micro fuel cells such as hydrogen fuel cells are not energy harvesting devices as they use a fuel instead of harvesting energy from the ambient environment. However a biological fuel cell a sub-type of the fuel cell is an energy harvesting device and is a bio-electrochemical system that derives power from bacterial / algae interactions found in nature. There are two basic types of biological fuel cells. The first type is the

microbial fuel cell (MFC) where bacteria act on organic waste and oxidize it to give free electrons and the second type is the photosynthetic power cell (or Phototrophic biofilm microbial fuel cell, these have been called by different names) where the electric current is derived from photosynthetic process of algae or phototropic bacteria such as algae or cyanobacteria.

1.1.2   Energy harvesting devices

As discussed earlier, energy from motion and vibration can be harvested using small electromagnetic generators as linear generator and piezo-electric generators. Typical sources of vibrations for energy harvesting are bridges, human footsteps, vibrations in mechanical systems such as an internal combustion engine, etc. One such application is to generate power from a human footstep. Current prototypes using electromagnetic induction harvest power in the range of 200µW to 1W [5] [6] [8]. Use of piezo-electric devices is more popular for energy harvesting from vibrations compared to electromagnetic generators. They harvest power in the range of 1µW to 600µW. Expensive and rare state of the art piezo ceramic devices can harvest power in rage of 1000µW to 8000µW [5] [7] [8].

Electrical energy harvested from thermal gradient is called Thermoelectric effect. Despite there being three different principles such as the Seebeck effect, Peltier effect and Thomson effect, the most commonly used is the Seebeck effect. According to Seebeck effect, electricity is generated when there is a temperature difference at a two different metal junction. For example, copper and constantan metal junction produces around 41µV for a temperature difference of 1 Kelvin between the metals [9]. This technology

can be used wherever there is heat is wasted, such as internal combustion engines, laptops and electronic devices as the processors and batteries produces a good amount of heat when used. Thermoelectric effect is the technology that powers "Voyager 1", the farthest manmade object in space and is about to leave the solar system and enter the interstellar space. The thermoelectric device is a Radioisotope thermoelectric generator. The Radioisotope thermoelectric generator has been powering the Voyager 1 spacecraft for more than 35 years [15]. Current commercial thermoelectric generators develop about 3 mW for a temperature difference of $25^{o}C$ [10].

A fuel cell is a device that converts the chemical energy from a fuel to electricity by oxidizing the fuel using an oxidizing agent. Hydrogen is the most common fuel, but hydrocarbons such as natural gas and alcohols like methanol are sometimes used.
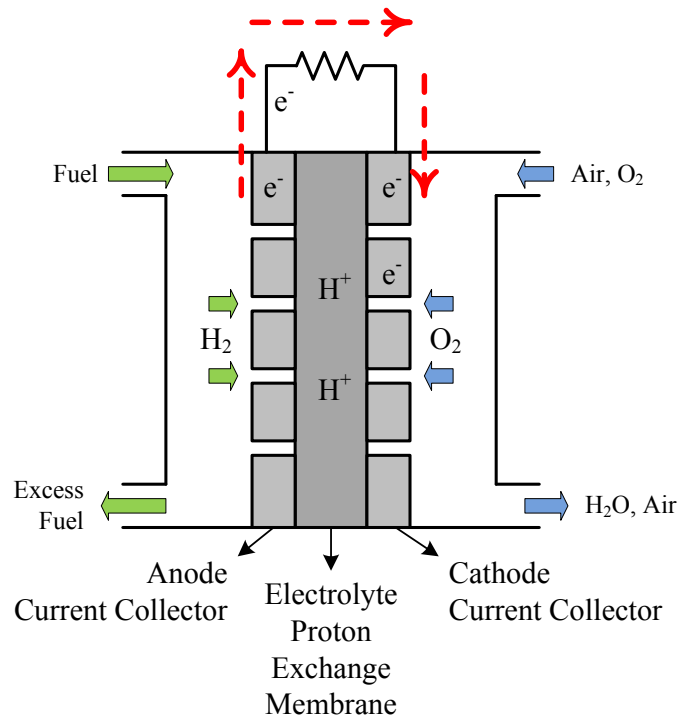
Fig. 1.1 Typical fuel cell

5

Shown in Figure 1.1 above is a typical fuel cell. In contrast to the batteries, fuel cells use continuously replenished reactants. They were first proposed by W. Grove [19] in 1839. The most common fuel cell types are Proton exchange membrane / Polymer electrolyte membranes fuel cell (PEMFC), solid oxide Fuel cell (SOFC) and molten carbonate fuel cell (MCFC) [20]. There are many types of fuel cells, but their constructions are similar, they are made up of an anode, a cathode and an electrolyte that allows transportation of charges between the two sides of the fuel cell. Electrons are drawn from the anode to the cathode through an external circuit, producing electric current. The main difference among fuel cell types is the electrolyte. They are classified based on the type of electrolyte used. Fuel cells are built in several different sizes. Individual fuel cells produce relatively small electrical potentials, about 0.7 volts. Hence cells are "stacked", or placed in series, to increase the voltage and meet the requirements as required.

Conventional fuel cell or micro fuel cells, though renewable and green are not considered energy harvesting devices. However special fuel cells such as the Microbial fuel cell and Photosynthetic fuel cells can be classified as energy harvesting devices when fabricated in the micro scale. The Microbial fuel cell (MFC) is functionally similar to the conventional fuel cell types by using oxidation. Bacteria in MFC convert chemical energy to electrical energy, they oxidize diverse organic substrates which produce free electrons and transfer these electrons to anodic electrodes and thereby generate electricity [11]. The usage of a microbial fuel cell for generation of power has been investigated since 1911 [12] and the system concept was demonstrated in 1974 [13]. Latest MFC have a power density of around 5 to 7mW/m^2 [11].

The Photosynthetic power cell, produce power by extracting the electrons from the electron transfer chain during photosynthesis. The device mechanism is explained in the Section 1.3. PSCs are better in numerous way to MFCs. Power density, the main consideration, is large compared to MFCs. Current PSCs have achieved a power density of more than 100 mW/m^2 [14]. The developed device explained in this thesis, has a power density of more than 200 mW/m^2. The working and results of the device are explained in detail in the following chapters, before which we will understand the photosynthetic process.

1.2   Photosynthesis and Energy

Photosynthesis occurs in plants, algae, and many species of bacteria. Photosynthetic organisms are called photoautotrophs, since they produce their own food. They convert the energy from sunlight to chemical energy with the help of carbon dioxide and water. Photosynthesis is vital for all aerobic life on Earth. In addition to maintaining normal levels of oxygen in the atmosphere, photosynthesis is the source of energy for nearly all life on earth, either directly, through primary production, or indirectly. The average energy captured by photosynthesis is immense, approximately 130 terawatts [16] [17] which is about six times larger than the power consumption of human civilization [18]. As well as for energy, photosynthesis is also the source of the carbon in all the organic compounds in organisms.

1.3   Photosynthetic power cell and energy harvesting

1.3.1   Energy conversion

Photosynthetic power cells (PSC) convert energy from sunlight to electrical energy through the biochemical processes occurring in different micro-organisms and by inducing redox reactions. The PSC unlike solar cell can produce power during dark period as well, and unlike the fuel cells it replenishes itself without having to supply additional fuel when energy is consumed. The operation of the device is based on the electron transfer that occurs during photosynthesis and respiration which are the same reactions when reversed. Thus it makes the PSC functional during light and dark and self-restoring. Following are the chemical reactions that occur during photosynthesis and respiration [24].

$Photosynthesis\ (light):$ $\quad CO_2 + H_2O\ ---\!\!\rightarrow (CH_2O) + O_2$ $\quad\quad\quad\quad$ (1.1)

$Respiration\ (dark):$ $\quad\quad (CH_2O) + O_2\ ---\!\!\rightarrow CO_2 + H_2O$ $\quad\quad\quad\quad$ (1.2)
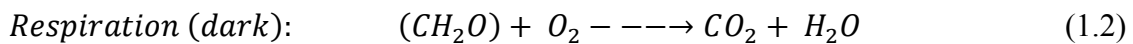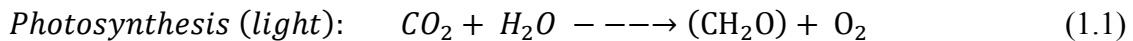
The photosynthetic process will be explained in Chapter 2 where the focus is on biological process and how it generates energy (free electron). Both photosynthesis and respiration involve electron transfer chains, from which a free electron can be extracted. In PSC, these electrons are extracted with the help of redox reactions and are passed through an external electrical circuit which gives raise to the electric current.

1.3.2   The Device

The PEC is similar in construction to that of an electrochemical cell like the fuel cell. The device consists of two identical half cells, each forming the anode and the cathode

separated by a proton exchange membrane (PEM) which is a sulfonated copolymer, usually Nafion. The anode and the cathode sides are sealed with glass on top to allow light to pass thorough for photosynthesis. A porous gold electrode is fabricated on top of both csurfaces of the Proton Exchange Membrane (PEM) which acts as the current collector. The PEM allows only the positive ions to the cathode side and blocks the electrons. The gold electrode helps in trapping the free electrons.
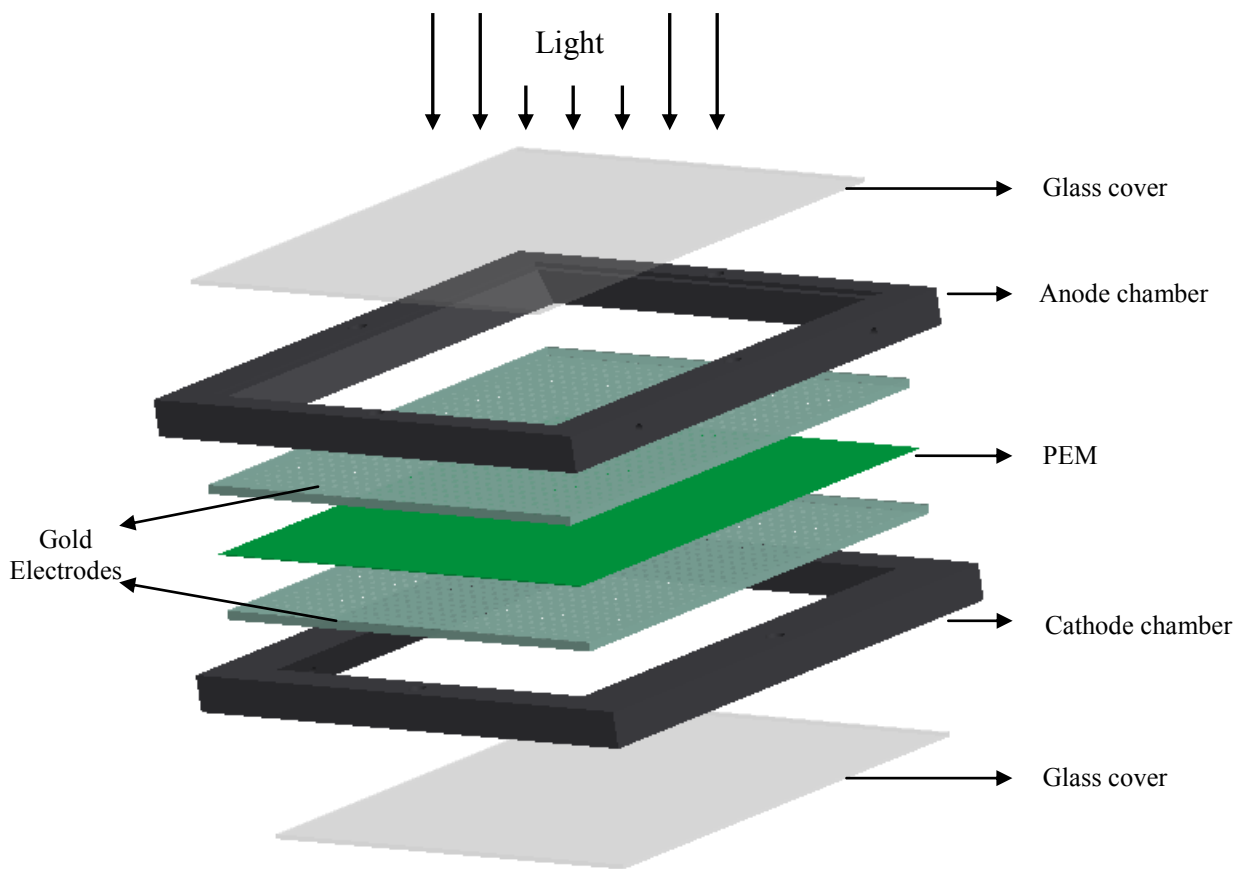
Fig. 1.2 µPSC Schematic Assembly [51]

The schematic assembly of the device is shown in Figure 1.2 above. The anode chamber is filled with the algal/bacterial medium (anolyte) and cathode chamber with the potassium ferricyanide (catholyte). Thin gold sputtered aluminum strips are attached to

the electrodes anode and cathode, to which any external electrical connection can be made. The fabrication of these main components is of a major difference between this work and earlier photosynthetic power cells. The fabrication process will be discussed in detail in the following chapter where each component is explained separately. One of the main differences to be mentioned is that unlike the previous works which were silicon based devices, the device fabricated in this work is a polymer-based MEMS device [51].

1.3.3   Operating principle

PSCs generate electricity from both photosynthesis and catabolism of endogenous carbohydrates in the light and from catabolism alone in the dark. The implemented PSC is illustrated in Figure 1.3 below [24] [25], which shows the anode and cathode reaction chambers separated by a proton exchange membrane (PEM) and is connected to an external circuit through electrodes.
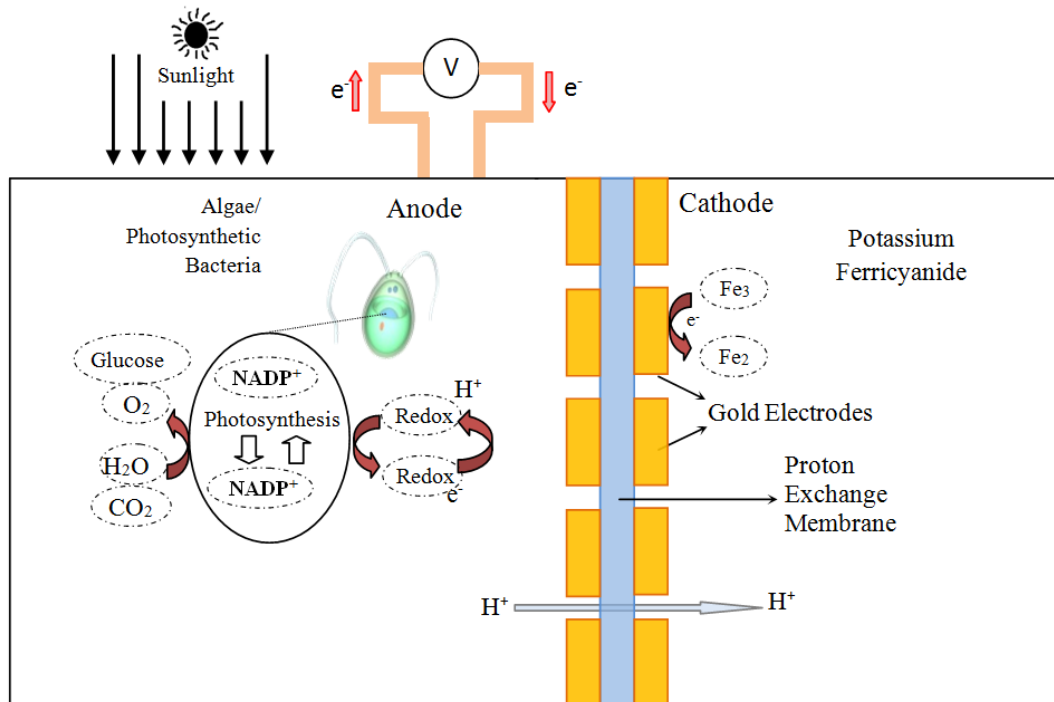
Fig. 1.3 PSC - Principle of operation

In the anode chamber, a live culture of algae or a photosynthetic bacterium such as the cyanobacteria is suspended in a growth media solution with a redox coupler or an electron mediator. During the presence of light, photosynthesis takes place in the microorganisms. The microorganisms convert CO_2 and H_2O into O_2 and carbohydrates (e.g. glucose). During photosynthesis, electrons are transferred by diffusion of electron carriers NADPH or along a electron chain carried out in the series of thylakoid bound enzyme complexes called the photo-systems. These electrons (and protons) are siphoned from the normal photosynthetic process either from NADPH or from the transport chain by redox coupler / electron mediator molecules that have diffused into the microorganisms. The reduced (electrons and protons carrying) compounds diffuse out of the microorganism's cell, through the mediator solution, the electrons close to the anode are attracted by the redox potential of the catholyte. Due to this potential, the electrons then travel through the connected external load into the cathode chamber, similar to a MFC. At the cathode, they reduce the oxidant ferricyanide (Fe_3). Meanwhile, the protons (H^+) at the anode diffuse across the PEM from the anode into the cathode, where they reduce the oxidant (Fe_2) or combine with O_2 and electrons from the reduced oxidant to release H_2O [24] [25].

1.3.4   Energy harvesting

The electrical energy from the photosynthetic power cell has to be harvested or be used directly for an application. Either the energy is to be stored in a battery / ultracapacitor or is used to power a device; a power electronic converter is required to condition the power (voltage and current) as needed for an application. Batteries need a specific voltage to be charged. Latest battery technologies such as the lithium ion (Li-ion) and lithium polymer

(Li-po) have a nominal voltage of 3.7 Volts and a maximum voltage of 4.2 Volts and have to be charged in a particular and precise way [23]. Figure 1.4 below shows the charging characteristics of a Li-ion battery [23] [22].
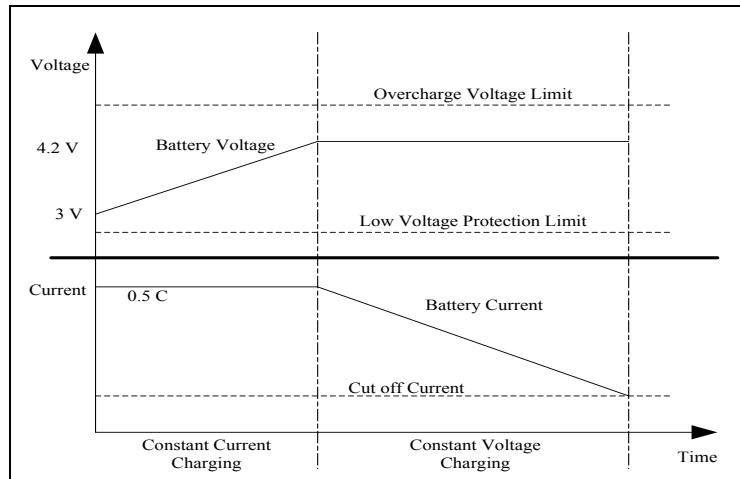
Fig. 1.4 Lithium Ion battery charging algorithm [23]

The required power conditioning can only be achieved by a suitably designed power electronic converter. In this thesis work, a suitable power electronic converter for the photosynthetic power cell (PEC) is identified, analyzed and is designed. The power electronic converter required for this application would be a DC-DC power converter. The power converter should be able to perform maximum power point tracking (MPPT) for the PSC and also provide regulated voltage and current depending on the load. This is usually achieved by using two cascaded DC-DC converters. In order to aid the analysis and design of the converter, a suitable electrical model for the cell has to be developed, which can be used for analysis and simulation. The electrical equivalent model of the cell cannot be arrived at without the mathematical model of the system. Thus a mathematical model, the cell's electrical equivalent model and simulation, and the analysis and design

of a suitable power electronic converter for the cell are dealt in detail in the following chapters.

1.4 History

1911 was the year when the first Microbial Fuel Cell (MFC) was reported by M.C. Plotter [26]. The MFC generated electrical energy directly by decomposition of organic compounds by bacterial activity, and the cell's electrodes were made of platinum. The principle of operational of Plotter's MFC was based on transfer of extracted electrons from microorganisms to the anode. The catholyte solution used had a different redox potential to that of the anolyte solution, this caused the electrons to travel from anode to cathode through the connected external circuit. The mediators in the anode along with the microorganism diffuse into the live cells and interact with the reducing agents in the cell. The consequent redox reactions give raise to electrons and protons. These protons are attracted by the reduced catholyte and the protons travel through a proton exchange membrane resulting in an additional potential gradient due to proton exchange [27] [28]. Research on MFCs did not advance until the year 1931, when Cohen brought Plotter's MFC back to life [27].

Practical studies of PSC done in 1976 are considered the real beginning. M. Allen and A. Crane [29] demonstrated a photosynthetic power cell with isolated thylakoids. Until this work, all the other previous works related to MFCs and PSCs used a living cell / whole-cell microorganisms (anaerobic for MFCs and photosynthetic organisms for PSC). Later in 1981 one of the earliest works of the above mentioned type was performed by

R.Bhardwaj et al. Later, many other experiments have been performed by using isolated subcellular photosynthetic components [24, 25, 27-45].

Based on these, experiments were conducted by isolating the reaction centers and performed with certain redox mediators. Some of the publications of this type were done by, A. Drachev and A. Jasaitis [33,34], K. Pakham and P. Mueller [35,36]. They were able to generate a potential of 0.2 V approximately.

Later in 1978, M. Aizawa [32] constructed a cell with platinum electrodes and alkaline solution, and used isolated chlorophyll. Generation of positive potential was reported by this PSC.

In 1980, A. F. Janzen [37] explored the possibility of photo-electrochemical conversion by piercing micro electrodes into the reaction centers. In this method, an open circuit voltage (OCV) of 0.08 V with a current density of 0.5 $\mu A/cm2$ was observed.

In 1985, one of first attempts to utilize cyanobacteria as the photosynthetic agent was carried out by K. Tanaka et al [38, 39], power measurements in range of few micro watts, both in dark and light were reported.

Results published by T. Yagishita et al. [40-42] in 1993 created a huge impact and brought a lot of attention to PSC. In this work, tests were performed with various micro-organisms. They reported a very high open circuit voltage of 800 mV. Also, they resistively loaded the cell and reported a current density of 320 $\mu A/cm^2$. The tests were done in cycles of light and dark and confirmed the generation of power during both light and dark periods. Their contribution to PSC research continued, in 1997 to 1999 they

investigated the influence of different parameters such as effect of light intensity, cell count of the micro-organism, and glucose addition to the cells [43, 44].

Meanwhile experiments using isolated chloroplast with various mediators were also conducted. One such work published by W. Haehnel and et al [46] reported OCV of 220 mV and 16 $\mu A/cm^2$ current density.

In 2003 a PSC fabricated by K. Lam et al. [24], reported an open circuit voltage of 400 mV with current and power densities of 30 $\mu A/cm2$ and 61 $\mu W/L$ respectively under both dark and light periods.

A recent work in 2006, M. Chiao et al. [25] used bulk silicon micromachining technology for fabricating the compartments of the PSC. They performed two experiments using two different micro-organisms – baker's yeast (Saccharomyces Cerevisiae) and blue green algae (Phylum Cyanophyta). The yeast based cell was a microbial fuel cell (MFC) and the one with the blue green algae was a photosynthetic power cell (PSC). They measured an OCV of 300-400 mV for both cells and power density was 0.04 nW/cm^2 and 2.3 nW/cm^2, respectively. This showed that the PSC had more power density than MFCs.

This was followed by the published work of K. Lam et al [24]. The theoretical understanding was given a lot of importance and calculated a theoretical maximum current density of 9.6 $mA/cm2$ under an illumination of 2000 μmol photons/m^2/s. But they were able to obtain only $1\mu A/cm^2$ from experiments. The OCV results were comparable to other cells.

Research and experiments, on PSC are still being pursued actively by many researchers around the globe.

The PSC developed by Mehdi Shaparnia, Dr. Muthukumarn Pakrisamy and Dr. Valter Zazubovich in 2010, was radically different to the earlier devices. Polydimethylsiloxane (PDMS) was used as the base and substrate instead of silicon. This reduced the cost. Also, the electrodes were directly fabricated on top of the proton exchange membrane (Nafion) using MEMS photolithography process. The device is presented in the Master's thesis of Mehdi Shaparnia 'Polymer Micro Photosynthetic Power Cell: Design, Fabrication, Parametric Study and Testing' [51], this fabrication is adapted for the work presented in this thesis.

1.5 Thesis motivation and contribution

Current energy demand and consumption levels are enormous, and this demand has to be met for any society to progress economically. The impact that the huge amount of energy production has on our environment is severe. So, as we human race continue to expand and consume more energy we are ethically and morally bound to protect and nurture our environment. Earth is our only home. Since energy demand and its consumption are never going to come down, one way of trying to tackle the problem would be to produce energy that does not have an impact on our environment. They say "Every drop makes an ocean", thus what every opportunities we have to explore new renewable energy source must be investigated. The photosynthetic electrochemical is one such area. Though the device is small, the ambitions are not of the same magnitude. This work is an attempt to harvest energy from the photosynthetic power cell. Earlier works on the cell have only been on demonstrating the capability.

The major contribution of this thesis includes:

a) Identification of important parameters that affect the energy produced from the photosynthetic power cell.

b) Mathematical and electrical equivalent modeling of the photosynthetic electrochemical cell.

c) Proven that the cells are scalable by stacking them in series and parallel.

d) Development of a simulation model of the cell.

e) Design and simulation multiple power electronic converters to harvest the energy from the cell and select the best suited converter for a scaled application.

f) Development of a custom MPPT algorithm that is more suited for PSC energy harvesting.

1.6   Thesis objectives and scopes

The work presented in the thesis is organized into 6 chapters.

Chapter 1 includes a brief introduction to the area of renewable energy, energy harvesting and the photosynthetic power cell. A brief idea on the PSC device, construction and working of the cell has been outlined along with the history of the cell.

Chapter 2 discusses on how energy is produced in photosynthesis and how it is harvesting using the cell. Also the fabrication and construction of the cell is explained.

Chapter 3 focuses on testing of the fabricated device and results of power and energy produced by the cell are shown. From the obtained results the important parameters of the cell are identified and a math model of the cell is arrived at.

17

Chapter 4   deals with deducing the electrical equivalent model of the cell and developing a simulation model of the cell using MATLAB. The simulation model of the cell is used as energy source and basic power electronic converter models are analyzed, designed and simulated.

In chapter 5, the cell model is scaled and a suitable energy harvesting application is simulated. The prototype of the power electronic converter is designed and developed and is experimentally tested with a source that emulates the cell behaviour based on the simulation model of the cell and the results are discussed.

Chapter 6 outlines the conclusion, and future work directions.

CHAPTER 2

2 PHOTOSYNTHESIS, PHOTOSYNTHETIC POWER CELL AND FABRICATION

In this chapter, the understanding of the photosynthesis process is established followed by the working principle of the photosynthetic power cell. Finally, the device's detailed fabrication process is explained.

2.1 Photosynthesis

Photosynthesis is the process that occurs in plants and other organisms that produce their own food. They convert light energy from the sun to chemical energy that can be stored and used for the organism's living and activities. Photosynthesis usually occurs in plants, algae, and many species of bacteria. Photosynthetic organisms are called photoautotrophs, since they create their own food. During photosynthesis, plants, algae and cyanobacteria, combine carbon dioxide and water in a chemical process under the presence of light to produce complex hydrocarbons such as glucose and release oxygen as a byproduct. This produced hydrocarbon (sugar) thereby acts as the food for the organisms.

Apart from producing food, photosynthesis serves many other purposes for life support on Earth. Photosynthesis is vital for all aerobic life on Earth. It helps maintain normal levels of oxygen and carbon-dioxide in the atmosphere, photosynthesis is the source of energy for nearly all life on earth, either directly or indirectly and is the ultimate source

of the energy. In addition, photosynthetic organisms convert around millions of tons of carbon into biomass per year.

2.1.1   Photosynthesis and respiration

To put it in simple words, photosynthesis can be considered as 'work hours' of plants, during which they work to produce their food by taking in carbon-dioxide and give out oxygen. Just like any other living being they also rest after work. The 'rest period' is called the respiration period, during which they consume the produced food, and just like other living beings they breathe in oxygen and give out carbon-dioxide during respiration. Both these cycles involve electron transfer chains, oxidation and reduction reactions. Thus making electrons available during both photosynthesis and respiration period. This is how the PSC produces energy during light (photosysnthesis) and also during the absence of light (respiration). Photosynthesis and respiration are reversible chemical reactions. When photosynthesis is reversed the reaction is respiration and vice versa. The reactions are represented in equations 1.1 and 1.2 in Section 1.3.1.

2.1.2   Basics of Photosynthesis

The photosynthetic process begins when photons hits and gets absorbed by special a protein structure in the plant called 'photosynthetic reaction centers' that contain chlorophylls. In plants, these proteins are held inside organelles called chloroplasts, while in bacteria/algae they are embedded in the plasma membrane. Refer Figure 2.1 below to get a clear picture of the cell structure and matter that contribute for photosynthesis [47] [48] [49] [50].

20
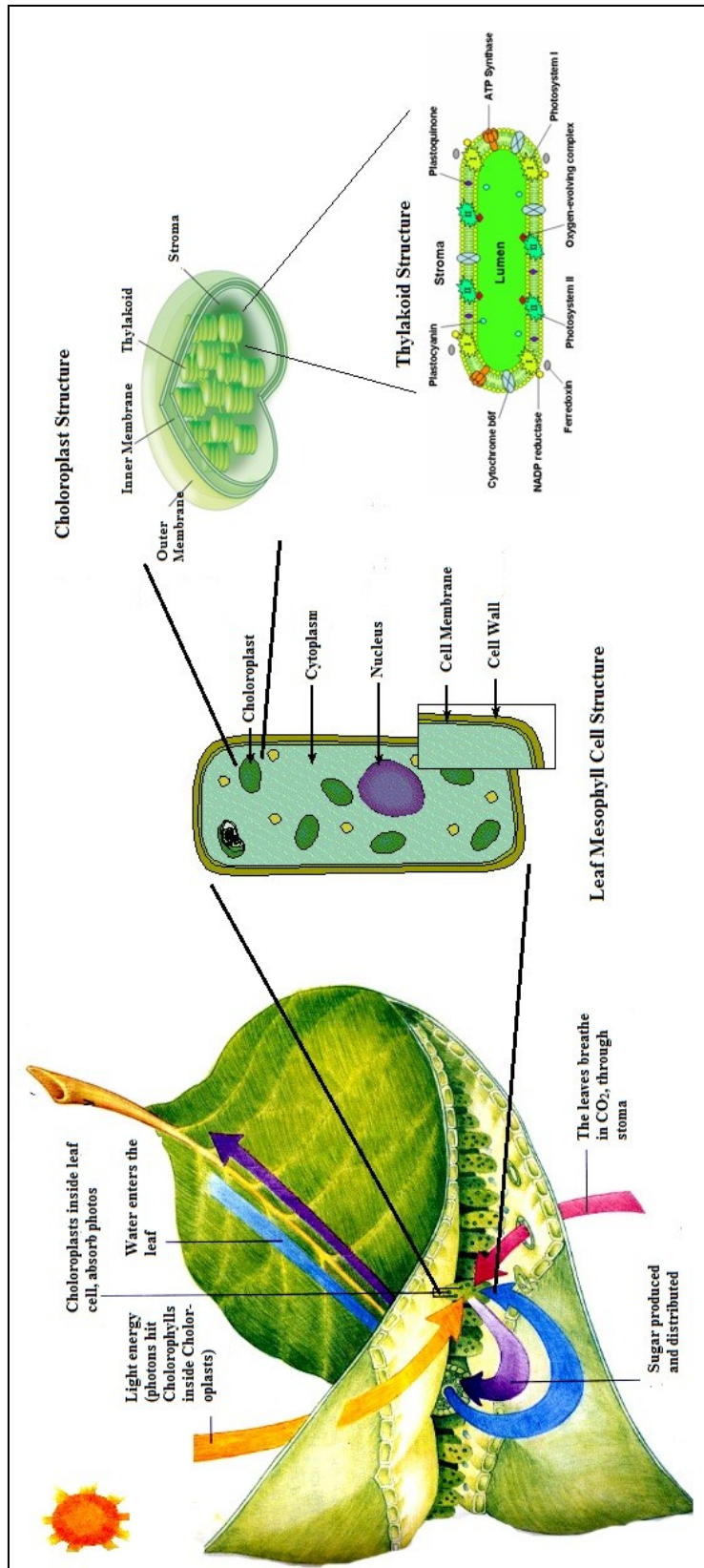
Fig. 2.1 Structure of plant leaf, cell, chloroplast and thylakoid [48]

The photosynthetic reaction center is a complex of several proteins, pigments and other co-factors assembled together to perform the primary energy conversion reactions of photosynthesis. When these reaction centers are 'hit' by a photon they give rise to molecular excitations, which in turn leads to a chain of electron transfer reactions along a series of protein-bound co-factors. These co-factors are light-absorbing molecules or pigments such as chlorophyll, phaeophytin and quinones. The energy of the photon is used to excite an electron to a higher level of molecular energy of a pigment. The energy created during this process is then used to reduce nearby electron acceptors. Subsequently on reduction they gain higher redox-potential. This chain of electron transfer steps form the initial phase of a series of energy conversion reactions result in the production of chemical energy during photosynthesis. These processes which form the initial phase of photosynthesis are dependent on energy from light (photon), hence these are called light-dependent or light reactions.

Apart from the processes mentioned above, a part of the light energy gathered by chlorophylls is converted and stored in the form of adenosine triphosphate (ATP). The rest of the energy is used for oxidation of compounds, such as water splitting. These electrons are then used in the reactions that turn carbon dioxide into organic compounds. These set of reactions is called the Calvin cycle. These reactions are basically post processing of energy that happen after the initial energy from light is absorbed. These reactions are the light independent reactions. They are also referred to as dark reactions. This should not be confused with 'respiration' of plants. This process occurs only when light is available. The light-independent reactions of photosynthesis are chemical reactions that convert carbon dioxide and other compounds into glucose. These reactions

occur in the stroma, the fluid-filled area of a chloroplast outside of the thylakoid membranes. These reactions act on the products of light-dependent reactions and perform further chemical processes on them.

Photosynthesis requires the photons in the visible light spectrum. Visible light spectrum is just a portion of the gamut of electromagnetic spectrum from the Sun. Plants do not absorb energy from the entire spectrum, they absorb only those in the visible light spectrum, especially those at the blue and red end of the visible light spectrum. The remaining green portion of the spectrum is reflected, which contributes to the green color of the pigments.

2.1.3   Light dependent and light independent reactions

As explained above photosynthesis has two stages, they are light dependent and light independent. During the light dependent reaction photons are absorbed and excite molecules to produce high energy molecules. In the light independent reactions these high energy molecules are utilized for processing carbon dioxide and water to produce carbohydrates [50].

Absorption of a photon initiates a primary photochemical charge separation (e⁻) from a chlorophyll (or group of chlorophylls), which are the primary electron donors and is attracted by the primary electron acceptor pheophytin, which passes the electron to a quinone molecule, resulting in reactions going through a series of intermediate electron-transfer steps. The transport of the electron along the electron transport chain leads to the eventual reduction of NADP to NADPH+. The chlorophyll regains this lost electron by

oxidizing a water molecule through a process called photolysis and release oxygen. This is represented by the following equation.

$$2H_2O + 2\,NADP^+ + 3\,ADP + light \longrightarrow 2\,NADPH + 2H^+ + 3\,ATP + O_2 \qquad (2.1)$$

In the light-independent reactions, the plat cell captures CO_2 from the atmosphere and processes it along with NADPH, ATP formed during the light dependent reaction is utilized to form sucrose and starch. The overall equation for the light-independent reactions is given below.

$$3CO_2 + 9\,ATP + 6\,NADPH + 6\,H^+ \longrightarrow C_3H_6O_3 + 9\,ADP + 6\,NADP + 3H_2O \quad (2.2)$$
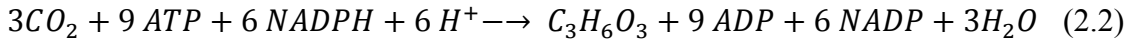
The overall reactions can be pictured as below.
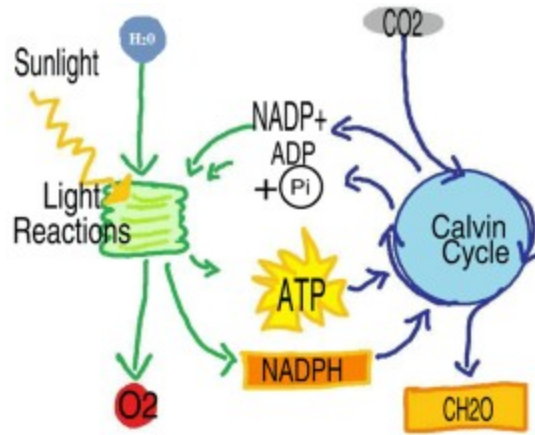
Fig. 2.2 Light dependent and light independent reactions [84]

Further reading, for a much detailed explanation on the photosystems and light harvesting complexes, electron transfer chain during photosynthesis and respiration refer the thesis work done by M. Shahparnia [51], which forms the basis of the work done in this thesis on PSC.

2.2 Parameters affecting photosynthesis

Three main environmental factors namely light irradiance, temperature and carbon-dioxide concentration influence the photosynthetic activity completely. Of these three, any one of them can become a limiting factor, i.e. if one factor has a greater influence it directly affects the total rate of photosynthesis irrespective of the influence of the other two factors masking the effects of the other factors. For example, if the temperature is not suitable for photosynthesis despite the availability of light and carbon-dioxide, the plant will be under respiration rather than carrying out photosynthesis. The effect of these parameters can only be observed in a controllable environment and a number of studies have been done to understand them [52].

2.2.1 Effect of light irradiance

The rate of photosynthesis depends on the irradiance of light (illuminance in photometry). During complete dark period (no light), plants respirate. The relation between light intensity and rate of photosynthesis can be better understood from the graphs below [52] [53].
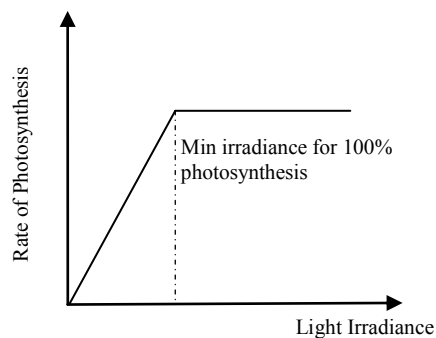
Fig. 2.3 a Generalized effect of Light irradiance on rate of photosynthesis [52]
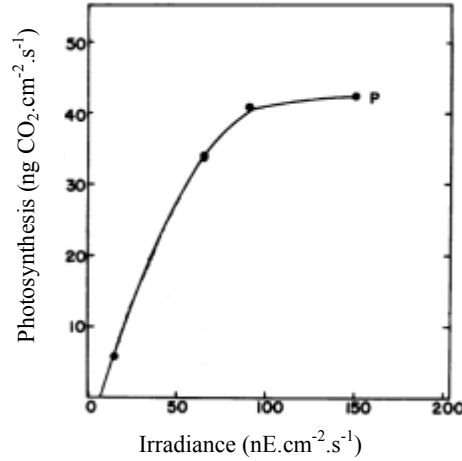
Fig. 2.3 b Effect of Light irradiance on rate of photosynthesis [53]

The minimum light irradiance $\left(\frac{E}{cm^2s}\right)$ for maximum photosynthetic activity depends on the wavelength of the incident light and is usually of the order of 50 to 100 $\left(\frac{nE}{cm^2s}\right)$ as shown in Figure 2.3b [53]. The photosynthetic activity is a measure based on the amount of carbon-dioxide absorbed per unit area per second. Figure 2.3b, shows the photosynthetic activity of common chlorophyll based plants and can be observed that the rate of photosynthesis saturates around 85 to 100 $\left(\frac{nE}{cm^2s}\right)$.

Where,

Irradiance is the measure of luminous flux per unit area.

E (Einstein unit) = 1mol of photons = 6.022 x 10^{23} photons

The energy of a photon is given by the equation:

$$\frac{hc}{\lambda} \qquad\qquad (2.3)$$

Where,

h → *planks constant*

c → *the speed of light, and*

λ → *wavelength of the incident light*

Green plants usually absorb the light close to red and blue spectrum. The wavelength of red light is higher than that of blue light. On conversion of units, power per unit area of blue light is around 165 W per m². Figure 2.4 below shows the visible light spectrum and absorbance of wavelength of chlorophylls.
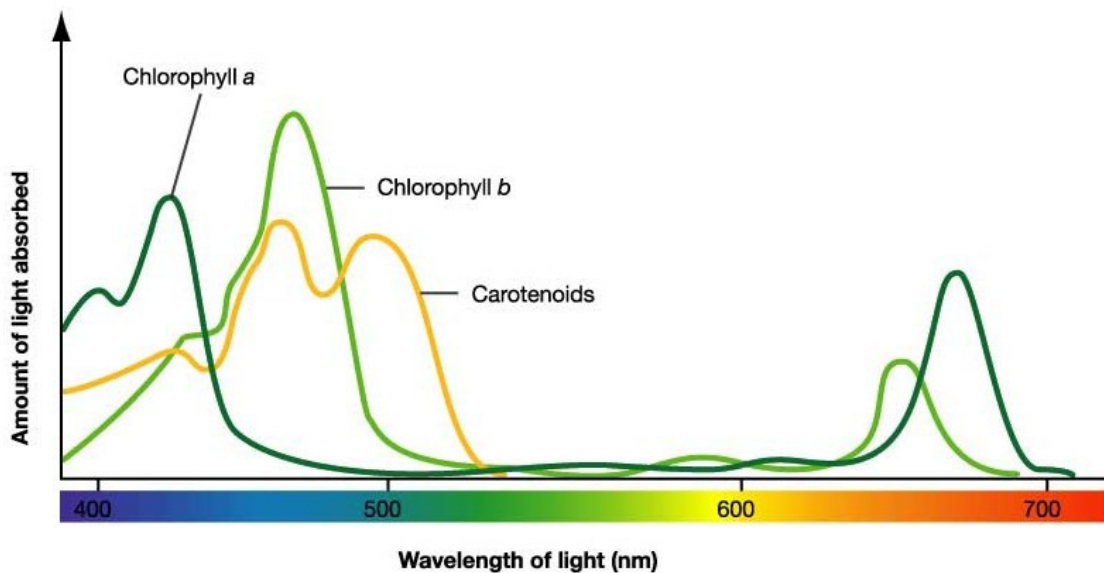
Fig. 2.4 Absorption spectrum of plants [55]

The maximum and minimum solar irradiance incident of earth is 1413 W per m² and 1321 W per m² [54], which translates to an average of 1367 W per m². Plants only need a minuscule 12% of the incident power for 'peak' photosynthetic activity and can be assumed to be easily available during normal daylight even during overcast conditions.

2.2.2 Temperature

The effect of temperature on photosynthesis is a very important consideration. It has to be noted that the light dependent reactions are not affected by changes in temperature. The light independent reactions are reactions catalysed by enzymes, the light independent reactions of photosynthesis are dependent on temperature. As the temperature increases the enzymes approach their optimum temperature of operation and the overall rate increases. The rate of increase approximately doubles for an increase of temperature by 10 °C. Once the temperature continues to rise beyond the optimum temperature the rate begins to decrease rapidly, until it comes to a halt, as enzymes are denatured [56] [57].
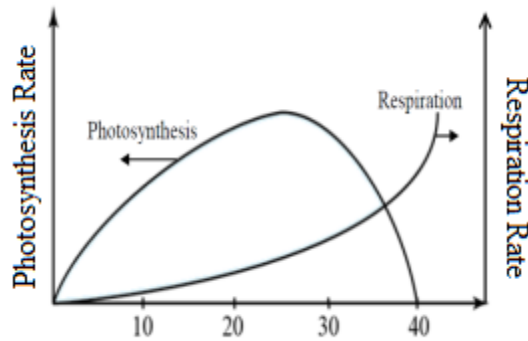
Fig. 2.5 a Generalized effect of temperature on rate of photosynthesis [56]
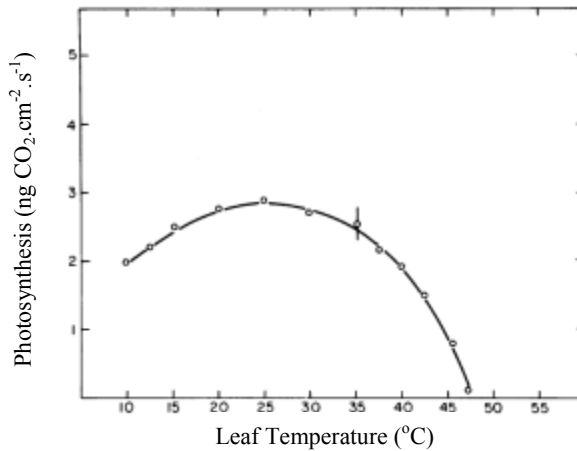
Fig. 2.5 b Effect of Temperature on rate of photosynthesis [57]

28

2.2.3 Concentration of Carbon-dioxide

An increase in CO_2 concentration leads to a higher rate of photosynthesis. However it effects can only be observed and controlled in a closed chamber and not in the real world. Though there is a variation in the rate of photosynthesis with respect to carbon-dioxide concentration, carbon-dioxide levels in atmospheric air is almost constant. Thus it need not be considered as an important parameter when modeling the PSC. Figure 2.6 below shows the effect of carbon-dioxide concentration on photosynthesis.
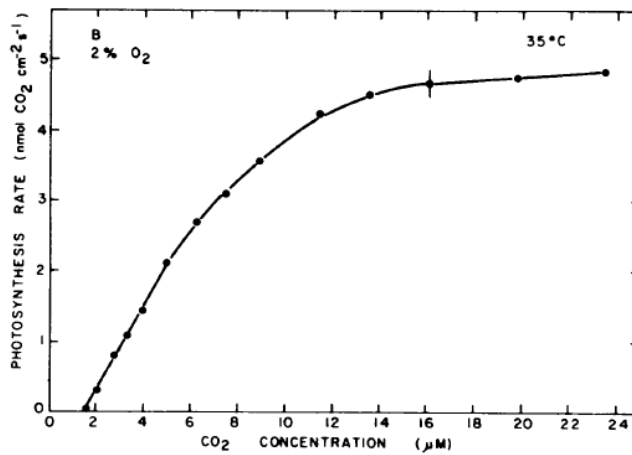
Fig. 2.6 CO_2 concentration vs. rate of photosynthesis [56]

2.3 PSC working principle

In the anode chamber, a live culture of photosynthetic microorganism such as green algae (chlamydomonas reinhardtii) or photosynthetic bacteria (cyanobacteria) is suspended in a growth medium solution mixed with an electron mediator or a redox coupler such as methylene blue ($C_{16}H_{18}N_3SCl$). Under the presence of light, the photosynthetic microorganisms carry on photosynthesis, producing carbohydrates (e.g. glucose) and O_2 from CO_2 and H_2O. During photosynthesis, electrons are being transported by NADPH

(NADPH are diffusional electron carriers) or along the series of enzyme complexes bound to the thylakoid membrane of the electron transport chain as explained in the sections above. These electrons (and protons) are siphoned from their normal photosynthetic function either from NADPH or the transport chain by the redox mediator molecules, by diffusion. This gives raise to electrons and protons. The mediators make their way back, through the buffer solution, and eventually donate the electrons to the anode. Then, just as in any fuel cell, the electrons then travel through an external load to the cathode chamber, where they reduce the oxidant ferricyanide (Fe(III)) [25]. These flowing electrons cause the electric current. The protons cross from the anode into the cathode through the PEM and combine with the reduced oxidant (Fe(II)). This is process by which the PSC produces electric power.

2.4 Fabrication & Components of Photosynthetic power cells

Now that the photosynthetic process and the working principle are understood, it would be easier to understand the importance of every component that makes the cell, and how they are fabricated. The fabrication work is based on the earlier work done by M. Shahparnia [51].

The cell is made up of two identical halves. Each half houses a chamber; the chamber forms the anode compartment and the cathode compartment of the cell as shown in Figure 2.7. Each chamber has a volume of 2 ml.
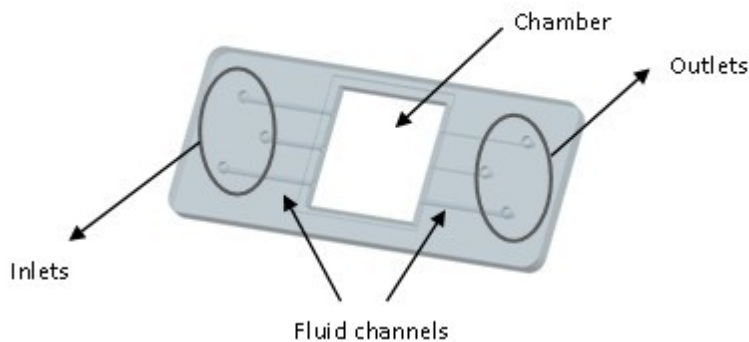
Fig. 2.7 The device's Half Cell

The half cells are fabricated using Polydimethylsiloxane (PDMS), with the help of a brass mould (Fig 2.8). PDMS is a polymeric organosilicon compound; these compounds are commonly referred to as silicones. PDMS is one of the most widely used silicon-based organic polymers, because of its superior inherent physical and chemical properties. PDMS is considered inert, non-toxic, non-flammable and optically clear.

The two half cells are separated by the proton exchange membrane and the chambers are covered with glass on both sides. The electrodes, anode and cathode are fabricated directly on both surfaces of the PEM.
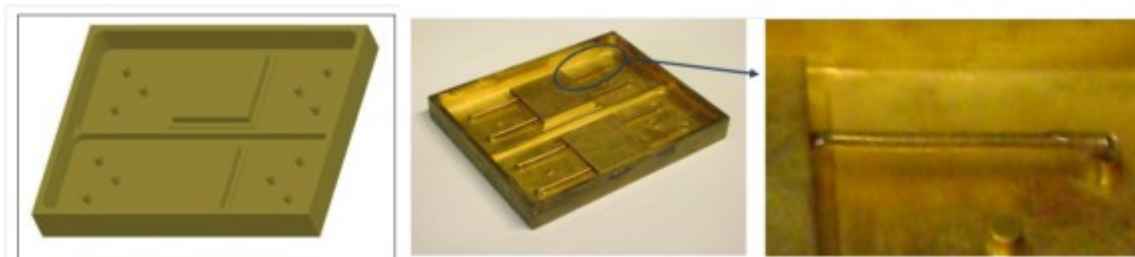
Fig. 2.8 Brass mould

2.4.1 Half cells

The half cells are fabricated using PDMS. First, the PDMS base and curing agent are mixed at a ratio of 10:1. Once the right amount of PDMS and curing agent needed are mixed, it is carefully poured in the mould shown in Figure 2.8. After pouring the uncured PDMS into the mold, the mixture is degasified in vacuum chamber for approximately 15 to 20 minutes. This removes the trapped air in the mixture. Air in the form of bubbles is trapped while mixing the base and curing agent, and pouring into the mould. Next, baking is done at 60 to 75°C for about 12 hours to finish the treatment and a solid half cell is fabricated, out of PDMS. Refer the annexure for the dimensions of the mould. Figure 2.9 below shows the dimensions of the half cell. The half cells are interchangeable as anode and cathode chambers as they have the same dimensions.
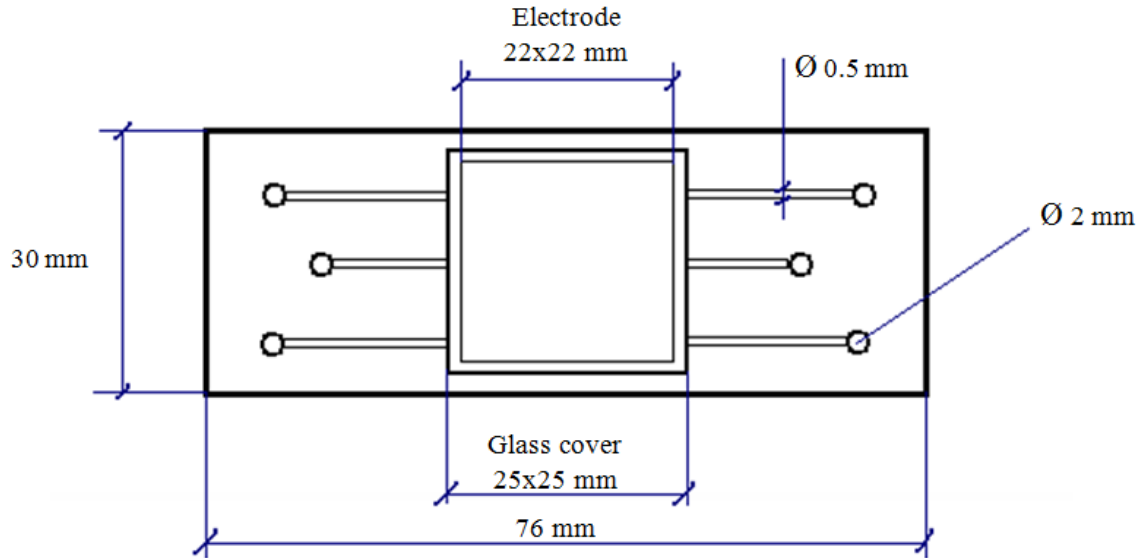
Fig. 2.9 Device half cell dimensions

2.4.2 Anode Compartment

The anode compartment contains the algae / photosynthetic micro organism suspended in a suitable growth media and a mediator such as methylene blue, and is covered by glass on the top and by the PEM at the bottom. The device is always placed with the anode on the top, so that it receives light. In all of the experiments, green algae (chlamydomonas reinhardtii) suspended in HSM solution (Sueoka's high salt medium) was used. The media helps in growth and reproduction of algae.

2.4.3 Cathode Compartment

The cathode compartment contains a solution with a high redox potential such as potassium ferricyanide solution. A 25% potassium ferricyanide solution was used in all the tests. This concentration level was selected based on the suggestion from the earlier work [51].

2.4.4 Proton exchange membrane

A proton exchange membrane or polymer electrolyte membrane (PEM) is a semi permeable membrane that conducts only protons. This helps in the separation of reactants and transport of protons, and is usually exploited by the membrane electrode assembly (MEA) of a proton exchange membrane fuel cell (PEMFC).

PEMs are made from either pure polymer membranes or from composite membranes with materials embedded in a polymer matrix. The most common and commercially available PEM is Nafion®, a product by DuPont. Proton exchange membranes are

primarily characterized by conductivity (σ), permeability (P), and thermal stability. PEMFC use a solid polymer membrane (a thin plastic film) as the electrolyte.

Nafion® was chosen as the proton exchange membrane for the device. There are different membranes available commercially with different parameters, only three types were used for the device and their parameters are given in the table below.

PEM	Thickness (μm)	Conductivity σ (S/m)	Weight (g/m^2)
Nafion® NRE – 212	51	0.1 (minimum)	100
Nafion® N – 115	127	0.1 (minimum)	250
Nafion® N – 117	183	0.1 (minimum)	360

Table 2.1 – Nafion Properties

2.4.5 Electrode

For the PSC device, the electrodes are integrated directly onto the surfaces of the PEM. Gold being noble and inert to the reactants was selected as the electrode material. Gold is sputtered on both surfaces of PEM and then etched using photolithography process. Electrode patterns were designed and tested in the earlier work [51] and the best one suggested in that work has been selected. The electrode pattern used is shown in Figure 2.10. A glass mask with the shown electrode pattern is used for the UV exposure step, during the lithography process. The thickness of the fabricated gold electrode is 100 nm.
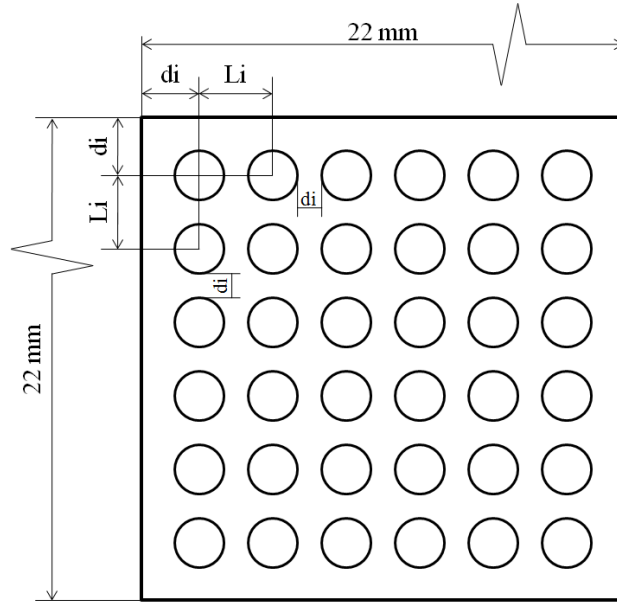
Fig. 2.10 Electrode design

The dimensions of the electrodes are given in the table below.

Diameter of pore (µm)	L (µm)	d (µm)
500	1000	500

Table – 2.2 – Electrode dimensions

The step by step photolithography fabrication process is explained in the table below.

Step. No.	Process	Description
1	Nafion preparation	The membrane is treated to increase the ionic conductivity of the membrane. Refer annexure for Nafion treatment.
2	Gold Sputtering	Gold is sputtered on both the surfaces of the membrane at a thickness of 100 nm using the Denton sputtering machine.
3	Silicon Wafer preparation	A 6 inch silicon wafer is prepared to be used as the base support layer for the photolithography base.
4	PR Spin coating (Wafer only)	The prepared wafer is spin coated with positive photoresist (PR) S1813 using the laurel SITE Coater.
5	UV Exposure (Wafer only)	The PR coated wafer is held under the glass mask and exposed to ultra violet radiation (UV).
6	Developing (Wafer only)	The UV exposed wafer is developed using the SU-8 developer in the SITE Coater. The electrode pattern will now be distinct on the wafer.
7	Nafion attachment to wafer	The gold sputtered PEM is attached to developed wafer, aligning with the electrode pattern on the wafer
8	PR Spin coating	Step 4 is repeated, now with the gold sputtered PEM on the wafer
9	UV Exposure	Step 5 is repeated, with the gold sputtered PEM on the wafer.
10	Developing	Step 6 is repeated, with the gold sputtered PEM on the wafer. The electrode pattern will appear distinct on the gold sputtered PEM.
11	Flipping of Nafion	The PEM is now flipped to process the other side, since only one side has been processed.
13	Repeat steps 7-10	The same steps from 7 to 10 are followed to process the other side of PEM. However care has to be taken when flipping and attaching PEM to wafer so that it aligns perfectly with the pattern and matches the other side.
16	Gold Etching	Once both the sides of the gold sputtered PEM are processed, the membrane is removed from the wafer and is etched using the gold etchant solution. Extreme care has to taken so as to not over etch the gold; it can easily be over etched in a matter of two or three seconds.
17	Nafion attachment to wafer	The gold etched PEM is again attached to the silicon wafer.
18	Full UV Exposure	It is now exposed completely in UV, i.e. 'without' the mask, to remove the PR.
19	Developing	Next step is to develop using the SU-8 developer.
20	Nafion flipping	The Nafion is flipped similar to step 11.
21	Repeat steps 17 - 19	Steps 17 to 19 are repeated and can be removed from the silicon wafer to complete the process. Now, the gold electrode will be fabricated on both the surfaces of the PEM.

Table – 2.3 – Step by step, Photolithography process

Figure 2.11 below helps visualize the process explained in the table.

1 – Silicon wafer

2 – PR spin coating

3 – UV exposure

4 – Developing

5 – Placing Nafion

6 – Nafion attachment

7 – Gold sputtering

8 – PR spin coating

9 – UV exposure

10 - Developing

11 – Gold etching

12 – Flood exposure

13 – Developing

14 – Nafion detachment

15 – Nafion flipping
and reattachment

16 – Repeat steps 7-13

17 – Final detachment
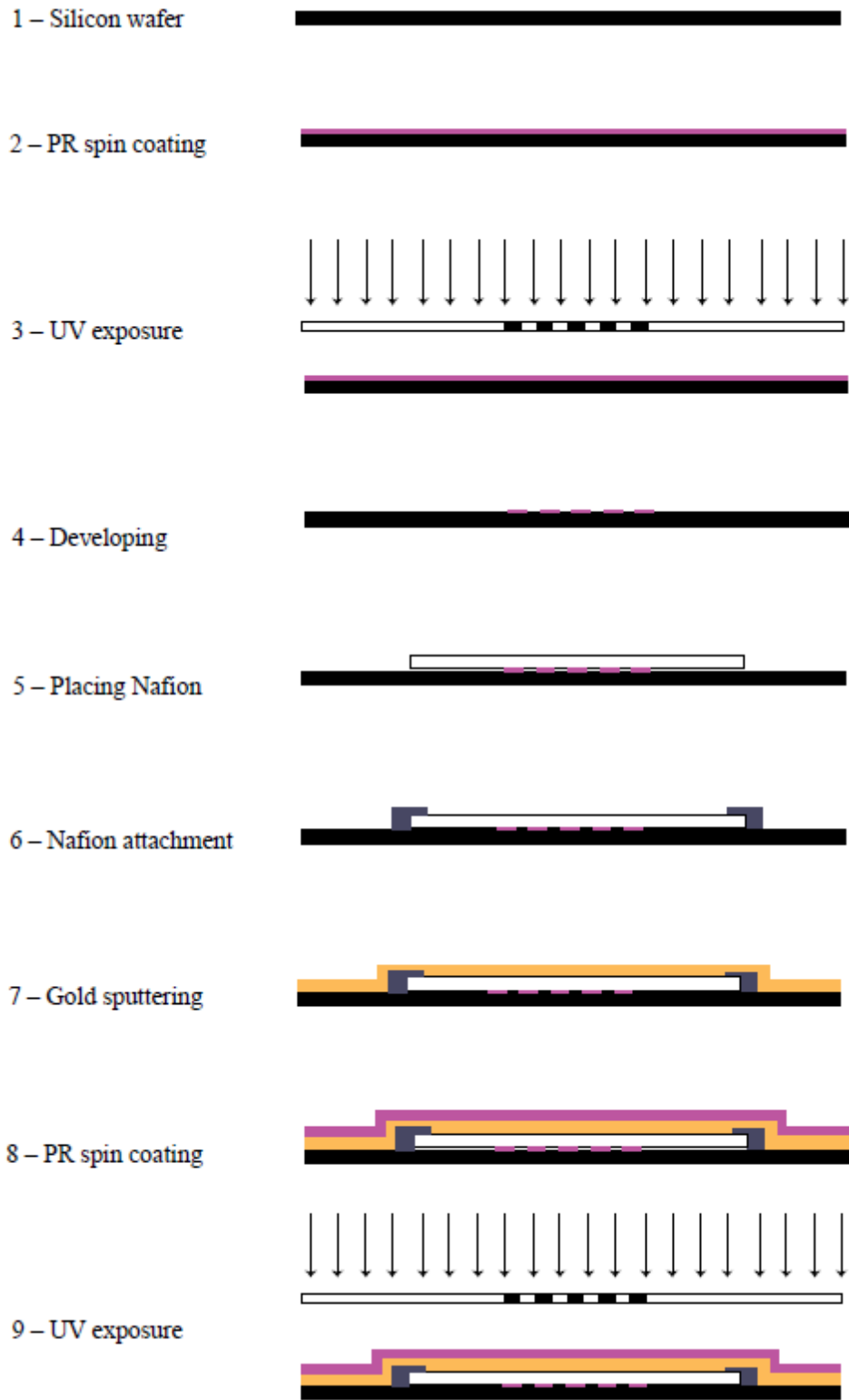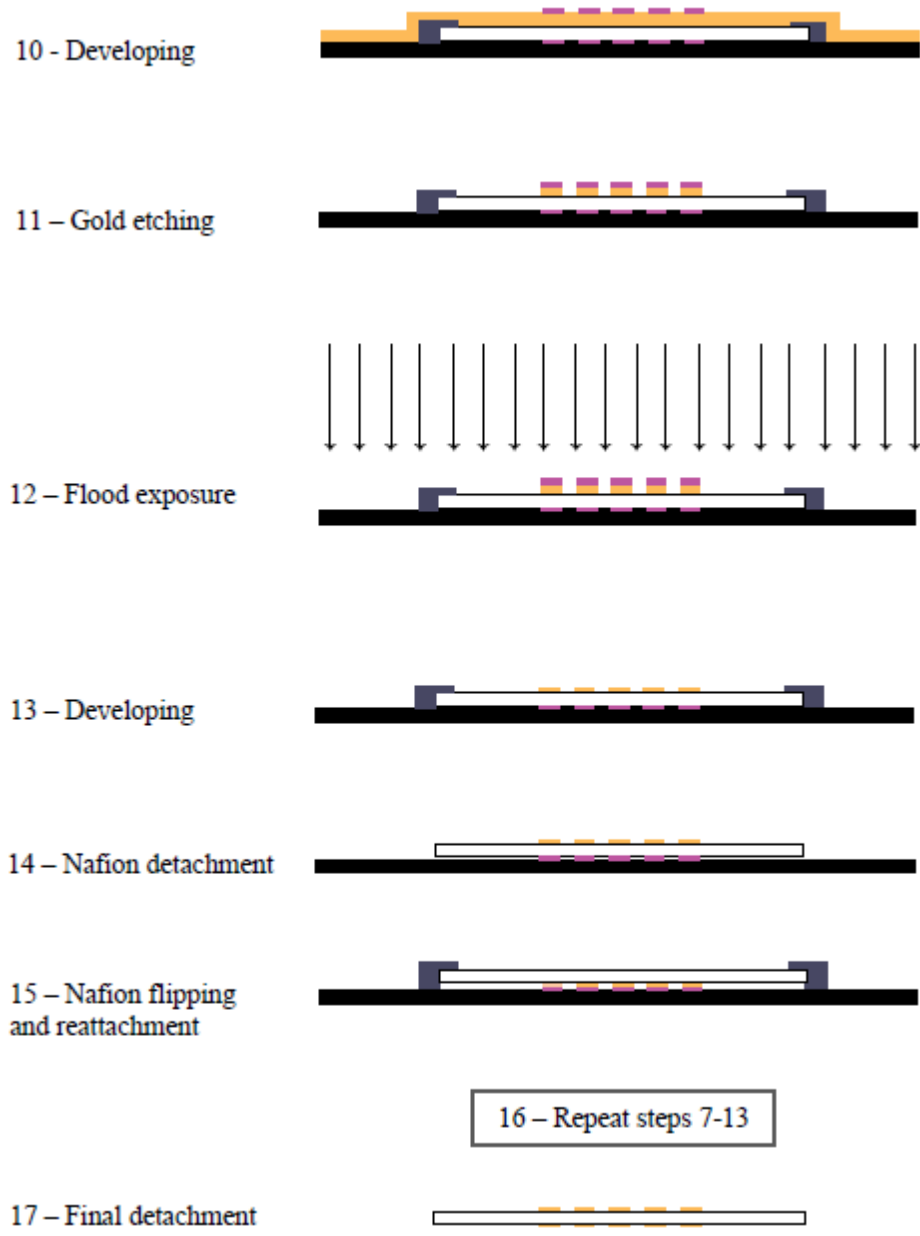
Fig. 2.11 Photolithography Fabrication process [51]

2.4.6 Assembly

Once the fabrication and preparation of all the components are done, the device is assembled. Exploded view of the unassembled model of μPSC and the assembled device are shown in the Figures 2.12 & 2.13.
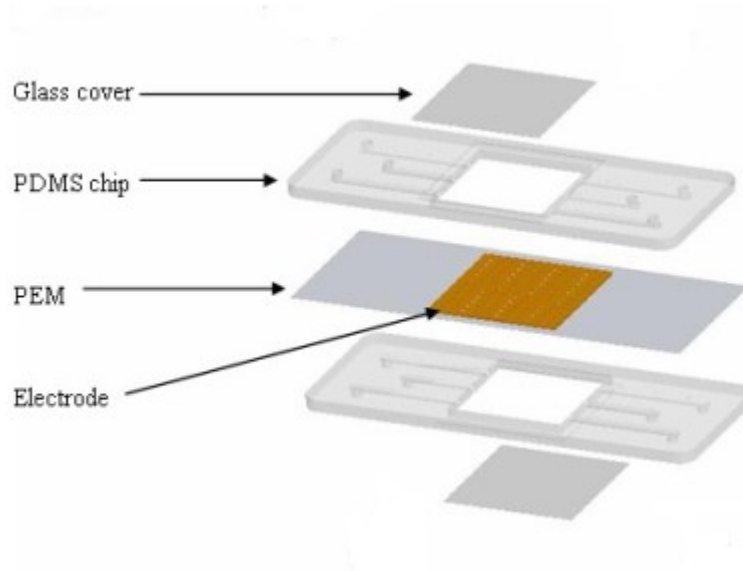
Fig. 2.12 Exploded view of the unassembled model of μPSC
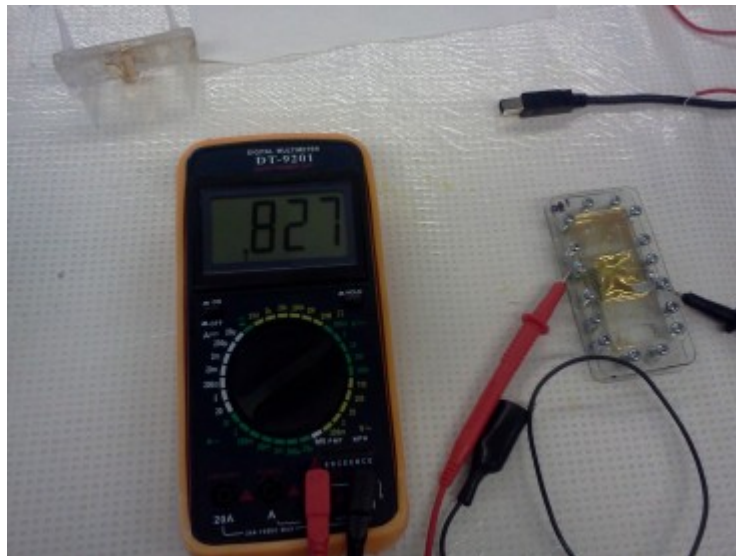
Fig. 2.13 Assembled device

The device is assembled by carefully combining the components together and sandwiching between two clear acrylic sheets, each with a thickness of 3 mm. The enclosure is made of acrylic sheets that have holes drilled on the sides and are bolted together. This ensures that there is no leak in the device and is highly robust. The dimensions (in mm) of the acrylic sheet enclosure used to bolt the device together are shown in the Figure 2.14 below.

Fig. 2.14 Dimensions of enclosure

The testing and the results of the PSC are discussed in the following chapter.

CHAPTER 3

3 TESTING AND CHARACTERIZATION OF THE CELL

The fabricated device is tested and the results are studied to characterize the cell by identifying the important parameters in this chapter.

3.1 Testing of the fabricated device

Once the half cells and the electrodes are fabricated they are assembled together to form the complete device as shown in Figure 2.10. Apart from the components assembly, the necessary reactants / solutions are prepared. A 25 % (w/w) Potassium ferricyanide $(K_3[Fe(CN)_6])$ solution is prepared and is used as the catholyte. A volume of 2 ml of the prepared catholyte is injected or pumped in to the cathode chamber through the channels with caution, such that there is no air bubbles formed in the chamber. A well assembled device has no leaks. The anode chamber is then filled with 2ml of the anolyte solution containing the green algae (chlamydomonas reinhardtii), growth medium and other reactants. The green algae samples are obtained from the Department of Biological Sciences, TOXEN center (Interinstitutional Center for Research in Environmental Toxicology), University of Quebec at Montreal, Canada.

3.1.1 Open Circuit voltage (OCV) testing

When the set up is ready, a simple digital multimeter is used as a voltmeter to observe the open circuit voltage produced by the cell. Open circuit voltage (OCV) observation is one of the best ways to test the cell. A quick inference can be drawn from the open circuit that

a cell produces. A cell that is assembled poorly or is made up of poorly fabricated components produce very low or zero voltage. If the device has leaks, the initial open circuit voltage produced will be good but reduces rapidly to zero. A good cell produces a steady open circuit voltage of 0.6 volts to 1 volt depending on various parameters. Thus, when a device is fabricated and assembled, the cell`s open circuit voltage performance is initially observed to check the quality device.

A sample open circuit voltage test is shown in the graph below, Figure 3.1. The voltage of the cell is observed for about 5 minutes without any load (OCV).
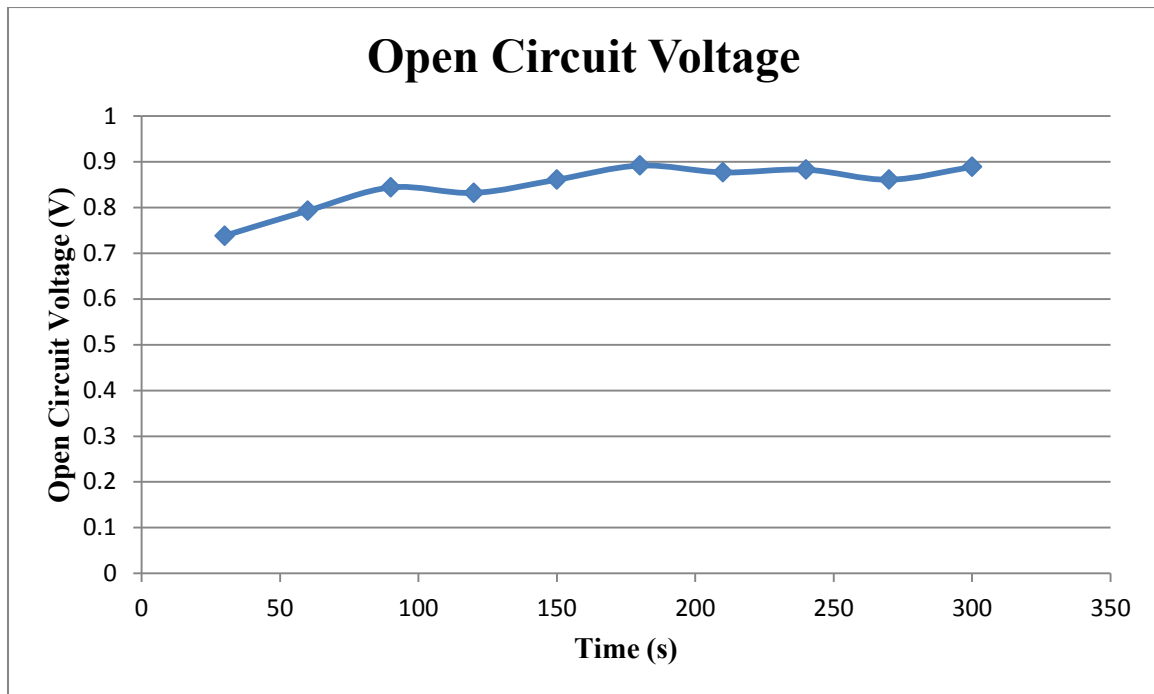
Fig. 3.1 Cell Open Circuit Voltage observation for 5 minutes

From the graph above, it can be inferred that the cell is able to produce voltage continuously and steadily. The real purpose of the cell is to produce power, this it would not suffice testing for the open circuit voltage alone. The cell has to be loaded and be

tested to find out if the cell is able to produce power. From the tests, it can be said that the cell produces around 0.9V under open circuit condition.

3.1.2 Load testing

The load testing is performed to observe if the cell is capable for producing power. A load of 1kΩ is connected to the cell and the now the voltage and current are measured and observed for five minutes.
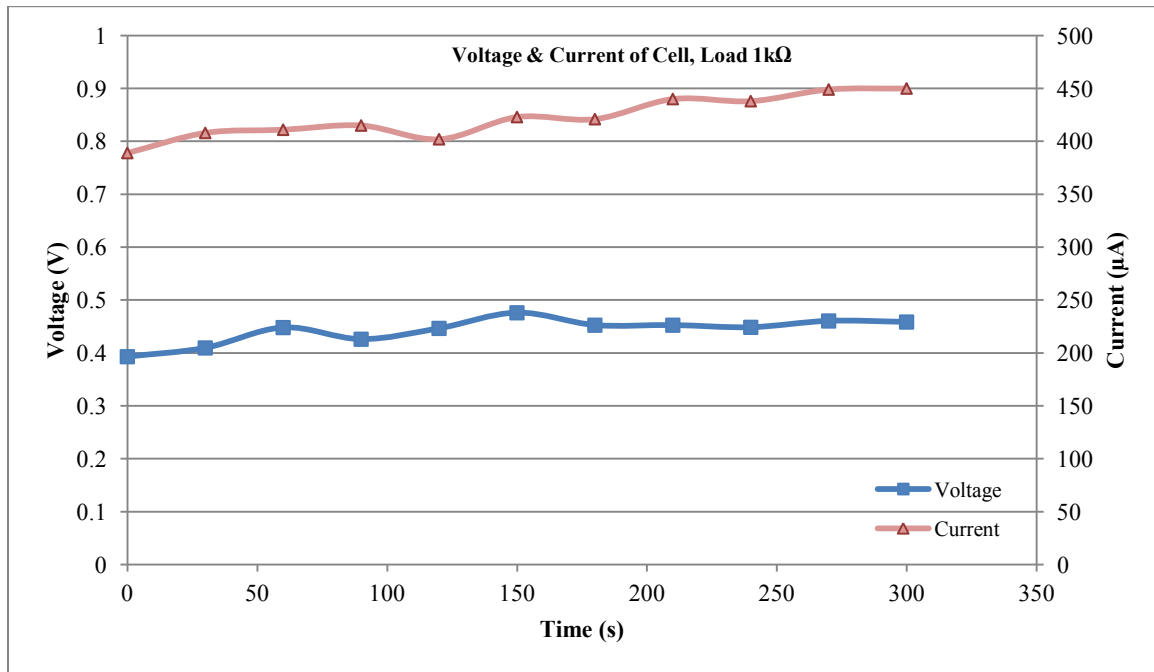
Fig. 3.2a Cell Voltage (V) and Cell Current (μA) under a load of 1kΩ

The graph above in Figure 3.2 shows the cell voltage (v) along the primary Y axis and cell current (μA) along the secondary Y axis when the cell is connected to a load of 1kΩ. The voltage and current are observed for a period of 5 minutes. From the graph, it can be concluded that the cell is capable of producing power. From the data, the cell average voltage is calculated as 0.476 volts and an average current of 423μA thereby producing an average power of around 200μW for 5 minutes when loaded with 1kΩ. The load of 1kΩ not necessarily extracts the maximum power from the cell. The load 1kΩ was

43

selected for demonstration purposes. The maximum power point of the cell can be found from the V-I characteristics and power characteristics of the cell. The first two tests are the main tests to identify whether the cell produces good and consistent power. The current was measured using a current sensing resistor of 0.91Ω. The current can be calculated by measuring the voltage across this resistor using the voltage divider relation. The circuit set up is shown in Figure 3.2b.
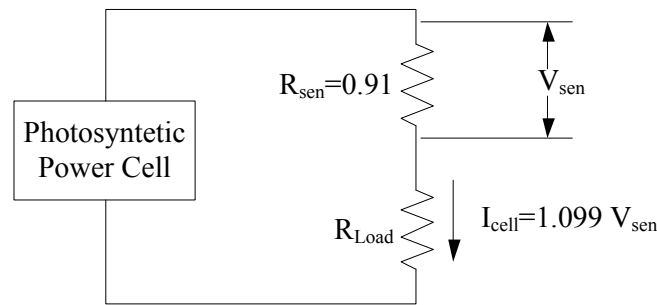
Fig. 3.2b Circuit for current and voltage measurement

The current from the voltage across the current sensing resistance R_{sen} 0.91Ω would be:

$$I = \frac{V_{sen}}{R_{sen}} = \frac{V_{sen}}{0.91} = 1.099\ V_{sen} \tag{3.1}$$

Measuring low voltage is easier and accurate than to measure low current. This is why it was chosen to use a resistive current sensor. If the current sensor resistance was lower than 0.91Ω it would lower the sensing voltage to few a micro volts, and that was the reasoning to not a very low current sensing resistor such as 0.1Ω or 0.2Ω.

3.1.3 Miscellaneous tests

Apart from these two tests, it is essential to prove that the algae are the main contributors for the continuous power production. To prove these, the device is tested with different anolytes such as water and just the growth medium without any algae in it.

The first test is to test the device with just water added to the anode compartment and potassium ferricyanide to the cathode compartment. The anode was filled with 2 ml of water. The graph below shows the results, OCV was observed for about 10 minutes.
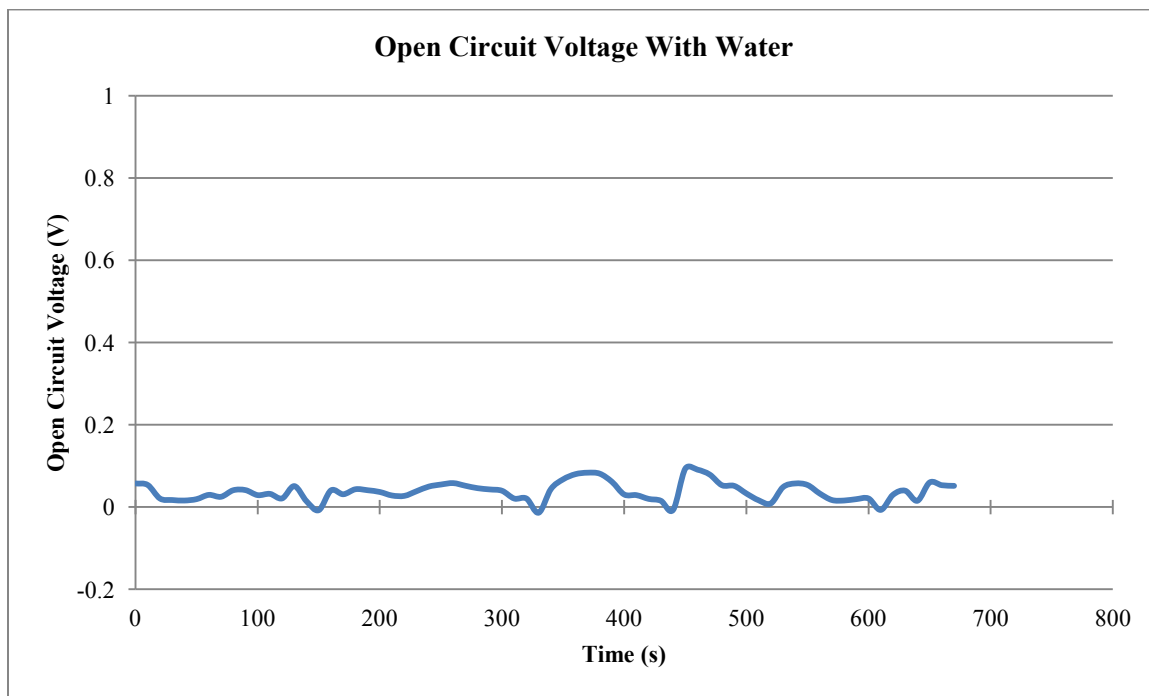
Fig. 3.3 OCV observation, when water is used as anolyte

It can be observed that there are minor fluctuations in voltage and this is because of some free ions present in water. These free ions are attracted by the redox potential of potassium ferricyanide in the cathode compartment. The water used was direct tap water, and when distilled water was used, similar open circuit voltages were observed, but the magnitude of OCV was slightly lesser than that of the OCV produced by tap water. Also, when both the sides were filled with the same fluid such as water and water or with potassium ferricyanide on both sides the cell did not produce any voltage at open circuit condition.

45

The same effect as mentioned above is observed when the growth medium alone is used in the anode. HSM media (Sueoka's high salt medium) was used as the grown media. Show below in Figure 3.4 is the voltage observed when only the media without any algae was used as anolyte and OCV was observed for about 25 minutes.

Open Circuit Voltage With HSM
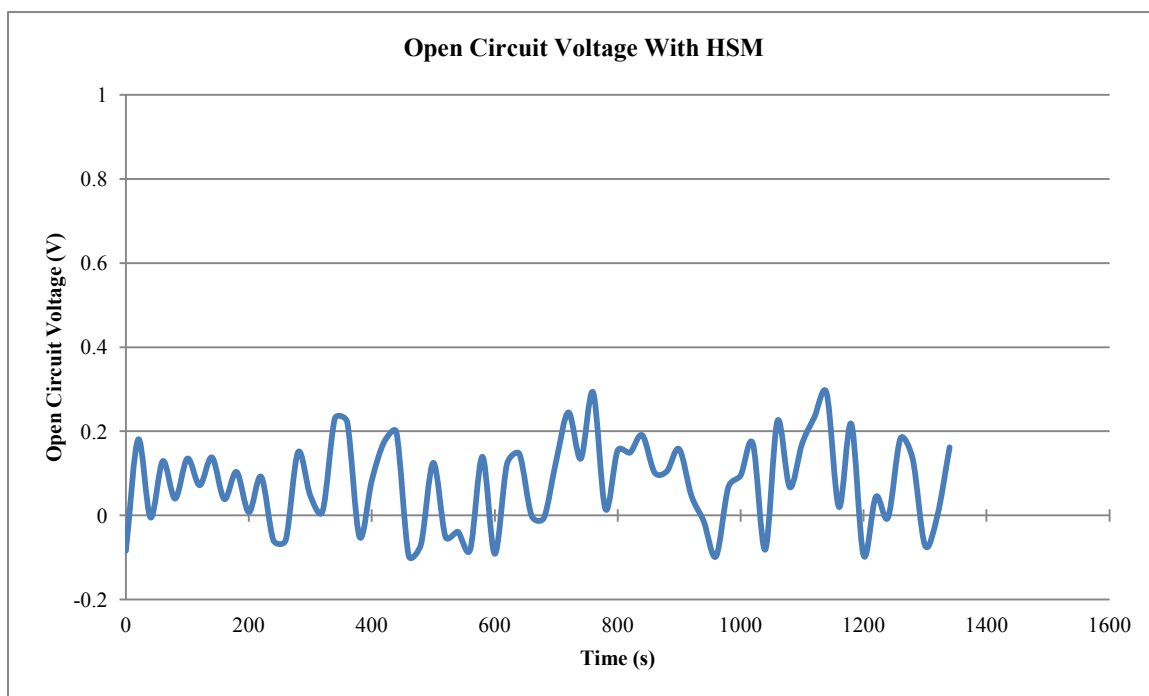
Fig. 3.4 OCV observation, when media (no algae) is used as anolyte

Apart from the free ions, there is glucose present in the media with along with traces of mediator, this gives raise to some free ions as above and produces some minor voltage. However, when loaded under this condition, i.e. with the media as anolyte, the current produced is too low to be measured with the devices. The current produced is probably in the range of few Pico amperes. This low current was not measurable and it is assumed to be zero. It can affirmatively be said that the media does not produce any power, though it produces some small amount of voltage as shown in Figure 3.4.

46

DT9805 Series USB Data Measurement and Acquisition Module, from Data Translation, Inc. was set up and used to obtain the data for the above tests.

3.2 Effects of Loading on PSC

It is necessary to identify the behaviour and the response time that the cell exhibits when loads are switched. For this test, the cell operation was started under open circuit conditions, when loads were switched when the voltage stabilized. First, the cell was in open circuit voltage condition, then a load of 100 Ω was switched after a time period of 5 minutes, and then a load of 500 Ω was switched on for 15 minutes and then a load of 1 kΩ and then a load of 2 kΩ were switched on. The results of the tests are highlighted in the graph below.
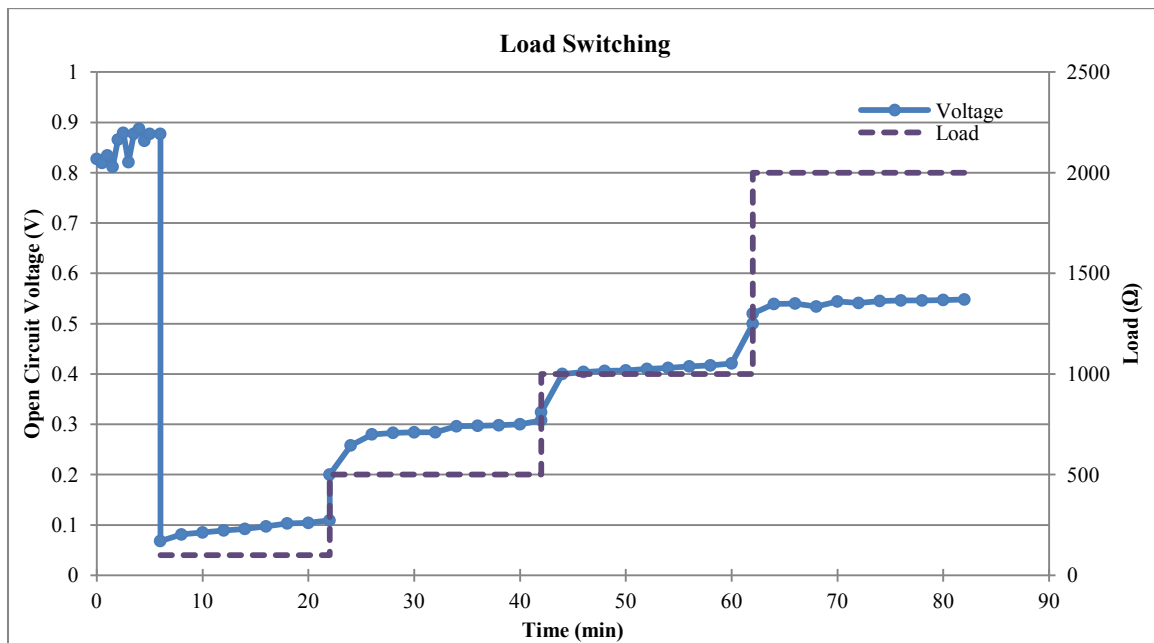
Fig. 3.5 Load switching and cell voltage response

It can be observed from the graph that the cell takes quite some time to stabilize when loads are switched and is approximately 4 minutes.

47

3.3   Voltage – Current (V-I) Characteristics of PSC

Voltage – Current (V-I) characteristics are studied to determine the basic parameters and used to model its behavior in an electrical circuit of any electrical or electronic device. In order to model the cell it becomes essential to obtain the V-I characteristics of the cell. Now, that the cell is tested for and has been proven that it is capable of producing power continuously, it can be tested to obtain the Voltage – Current (V-I) characteristics of the PSC. The V-I characteristics are obtained by loading the cell and varying the load linearly. The cell was initially loaded at approximately at 1Ω and was increased gradually up to 10 MΩ. The graph below illustrates a V-I characteristics obtained for one of the cell (loading shown up to 10kΩ only), under ambient temperature and lighting conditions.
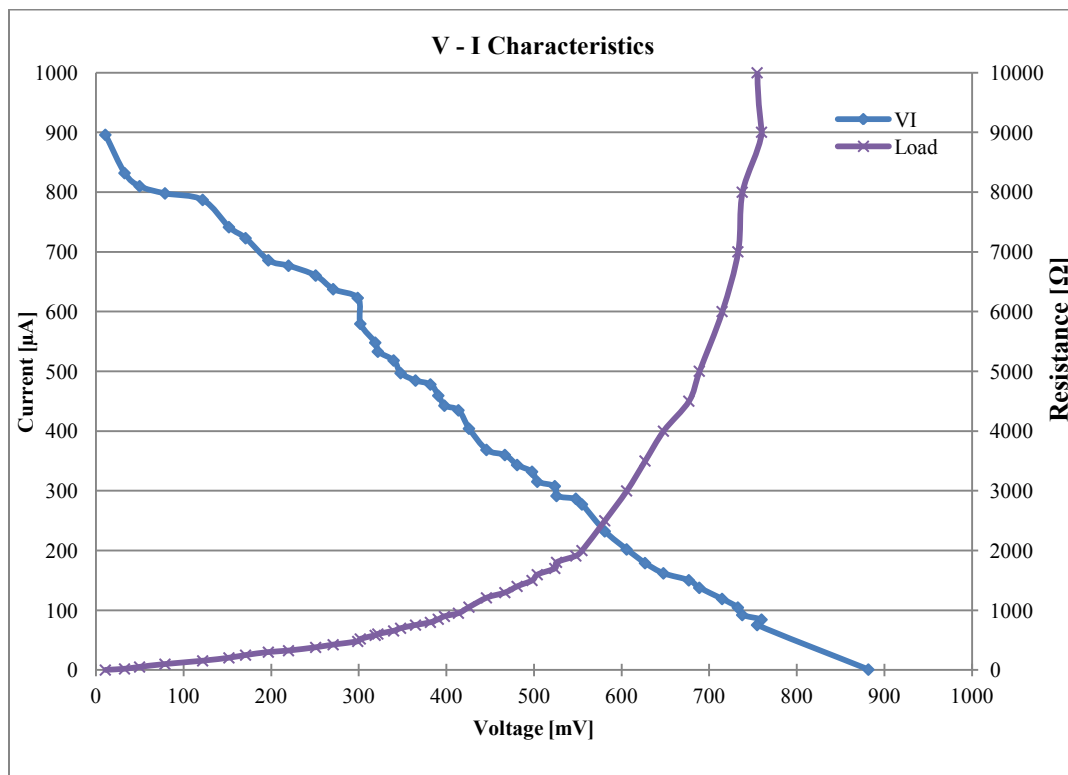
Fig. 3.6 V-I Characteristics of μPSC

The test parameters for the above obtained characteristics are:

Photosynthetic Organism	Anolyte Concentration	Algae Quantum yield	PEM	Light Irradiance
Green Algae	1.3 million cells per ml in HSM	0.786	Nafion 117	210 lux

Table – 3.1 –Testing Parameters of PSC

The effects of the above mentioned parameters are discussed in a detail in Section 3.5, where the main parameters are identified and the system is modeled based on that. It has to be noted once again that, the catholyte concentration for all the experiments are 25 % (w/w) potassium ferricyanide solution, also the electrode pattern is as shown in Section 2.4.5. The current was measured using the method as explained in Section 3.1.2.

3.4   Power Characteristics of PSC

The power characteristics of the cell are obtained from the same experiment. The power produced by the cell is plotted against the voltage of the cell. The power characteristics of the cell (same as experiment in Section 3.3) are shown in Figure 3.7 below.
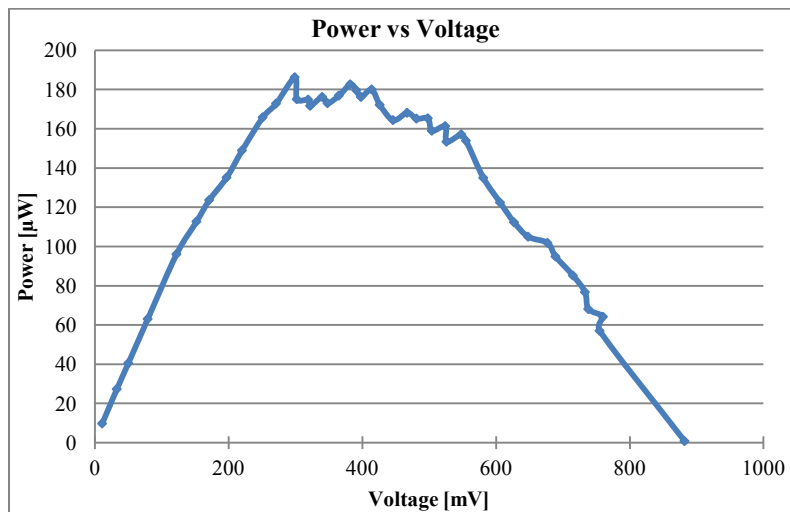
Fig. 3.7 Power Characteristics of µPSC

The cell generates a peak power of about 190μW. From the graph, it can be inferred that the preferable working range for PSC would range from 300 to 600mV. The peak power of 190μW of the cell corresponds to 39.25μW/cm^2, as the area of the cell is 2.2 cm x 2.2 cm. These characteristics can be used to achieve the maximum power point (MPP) of the cell.

From the sections above, it can be safely said that the cell has been tested and also the performance and characteristics of the cell are obtained. The next step would be to examine the various parameters affecting the cell's performance and characteristics, and that is exactly what will be achieved in Section 3.5 below.

3.5 Identification of vital parameters influencing cell performance

The cell's characteristics and performance are dependent on so many parameters. However, the ultimate parameter is the rate of photosynthesis, which is explained in Sections 2.2.1, 2.2.2 and 2.2.3 on how it is affected by the effect of light, temperature and carbon dioxide concentrations. To set up a controlled environment to control temperature and carbon dioxide concentration and monitor their effect is difficult and expensive, thus they have been performed at the ambient conditions. It is relatively easier to control the light irradiance and measure the irradiance. Hence, the effect of light irradiance on the cell's performance is studied.

Apart from the ambient factors such as the light, temperature, etc, influencing the cell, other parameters such as different Nafion thickness, electrode pattern, concentration of algae in the growth medium, concentration of potassium ferricyanide, algae's efficiency in absorbing photons and releasing electrons, etc, too play a vital role in the performance

50

of the cell. Some of the above mentioned parameters are studied by an earlier work [51], and will be highlighted in Section 3.5.4 and the also other factors are discussed in detail.

3.5.1 Nafion thickness

The Nafion PEM is available in different thickness. Thicker the Nafion, more robust it is and thicker Nafion has more electron resistance than thinner Nafion. The different available Nafions are mentioned in Table 2.1 in Section 2.4.4. Out of these three Nafions, only two membranes 115 and 117 were tested as the results shown in Figures 3.8-3.9 below were quite conclusive.
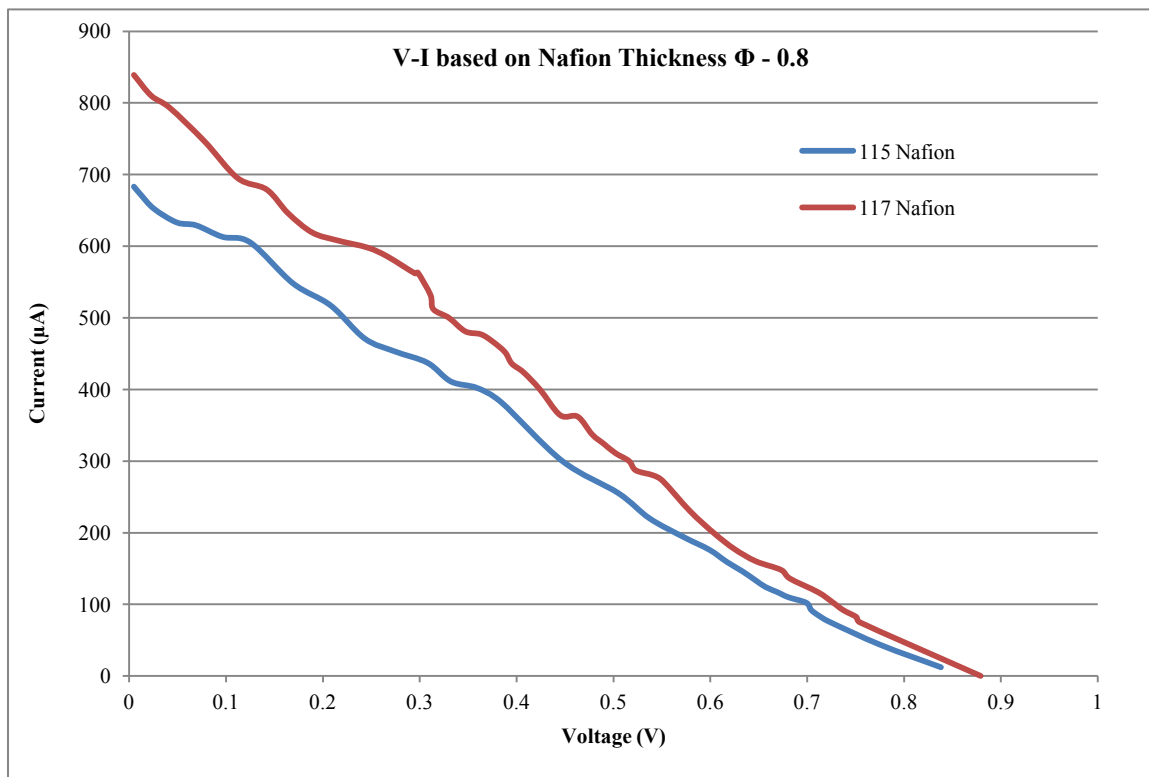
Fig. 3.8 V-I characteristics for different Nafion Membranes
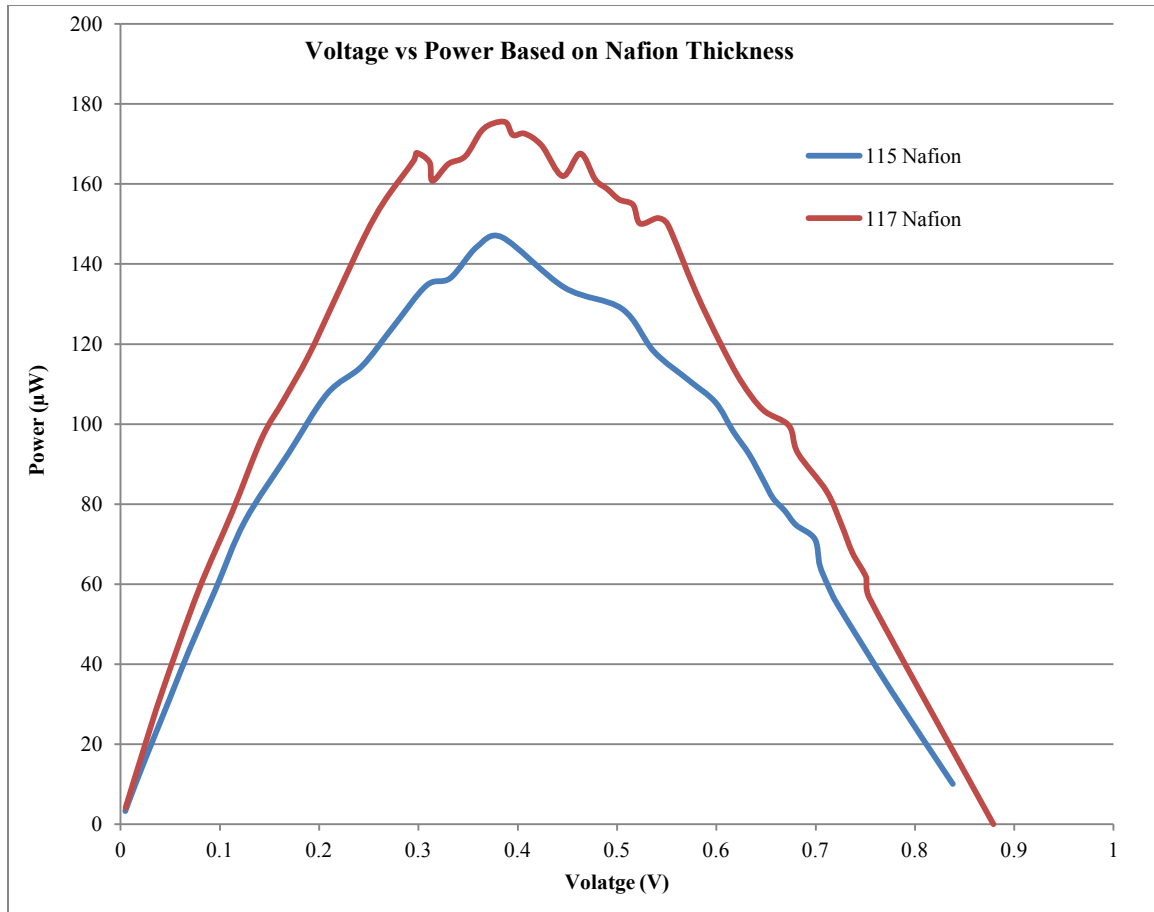
Fig. 3.9 Power characteristics for different Nafion Membranes

All the other parameters were the same for both the tests while the only difference was the different type of Nafion used. The cell produces more power and voltage when a thicker PEM membrane is used. This is caused because the thicker membrane has more resistance for the electrons and therefore more electrons are made to travel through the external circuit instead of passing through the membrane. This increased resistance causes the increase in power compared to the thinner Nafion.

It is quite conclusive to use the thicker membrane than the thinner membrane, though thicker membranes cost slightly more than thinner membranes.

3.5.2 Light Intensity

It was clearly seen how the light irradiance affects the rate of photosynthesis in Section 2.2.1, but that does not give a clear idea on how the cell's performance is affected. It should be noted that the photosynthesis rate saturates around 165 W per m^2 (41.085 lux) for algae or organisms with chlorophyll as the main photosynthetic pigments. Bright sunlight provides an irradiance of approximately 100,000 lux or lumens per square meter on the Earth's surface and is spread over the electromagnetic spectrum. Table 3.2 below, gives an idea about the light irradiance with examples [59].

Light irradiance	Description
100,000 lux	Bright sunlight
20,000 lux	Shade illuminated by entire clear blue sky, midday
10,000 lux	Typical overcast day, midday
400 lux	Sunrise or sunset on a clear day (ambient illumination).
40 lux	Fully overcast, sunset/sunrise
0.25 lux	Full Moonlight
0.002 lux	Starlight clear moonless night sky

Table 3.2 : Light irradiance examples

For these test a closed opaque cardboard chamber was made and was fitted with four 60W incandescent bulbs inside along with it was placed the lux meter to measure the light irradiance. There was no ambient light entering the chamber. When there was no bulbs on it was completely dark inside the chamber, and each light were turned on one by one to increase the lux and find out its effects. Apart from performing the tests inside the chamber, the same test was done in ambient light in the lab and also in directly in sunlight (was placed directly under sunlight near a window). The V-I and power characterisation of the cell was then performed. Nafion 115 was used as the PEM for all of these experiments. The graphs below show the V-I and power characterisation of the cell under different lighting conditions.
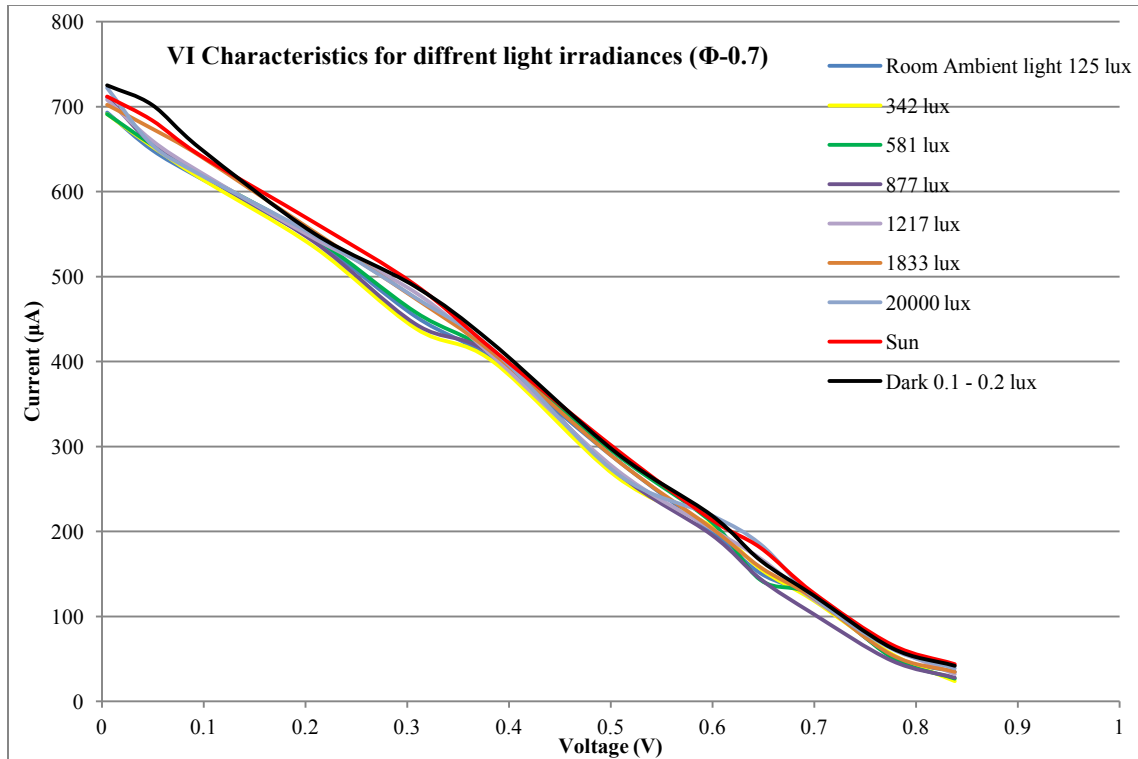
Fig. 3.10 V-I characteristics for different light irradiances
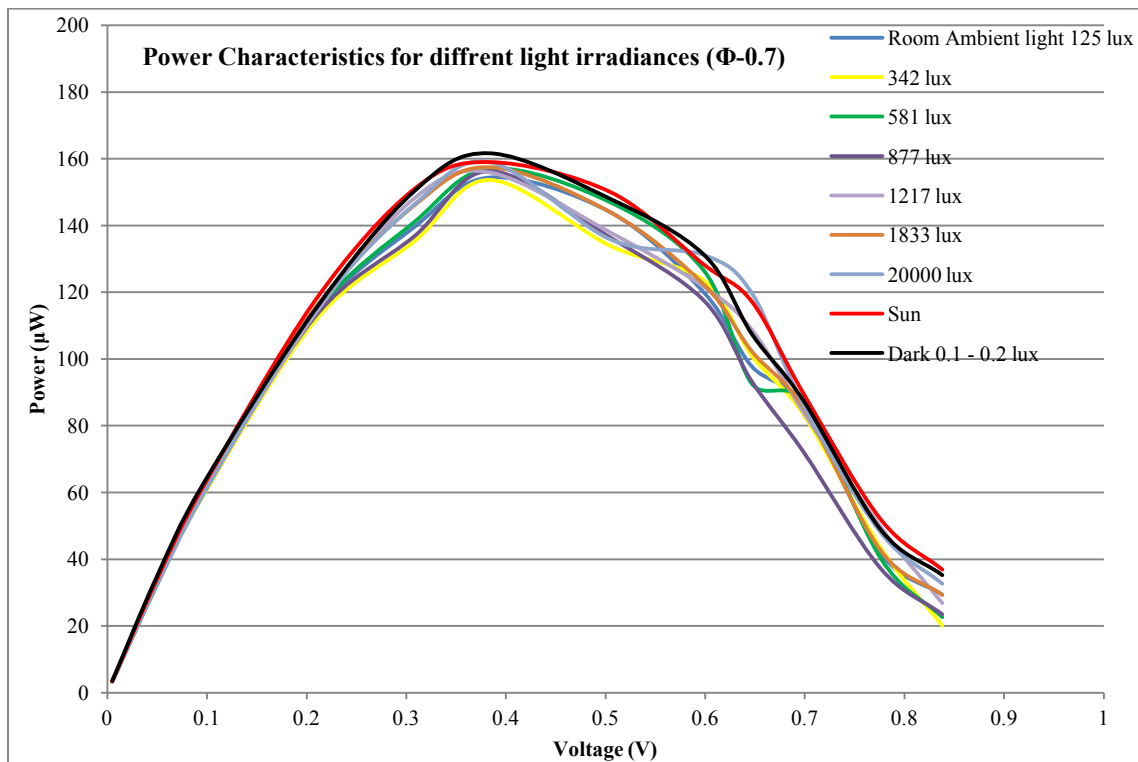
Fig. 3.11a Power characteristics for different light irradiances

54
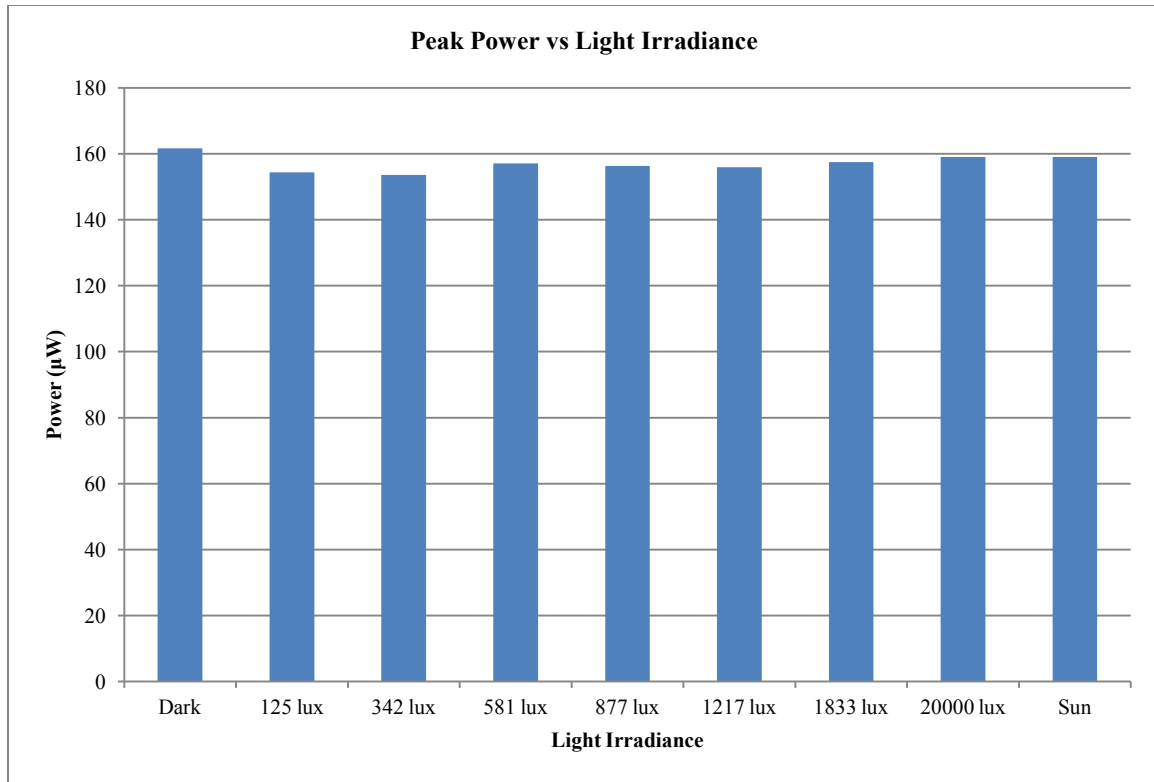
Fig. 3.11b Peak Power produced by cell at different light irradiances

3.5.3 Quantum yield

Since the goal of the device is to produce maximum power, we can assume that the best PEM will always be used and under the minimum light irradiance of 41 lux. Thus it is not necessary to model the cell based on the above two parameters. However, the tests above did not give consistent results in the beginning, even on using the same PEM, same lighting conditions, algae concentration and other physical parameters. On further investigation, the most important factor was determined which was the Quantum yield of photosystem of algae. For the tests performed initially, though the same concentration of algae samples were used, they did not have the same quantum yield and thus led to different voltages and power levels. On using the algae with same quantum yield it was observed that the test provided consistent results.

55

Quantum Yield (Φ) is defined as the number of molecules or electrons given out per photon absorbed by the system. It will be easier to understand the quantum yield Φ with an example of fluorescence, where it is the number of photons emitted to that of photons absorbed [58].

$$\Phi = \frac{number\ of\ molecules\ affected}{total\ number\ of\ photons\ absorbed} \qquad (3.2)$$

In a photo chemical process when a molecule changes state after absorbing a light quantum (photon), the quantum yield is the ratio of number of changed molecules to the number of photons absorbed. As it is not possible to absorb all the photons efficiently, quantum yield will always be less than 1. The value of Φ for a particular process can range from 0 to 1.0. Quantum yield of a process is 0 when the involved molecule or particle does not change its state of excitation, and it is 1.0 when the process is excited with the same level of energy.

Quantum yield (Φ) of the algae (chlamydomonas reinhardtii) samples of used ranged from 0.5 to 0.8. It was observed that higher the quantum yield, higher the power output of the cell. Presented in the graph below are the test results where V-I and power characteristics are observed for different quantum yield. The tests results shown in Figure 3.12 below were conducted with chlamydomonas reinhardtii with a quantum yield of $0.589 \approx 0.6$, Figure 3.13 with a quantum yield of $0.712 \approx 0.7$ and Figure 3.14 with a quantum yield of $0.796 \approx 0.8$, other parameters for the tests remained same and were performed in ambient light conditions.
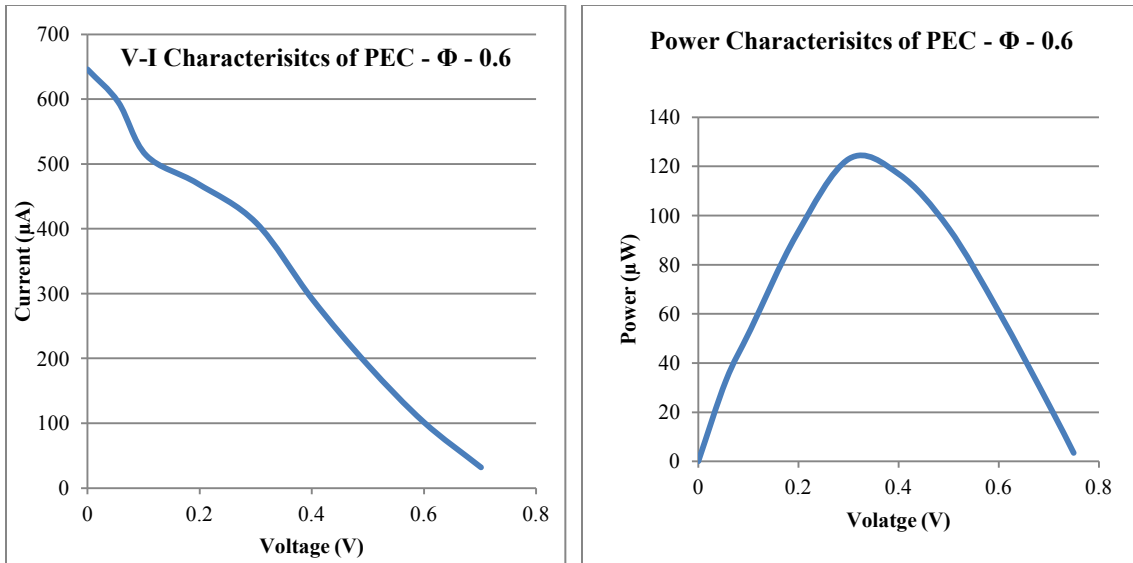
Fig. 3.12 V-I & Power characteristics of PEC with Φ = 0.6
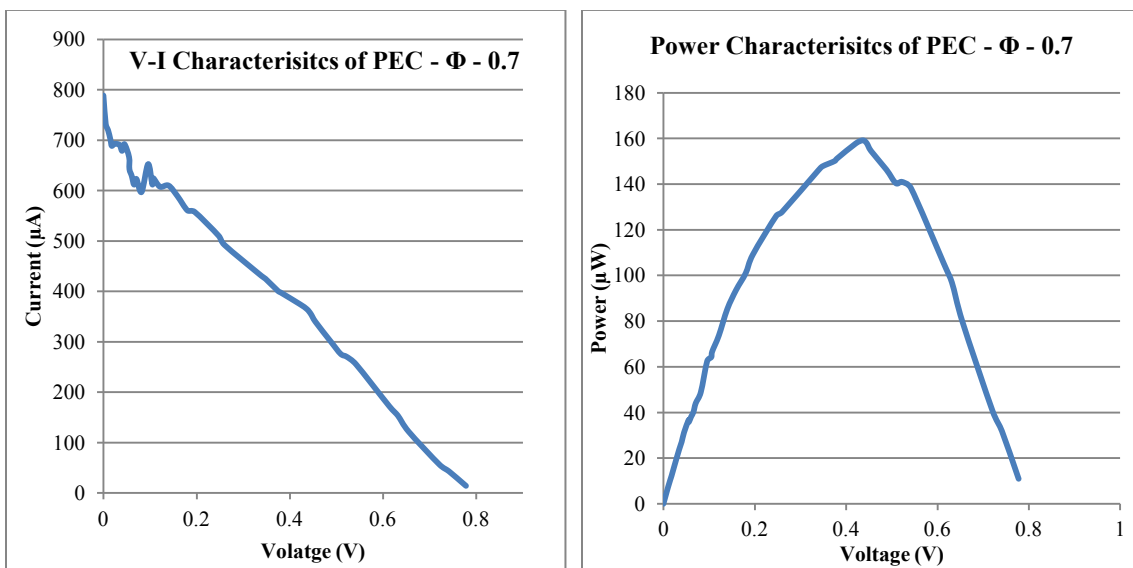
Fig. 3.13 V-I & Power characteristics of PEC with Φ = 0.7
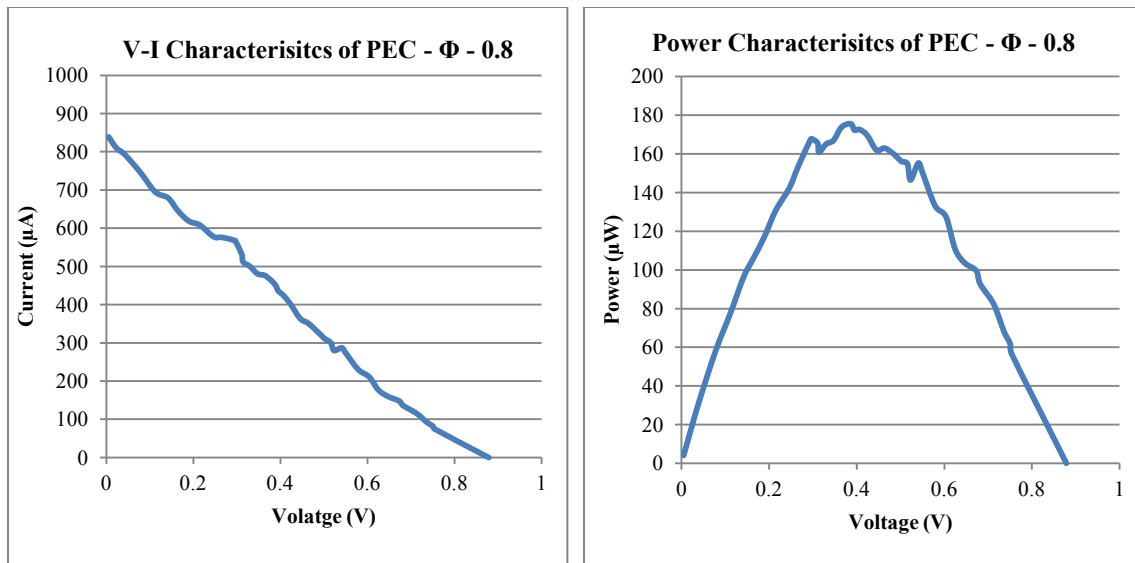
Fig. 3.14 V-I & Power characteristics of PEC with Φ = 0.8
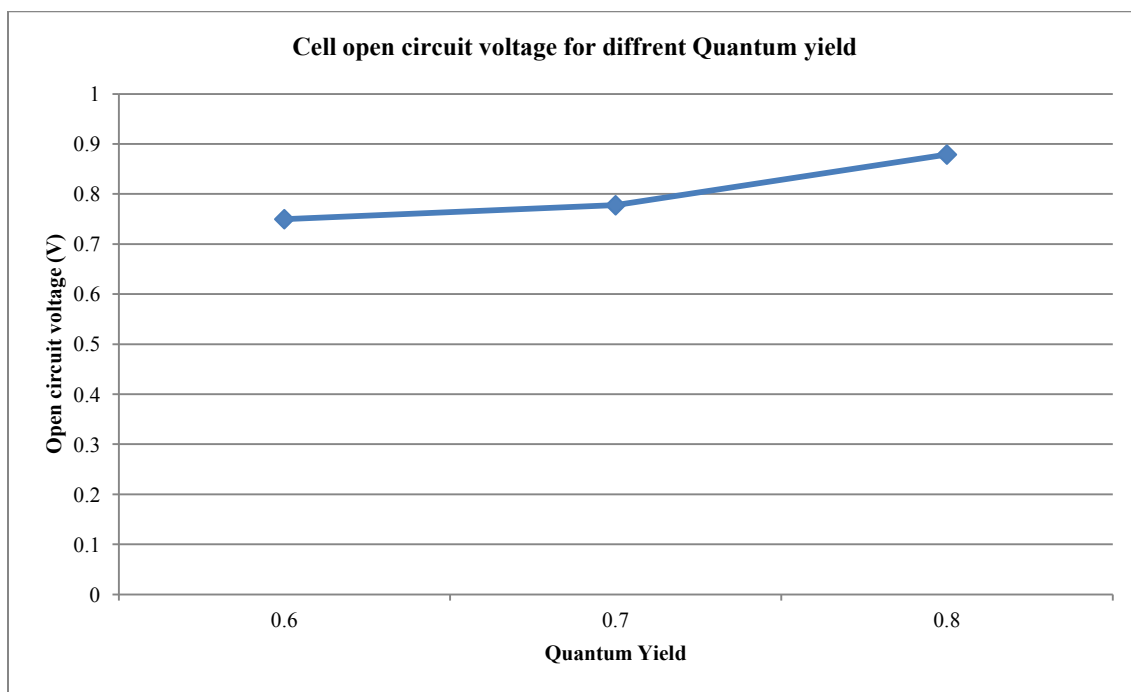
Fig. 3.15 Cell open circuit voltage for different quantum yield
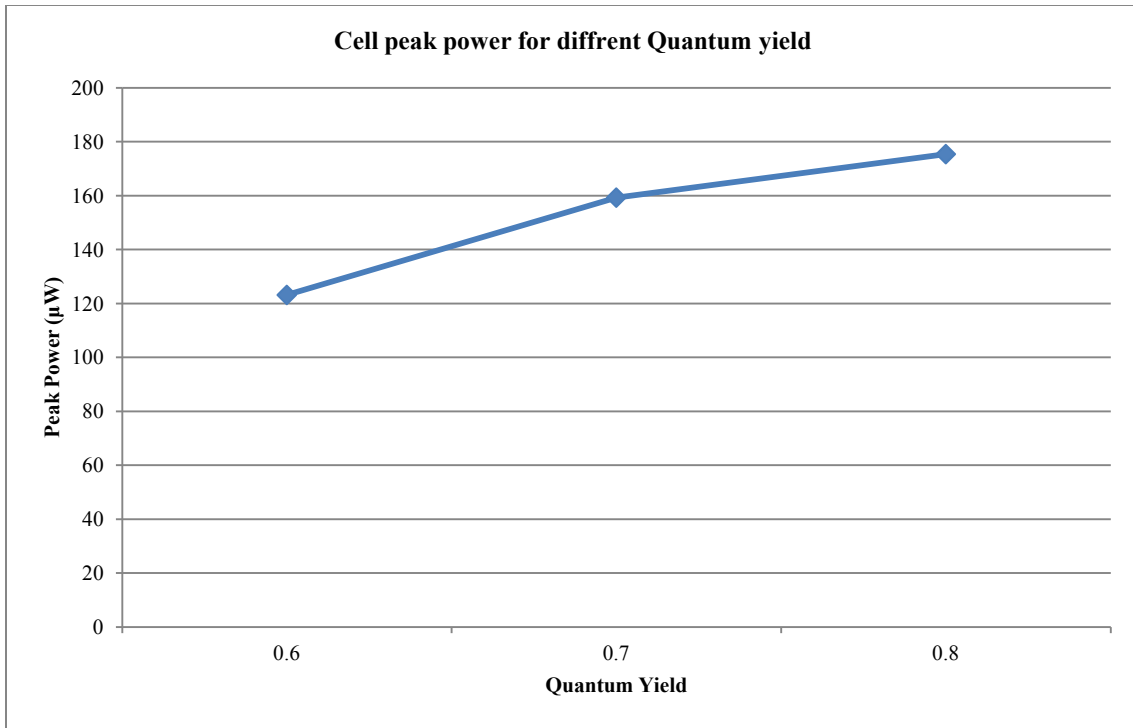
Fig. 3.16 Cell peak power produced for different quantum yield
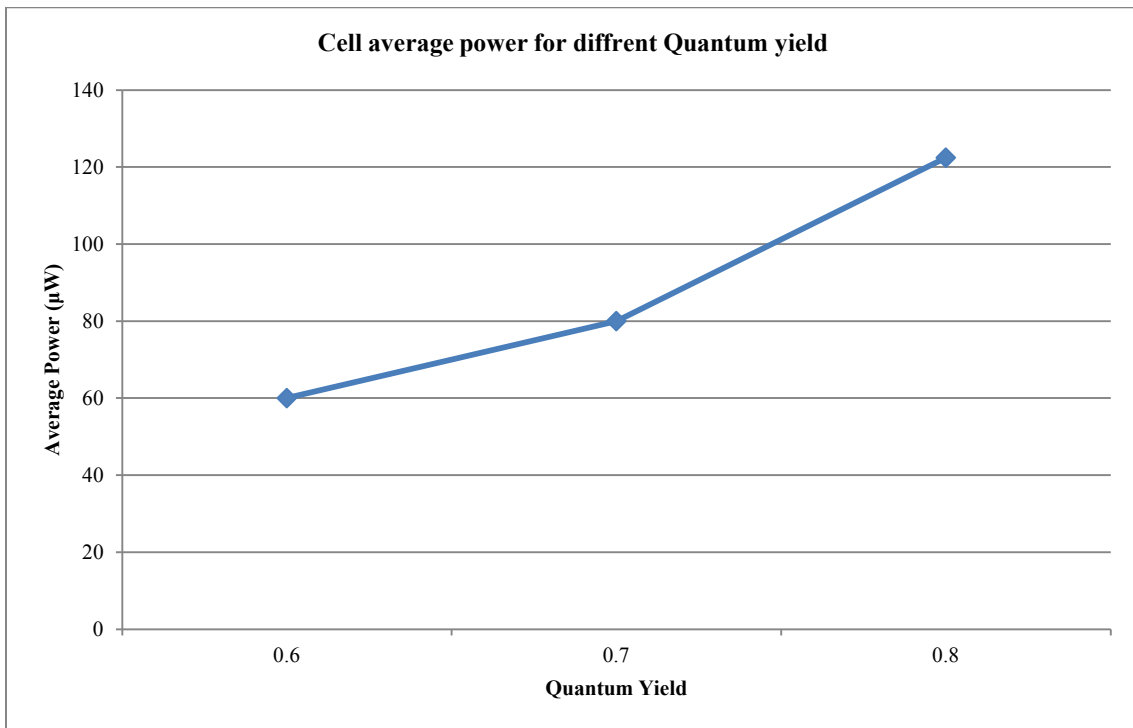
Fig. 3.17 Cell average power produced for different quantum yield

It can be clearly observed that the quantum yield of the samples significantly changes the characteristics of the cell as shown in Figures 3.12-3.17. The cell with a quantum yield of 0.6 produces approximately a peak power of 125 µW, while that with Φ=0.7 produces around 150 µW and the cell with $\Phi = 0.8$ produces around 180 µW. Also the open circuit voltage produced by the cells increases when quantum yield increases as shown in Figure 3.17.

3.5.4 Other factors

Other factors such as algae concentration in the media affect the power produced. It was observed that when the cell concentration of algae is greater than 0.7 million cells per ml, the open circuit voltage and the peak power produced saturates, and relation is not linear. Since we always need the maximum power extracted from the cell the cultures used should have a concentration of more than 0.7 million cells per ml.

Concentration of the catholyte (potassium ferricyanide) also affects the power produced by the cell. It was observed that when the cell saturates at 25% (w/w) solution [51]. Thus 25 % is always the preferred concentration, and this was used for all the experiments.

The electrode pore density study was done in the previous work [51] as mentioned before. The electrode patter was selected from the work and is explained in Section 2.4.5.

Bonding, though it is a part of the assembly, a badly bonded performs terribly. It is very important to assemble the cell and extreme care should be taken care to avoid, leaks, air bubbles, evaporation etc. Fabrication of the electrode also plays a vital role, poorly fabricated device that is not robust, does not produce good results. Material used for the electrode also plays an important role. Lesser the resistance of the metal used for the

electrode more efficient the cell is, also it should be possible to sputter the metal on to the membrane. Sputterable materials such as silver, copper and platinum react with algae and other micro-organisms and are either reduced or oxidized heavily, thus making gold the only metal that can be sputtered on to the membrane. Same can be said about attaching the external leads to the electrodes. An aluminium foil was gold plated and was attached to electrode without any bonding material, the snug fit of the cell keeps the leads in contact with the electrodes of the cell. From the above tests and results, we can draw an inference to indentify the best parameters for the cell to be modeled on.

3.6   Results and Inference of influencing parameters

It is understood the cell's performance saturates when the light irradiance is around 41 lux which is easily available, and even when light is not present the cell performs in a similar way, it should be only ensured that the organisms get both the light and dark cycles to sustain. The cells die if either period is there prolonged period.

As our goal is to produce maximum power, the membrane with maximum thickness can be used.

The cells perform relatively well under ambient temperature and carbon-dioxide concentration conditions and these parameters are uncontrollable in the real world.

Quantum yield of the cells give a very good idea about the cell's performance and thus can be used as one of the main parameters to model the cell.

Now that our parameters are identified, the various modeling techniques can be looked upon and the best suited method for the application can be used to achieve the model of the cell.

3.7 Mathematical Modeling

A mathematical model is an absolute necessity for any system to be analyzed, optimized and controlled. By analysis, one can build a descriptive/simulation model of the system any study the system to optimize it, also one can try different control techniques and approaches in simulations and find the best suited one. A mathematical model describes a system in terms of equations defining the relationship between a set of variables and would represent the properties of the system [60].

Thus a mathematical model developed for the cell, should be able to provide the output states such as cell voltage, current and power in relation to dependent parameters such as Nafion thickness, quantum yield of algae, light intensity, etc as mentioned in the sections above.

There are a few different ways by which a system can be modeled. Based on the properties of the system it has to be classified under these criterions linear or nonlinear; deterministic or probabilistic (stochastic); static or dynamic and discrete or continuous. Classifying the system makes it easier to identify the best suited mathematical modeling approach.

The cell displays linear behavior. The cell voltage is not constant and varies in a random fashion, however the variation is small and the voltage seems to hover around an average

62

value. From Figure 3.1 it can be said that the open circuit voltage once stabilizes is around 0.9 volts and varies between a range of +/- 0.05 volts. Thus it can be said the average voltage produced is deterministic and the small perturbations in the voltages are probabilistic based on the movement of the algae. The average voltage can be modeled as a deterministic component and the small perturbations can be modeled as random perturbation based on a probabilistic distribution. The system is largely steady, and there is no parameter that is varying with respect to time, if we ignore evaporation of anolyte, as evaporation of anolyte will not occur when it is circulated from a reservoir.

Since data relating all the possible parameters and the system output variables are available, mathematical modeling approaches such as statistical modeling and neural network based model need not be adopted. Even if those models were developed, they eventually have to conform or fit to empirical data. Fitting to empirical data is the most common approach to evaluate and verify the model. An accurate model will closely match to real data. Instead, developing a model using curve fitting techniques is faster, more accurate and reliable [60].

Based on the results obtained it was determined that building a model based on curve fitting was the best option.

3.7.1   Experimental based modeling of the cell / curve fitting

Experimental based modeling of the cell or curve fitting is the process of formulating a mathematical function (polynomial equation/ curve), that fits best to all the data points with the least deviation. For the interpolation to be smooth between the data points, a smooth function can be constructed for an almost exact fit to the data. Fitting the curve

outside the range of the observed data is called extrapolation and has a greater degree of uncertainty as it would use the same method to relate the available data.

To develop a model for the cell, data from different experimental results are curve fitted and the relationship between the parameters is understood. These functions for different relationships are surface fitted (when more than two parameters are curve fitted it is referred to as surface fitting) and the final inter relational function is obtained.

Using the 'Basic Fitting' tool in Matlab, data for the V-I characteristics of the cell obtained in Figure 3.6 is curve fitted and the function is derived. The fitted curve function is shown in the graph below.
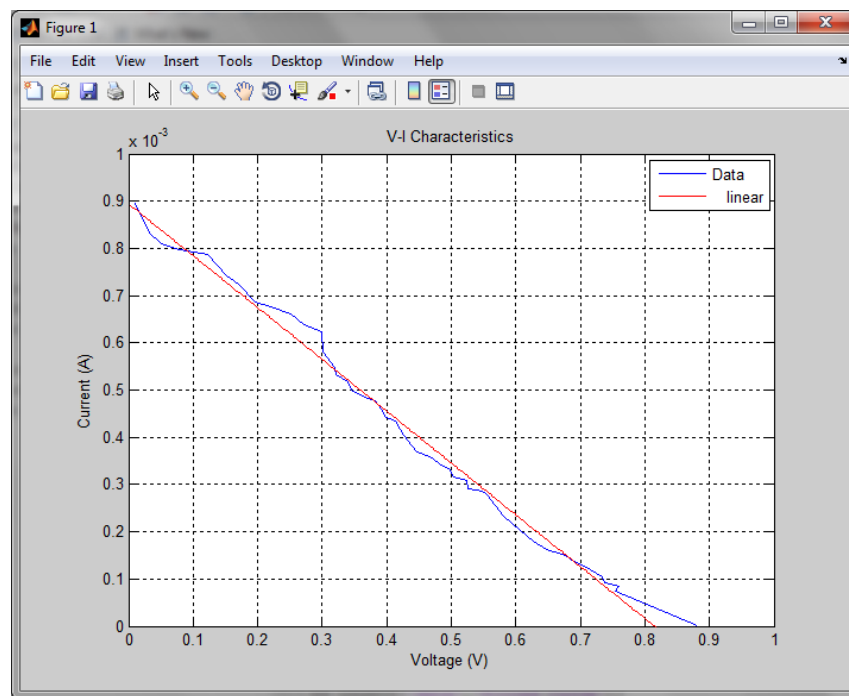
Fig. 3.18 Curve fitting of V-I Characteristics

From the fitted function, the relationship between cell voltage and current is obtained as.

$$I = -V * 10^{-3} + 0.83 * 10^{-3} \ (A) \tag{3.3}$$

This relationship in equation 3.3 holds true only for that particular operating parameters.

3.8   Summary

In this chapter, the developed cell was tested and the conclusive results proved that the cell generates electric power consistently. Once the cell was tested successfully, various parameters influencing the cell's performance were studied and the experimental results were presented in Sections 3.5.1, 3.5.2, 3.5.3 and based on the experimental data obtained it was best determined that experimental data based modeling (data fitting/curve fitting) technique would suit best to develop the mathematical model.

In the following chapter, curve fitting of the experimental data for the different parameters are done and the relationships are established. The different parameters are then interrelated using surface fitting and their relationship is obtained. Once the math model is established, electrical equivalent circuit model is developed. Simulation results of the developed electrical equivalent model are shown and are compared with real data. Apart from the efforts to model the cell, a suitable power electronic converter is chosen to harvest the energy produced by the cell.

CHAPTER 4

4 MODELING, ANALYSIS AND SIMULATION OF CELL

4.1 Experimental based modeling of the cell

Curve fitting is one of the most widely used approach for experimental data based modeling. Curve fitting functions are represented by polynomial equations. A simple first degree polynomial equation is of the form: $y = ax + b$ (4.1). First degree polynomial function is a simple line joining two points at a slope. When numerous data points are involved, a higher degree polynomial function such as second degree equation $y = ax^2 + bx + c$ (4.2) or a third degree equation $y = ax^3 + bx^2 + cx + d$ (4.3) is used to reduce errors.

There are many error functions defined for a polynomial, but the most commonly used error function for a polynomial curve fit is the sum of squares of the residuals. It is done by summing the distance to the fit curve of each data point and squared. For a simple function as shown in equation 4.1, the error function can be expressed as:

$$E\ (x; a, b) = \sum_{i=1}^{P}(y_i - ax_i - b\ )^2 \qquad\qquad (4.4)$$

From, differentiating the above equation the maximum and the minimum error conditions can be found.

However after curve fitting the experimental data, it can be said that the difference in the errors generated between a first, second and third degree polynomial function was not

substantial. The first degree (linear) polynomial results were satisfactory. Thus a simple first degree polynomial (linear) fit was used for modeling.

4.1.1   Curve fitting for experiments based on Nafion thickness

The experimental results for V-I and power characterises for the cell based on Nafion were shown in Figure 3.8 & 3.9. The experiment was conducted with two different membranes with different thickness and all the other parameters remained the same. The experimental data is curve fitted and the results are shown below.

Fig. 4.1 Curve fitting for experiments based on Nafion thickness

The curve fit equations for the curves are

$$I = -V * 0.842 * 10^{-3} + 0.686 * 10^{-3} \; (A) \qquad \text{for Nafion 115} \qquad (4.5)$$
$$I = -V * 10^{-3} + 0.83 * 10^{-3} \; (A) \qquad \text{for Nafion 117} \qquad (4.6)$$

Thicker the Nafion membrane used more is the power (voltage and current) generated by the cell. Nafion membrane 117 has a thickness 183 microns of and Nafion membrane 115 has a thickness of 127 microns.

4.1.2 Curve fitting for experiments based on Light Intensity

The experimental results for V-I and power characterises for the cell for different light intensities were discussed in Section 3.5.2. The experiment was conducted with a single cell, two different membranes with different thickness and all the other parameters remained the same. The experimental data is curve fitted and the results are shown below.
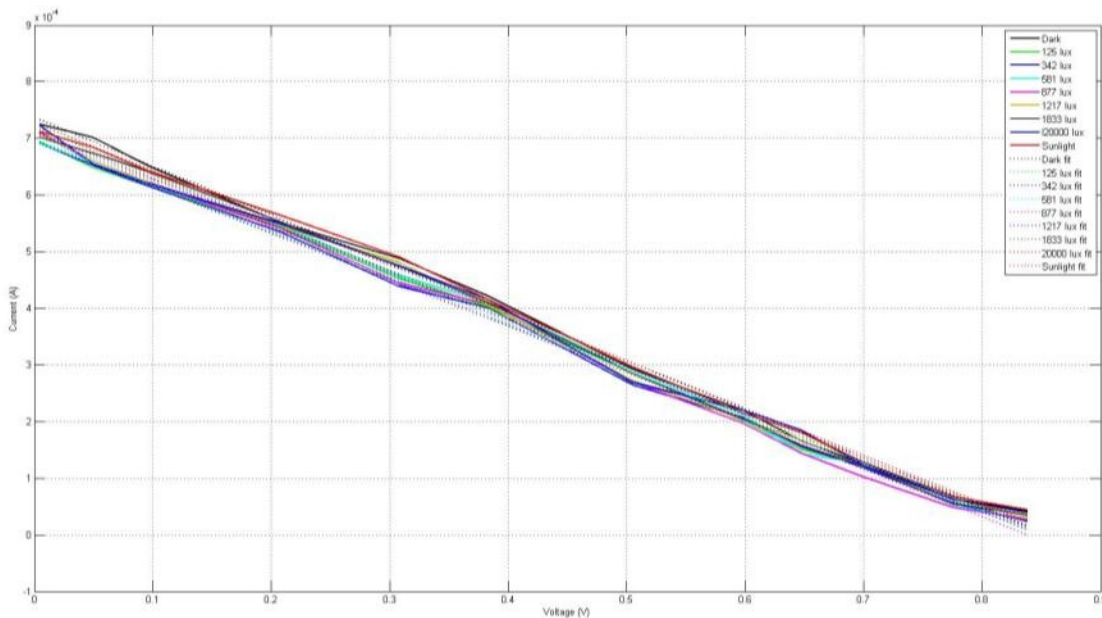
Fig. 4.2 Curve fitting for experiments based on light intensity

The curve fit equations for the curves are

$$I = -V * 0.858 * 10^{-3} + 0.736 * 10^{-3} \ (A) \qquad \text{for Dark} \qquad (4.7)$$
$$I = -V * 0.818 * 10^{-3} + 0.698 * 10^{-3} \ (A) \qquad \text{for 125 lux} \qquad (4.8)$$
$$I = -V * 0.819 * 10^{-3} + 0.695 * 10^{-3} \ (A) \qquad \text{for 342 lux} \qquad (4.9)$$
$$I = -V * 0.825 * 10^{-3} + 0.704 * 10^{-3} \ (A) \qquad \text{for 581 lux} \qquad (4.10)$$
$$I = -V * 0.843 * 10^{-3} + 0.707 * 10^{-3} \ (A) \qquad \text{for 877 lux} \qquad (4.11)$$
$$I = -V * 0.830 * 10^{-3} + 0.710 * 10^{-3} \ (A) \qquad \text{for 1217 lux} \qquad (4.12)$$

$$I = -V * 0.844 * 10^{-3} + 0.719 * 10^{-3} \ (A) \qquad \text{for 1833 lux} \qquad (4.13)$$
$$I = -V * 0.824 * 10^{-3} + 0.712 * 10^{-3} \ (A) \qquad \text{for 20000 lux} \qquad (4.14)$$
$$I = -V * 0.839 * 10^{-3} + 0.727 * 10^{-3} \ (A) \qquad \text{for Sunlight} \qquad (4.15)$$

It can be clearly observed that the cell produces maximum power during the dark period and slightly less during sunlight. Also, the difference in the power produced is not big during other light irradiances compared to that of the dark or sunlight i.e., the difference between the equations 4.7 to 4.15 is not great and they all can be approximated to a single fit.

4.1.3 Curve fitting for experiments based on Quantum yield

The effect of Quantum yield on V-I and power characterises for the cell was discussed in Section 3.5.3. All the parameters were the same for the cell except for the algae culture, whose quantum yield was different. The curve fitting of the results are shown below.
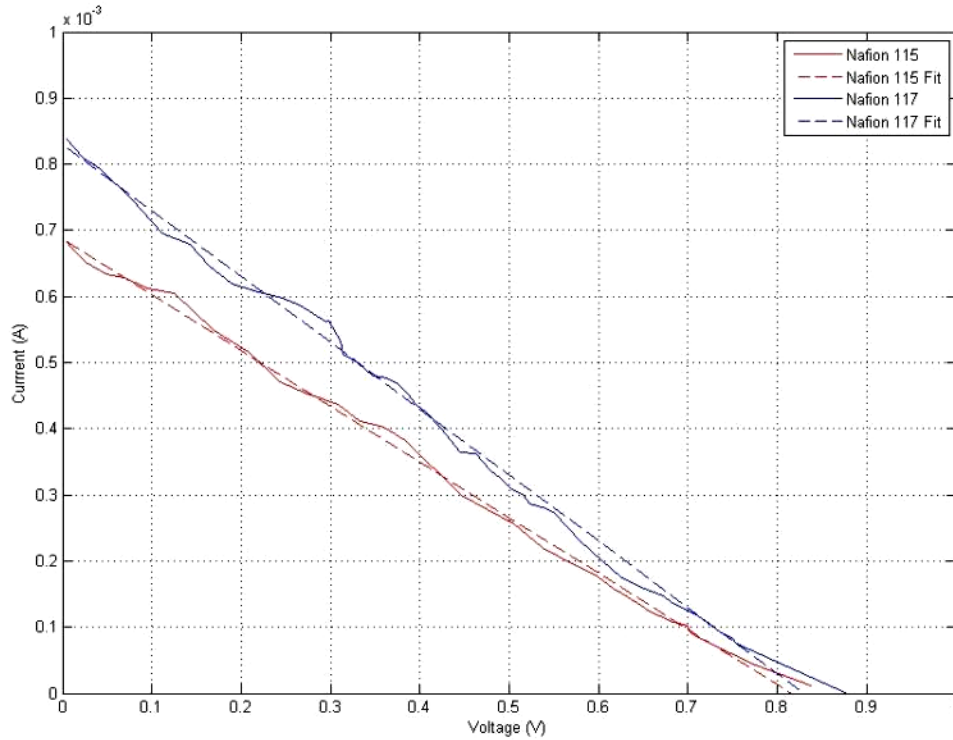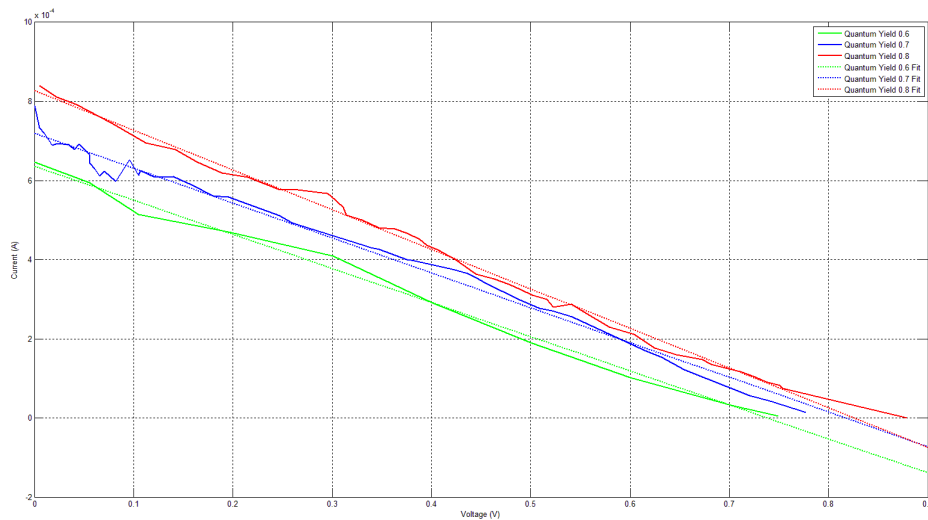

Fig. 4.3 Curve fitting for experiments based on Quantum Yield

The curve fit equations for the curves are

$$I = -V * 0.861 * 10^{-3} + 0.636 * 10^{-3} \ (A) \qquad \text{for } \Phi = 0.6 \qquad (4.16)$$
$$I = -V * 0.881 * 10^{-3} + 0.719 * 10^{-3} \ (A) \qquad \text{for } \Phi = 0.7 \qquad (4.17)$$

$$I = -V * 1.003 * 10^{-3} + 0.827 * 10^{-3} \ (A) \qquad \text{for } \Phi = 0.8 \qquad\qquad (4.18)$$

It can be seen that the constant term in equations 4.16, 4.17, 4.18 is approximately equal to the quantum yield multiplied with a factor of 10^{-3}. Also the change in the short circuit current and open circuit voltage is substantial with the quantum yield of the cell changing.

4.2   Mathematical model of cell

There are a few mathematical models that have been proposed for MFCs [61-64], they emphasize on models based on electrochemical model, biochemical model, biofilm model, bulk liquid model, etc. Most of these models are based on Nernst equations. The structure and parameters of the models are complicated, also the process of modeling is complex. A basic simple model, which can provide important and accurate predictions of the cell operating conditions so that the model can be used in simulations and be used for optimization of the performance of MFC, is more applicable. Therefore, establishing a simple model for the μPSC was given all the attention.

Since the main focus is to use the model in simulations, the mathematical model of the cell can be represented as a surface function based on the experimental data. The surface function is generated by interpolation of the curve fit functions for a particular parameter, thus giving rise to a 3D surface. From the derived 3D surface, any operating point for the cell can be obtained. For example, given a random quantum yield and a random operating cell voltage the cell's current can be obtained. This model can be used in simulations to study the behavior of the cell when connected with different loads.

4.2.1 Surface fitting

In order to obtain the operating point precisely based on the factor, it is necessary to have a surface fit from the fitted curves. The surface fit function represents a three dimensional surface, which corresponds to an operating point based on three different parameters. Surface fitting of equations based on Nafion thickness (4.5 & 4.6) are not necessary because the best thickness can be chosen when fabricating the device and will remain constant. Also surface fitting of equations based on light irradiance does not seem necessary as all the equations (4.7 to 4.15) can be approximated to single equation with the error between the functions being negligible. The curve fitting equations obtained for experiments based on quantum yield of the cell (4.16 to 4.18) were used for developing the surface fitting function.

The fitted curve equations are taken and are surface fitted to get a 3D surface. From the 3D surface any operating point based on the influencing parameter can be obtained, in our case it would be the quantum yield of the cell. The surface fit function for quantum yield is shown in Figure 4.4 & 4.5.
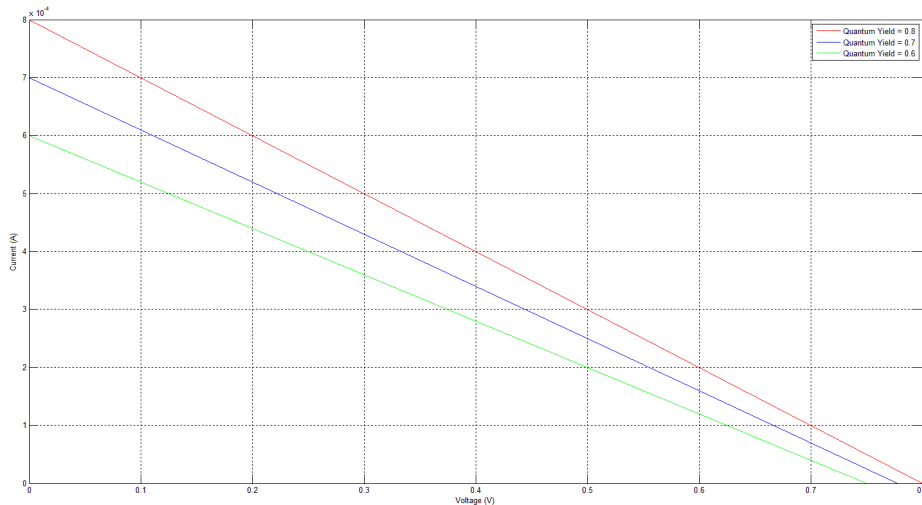
Fig. 4.4 Curve fitting curves based on Quantum Yield

71
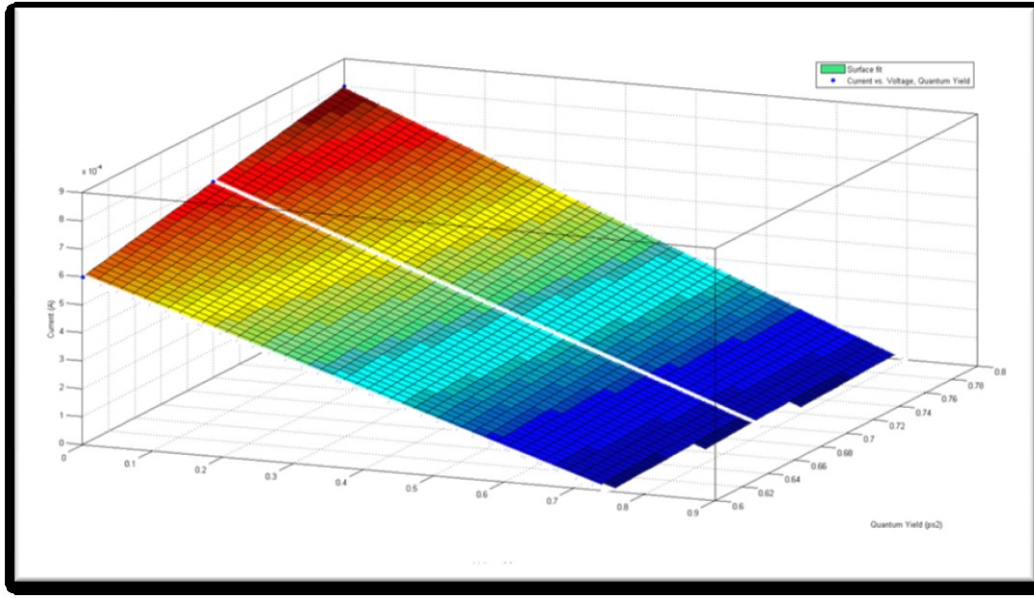
Fig. 4.5 Surface fitting based on Quantum Yield

The surface fit function is of the form z(x,y). The cell current is represented by the z axis, the cell voltage as x axis and quantum yield as y axis, i.e. the cell current is represented by the cell voltage and quantum yield of the cell.

4.3   Development of electrical equivalent model of the cell

The published work of Markvart et al., 2002, shows that that the primary photosynthetic reaction closely resembles the operation of the solar cell. The photosynthetic reaction rate and process can be represented in a form similar to the Shockley solar cell equation. The photosynthetic reaction produces both chemical and electrical energy (from the electron transfer chain). Energy divided into these two components are predictable and hence it is possible to optimize the amount of power produced, i.e., the maximum power point of the photosynthetic organism can be tracked. This can used to estimate the maximum energy that can be produced, and of the different losses that limit this amount [65]. Before that a simple understanding of the solar cell model is established in sections below.

72

4.3.1 Theory and equivalent circuit of solar cell

The solar cell converts light energy to electrical energy. When photons hit the solar cell they are absorbed by the cell which is a semiconducting device (silicon). The photon's energy is donated to an electron in the valence bond. The electrons in the valence band, are bound by covalent bonds between neighboring atoms, and this energy excites the electron into the conduction band. Once in conduction band the electron faces far less resistance and is free to move. Also, the loss of an electron from the covalent bond gives raise to a hole. Bonded electrons of neighboring atoms shift into the "hole", creating a hole with that ion, and in this way the hole moves through the semiconductor. Thus, the photons absorbed by the semiconductor solar cell give raise to mobile electron-hole pairs. The free electrons that flow through the semiconductor give raise to electric current. The band gap of the cell and excitation process is shown in Figure 4.6 [66].
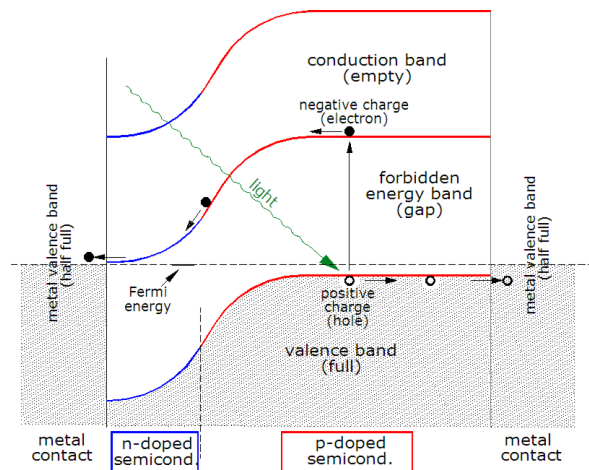
Fig. 4.6 Solar cell band Gap and excitation process [66]

This is similar to photon absorption by the photosynthetic subsystem of the plant and the subsequent electron transfer chain as explained in Section 2.1 and its subsections. The equivalent circuit model of the solar cell is show in Figure 4.7.
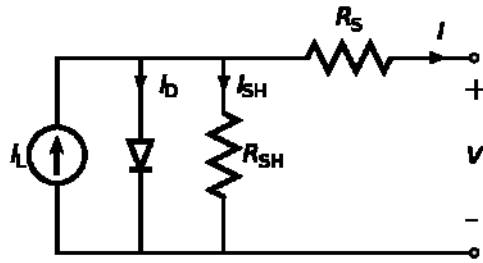
Fig. 4.7 Equivalent circuit of solar cell [66]

4.3.2 Solar cell model for electron transport in photosynthesis

A simplified photosynthetic electron transport chain is show in Figure 4.8 below [50]. The process is similar to the electron excitations in a solar cell.
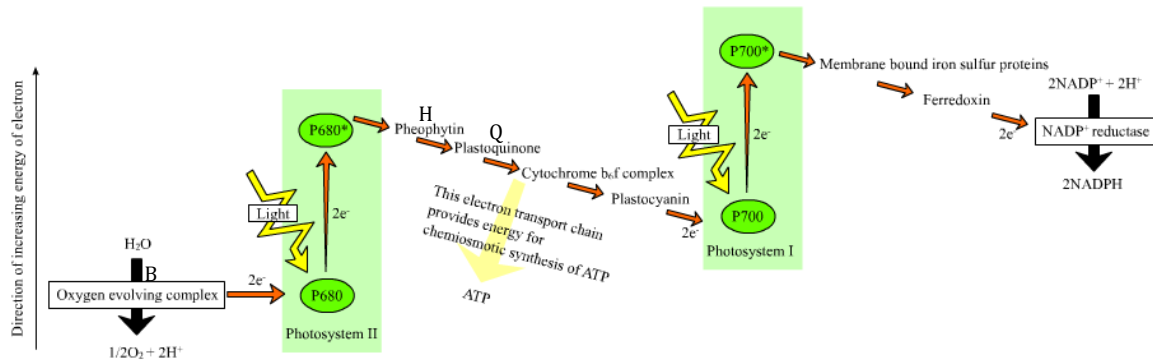
Fig. 4.8 Photosynthesis Z-scheme electron transport chain [50]

The electron transport chain occurs in the photosynthetic reaction centre, which is a protein complex binding component of the electron transport chain. The primary electron donor is a chlorophyll molecule (B), pheophytin (H) and a quinone (Q). Electron is excited by light from the ground state of P to an excited slate P* (transferred successively from B, H and finally Q). The ground state of the primary donor is replenished by an electron and the electron transfer cycle starts again [65].

A simplified schematic diagram for the model with the notations is shown in Figure 4.9.
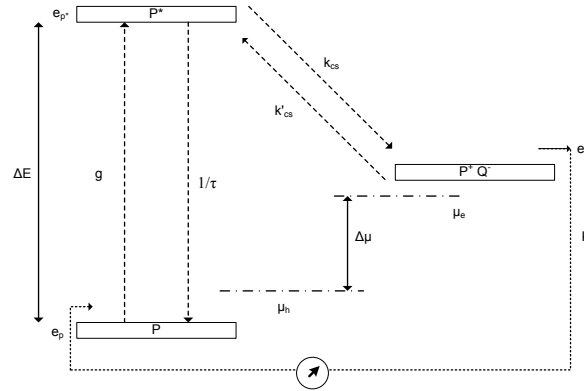
Fig. 4.9 Schematic model of electron transport in photosynthesis (based on [65])

Here,

$1/\tau$ is the lifetime of the electron in the excited state P*

g is the photoexcitation rate of P

K is the rate of electron removal from the photosynthetic reaction centre at Q (it's the actual rate of the photosynthetic energy conversion).

$\Delta\mu$ is the maximum energy generated per electron

k_{cs}, is the rate constant for charge separation from P* → Q, and

k_{cs}' is the rate constant for the reverse process.

The rate constants k_{cs} and k_{cs}' satisfy the detailed balance criteria:

$$\frac{k_{cs}'}{k_{cs}} = exp\left(\frac{e_q - e_{p*}}{k_b\,T}\right) \tag{4.19}$$

Where k_B is the Boltzmann's constant, T is the ambient temperature, and e_q and e_{p*} are the energies of the electron at Q⁻(state P⁺Q⁻) and in the excited state P*. The difference of these energies depends on the electric field when this exists.

The probability that an electron resides either in the excited state P*, Q⁻ or in the ground state of P (denoted respectively by p(P*), p(P⁺Q⁻) and p(P)), from Figure 4.9 are represented by,

$$p(P^+Q^-) = exp\left(\frac{\Delta\mu-\Delta E}{k_b\,T}\right) \tag{4.20}$$

$$p(P^*) = \frac{K}{k_{cs}} + exp\left(\frac{\Delta\mu-\Delta E}{k_b\,T}\right) \tag{4.21}$$

The rate of change of the electron between the states based on the probability of the electron states is represented by

$$\frac{1}{\tau}p(P^*) = g + \frac{1}{\tau}exp\left(\frac{-\Delta E}{k_b\,T}\right) - K \tag{4.22}$$

Substituting equations 4.20 and 4.21 in 4.22 gives

$$K = K_L - K_O\left(e^{\frac{\Delta\mu}{k_b\,T}} - 1\right) \tag{4.23}$$

Equation 4.23 is analogous to the Shockley solar cell equation. The reaction rates K_L and K_O which corresponds to the light and dark reactions respectively are given by:

$$K_L = \frac{\tau k_{cs}}{1+\tau k_{cs}}g \qquad\qquad K_o = \frac{\tau k_{cs}}{1+\tau k_{cs}}\,e^{\frac{-\Delta E}{k_b\,T}} \tag{4.24}$$

4.3.3   Electrical equivalent model of µPSC based on solar cell

Now that it is established that photosynthetic reaction models are similar to that of a solar cell. The electrical equivalent circuit of the cell can be developed based on the solar cell. Since the voltage current relationship is linear in the case of µPSC and also the fact that there is no diode like behavior, absence of diode voltage and diode current, the diode from the electrical equivalent circuit model of the solar cell should be omitted. Thus the circuit would be as represented in Figure 4.10 below.
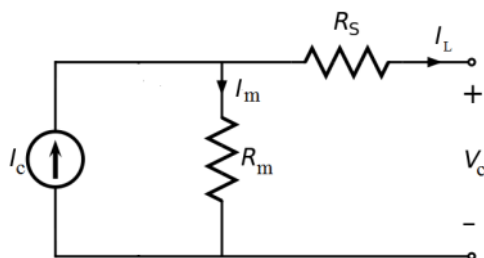
Fig. 4.10 Simple equivalent circuit representation of µPSC

The cell is represented using a current source (I_c – cell current), in parallel with a resistance R_m which is the resistance of the proton exchange membrane and is typically very high. Ideally R_m should be infinity. However that is not the case in the real world. Proton exchange membranes do leak some electrons through it, also they allow positive ions to the other side. This creates a potential difference across the membrane. The cell current I_c showing in the equivalent circuit model flowing through the R_m represents the voltage potential developed across the membrane. The series resistance R_s represents the total series resistance experienced by the load current. The series resistance R_s is made of resistance of the anode, resistance of the cathode, resistance of the solution (the electron has to move via the solution from the cell to the electrode and vice versa) and the resistance of the leads attached to the electrodes. Apart from the resistances, the cell also exhibits capacitive behavior. Since the proton exchange membrane is a dielectric by nature and that it is sandwiched between two electrodes it exhibits capacitance [67]. This capacitance is predictable and dependent on the dielectric constant of the proton exchange membrane and the area of the gold electrode (C_m as shown in Fig 4.11) [67]. This value typically ranges between 1µF to 10µF. Apart from the capacitance in the proton exchange membrane, the cell should theoretically have a large capacitance value in order to represent high time constant of the system (C_c as shown in Fig 4.11). However

77

calculating this time constant and its respective capacitance value for the electrical equivalent circuit is very complex, and has been ignored or kept very low for simplicity and this does not affect the voltage and cell current produced excet the way the cell reacts to changes in load and switching. The actual electrical equivalent circuit model used for simulation is shown in Figure 4.11.
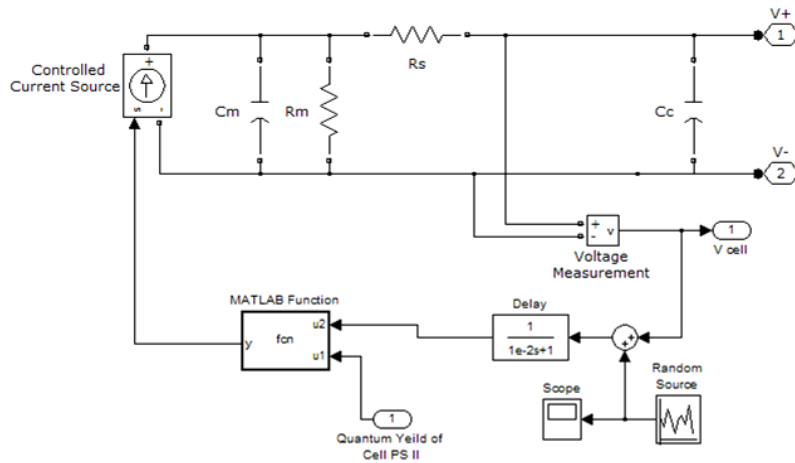
Fig. 4.11 Electrical equivalent circuit representation of µPSC

As briefed earlier the source is represented using a current source, in parallel with the resistance of the proton exchange membrane R_m. The membrane's capacitive behavior is represented by C_m and it is connected to the series resistance R_s. When the cell is under open circuit there is no load current and the current flows only through R_m producing the open circuit voltage. The MATLAB function block is used to relate the Quantum yield and the voltage produced to estimate the cell current. There is a small delay included for avoiding the algebraic loop error while simulating. The random source represents the minor perturbations that the cell continually produces around an average value (see experimental results from Section 3). Using this developed electrical model, the cell's

78

behavior for various loads are successfully simulated. The simulation results are presented in the following section

4.4 Simulation and results of developed electrical model of the cell

The developed electrical equivalent circuit model is connected to different resistive loads and is simulated. The simulation results are then compared with the practical results and presented.
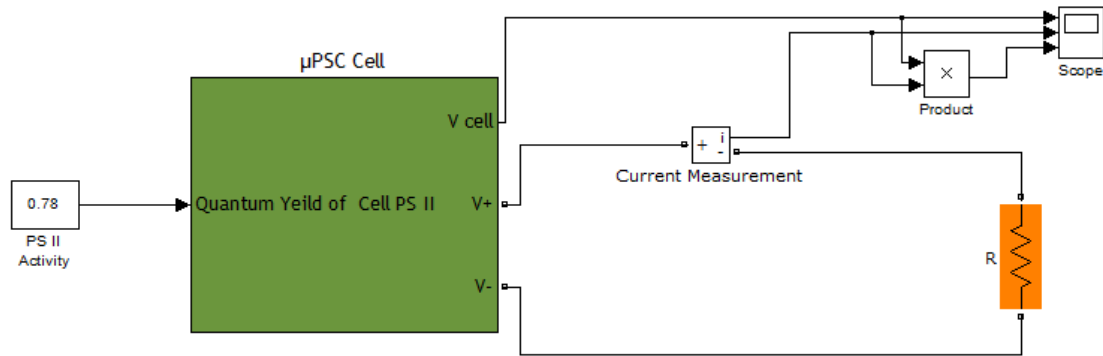
Fig. 4.12 Simulation of electrical equivalent circuit model of µPSC

The equivalent electrical circuit model shown in Figure 4.11 is masked under the green square box highlighting the µPSC and is connected to various resistive loads. First the equivalent circuit is simulated under open circuit condition and experimental results are compared followed by the loading of the cell with different resistive loads followed by short circuit condition towards the end.

4.4.1 Simulation results

The electrical equivalent model is simulated without any load. The only user entered parameter is the quantum yield of the cell.

The simulation was executed with a quantum yield of 0.78.
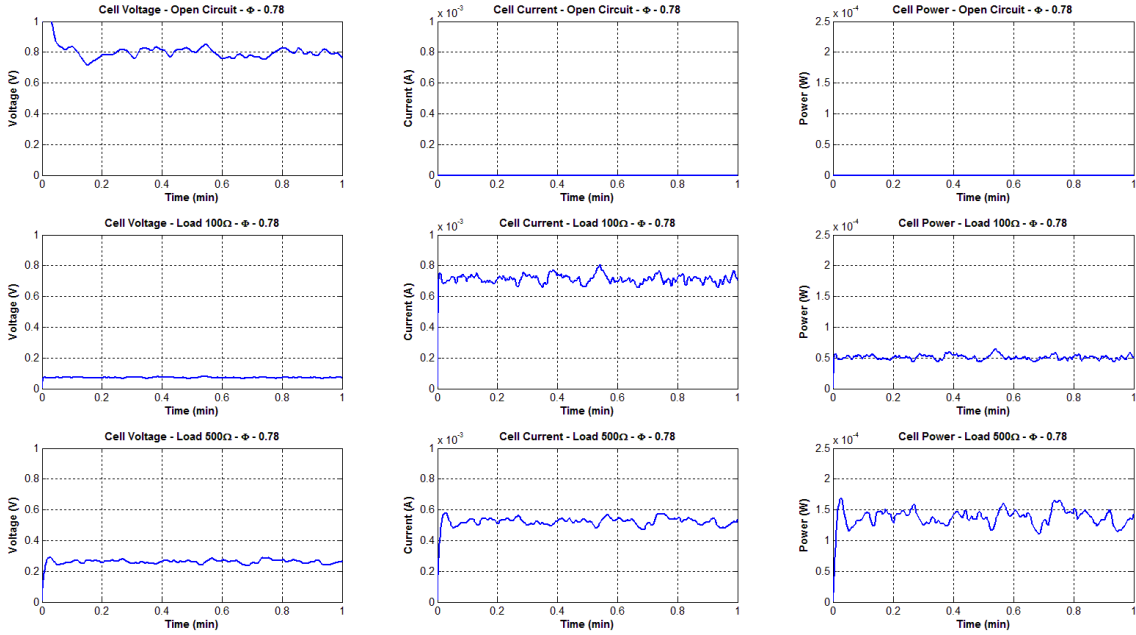
Fig. 4.13a Simulation results of μPSC electrical equivalent circuit model under different loading conditions of no load, 100 Ω and 500 Ω with quantum yield of 0.78

The simulation results are shown in Figure 4.13a. The different graphs provide the cell voltage, current and power for open circuit condition, 100Ω load and a load of 500 Ω respectively. The results make it apparent that the simulations reproduce the cell's behavior with very good accuracy. A cell with a quantum yield of 0.78 produces an average open circuit voltage of approximately 0. 8 volts with the voltage perturbing randomly around the average value and current drawn during open circuit condition is always zero. The experimental results for open circuit voltage are shown in Figure 3.1 (Section 3.1.1) and Figure 3.5 (Section 3.2). Also the values of voltage, current and power for the loads (100 Ω and 500 Ω) can be compared with the data points corresponding to that of the load with the experimental results of V-I characteristics of

the cell (Figure 3.11, 3.12, 3.13 Section 3.5.3) depending on the quantum yield of the cell. It should be noted that the simulation was executed for a total time of 1 minute.
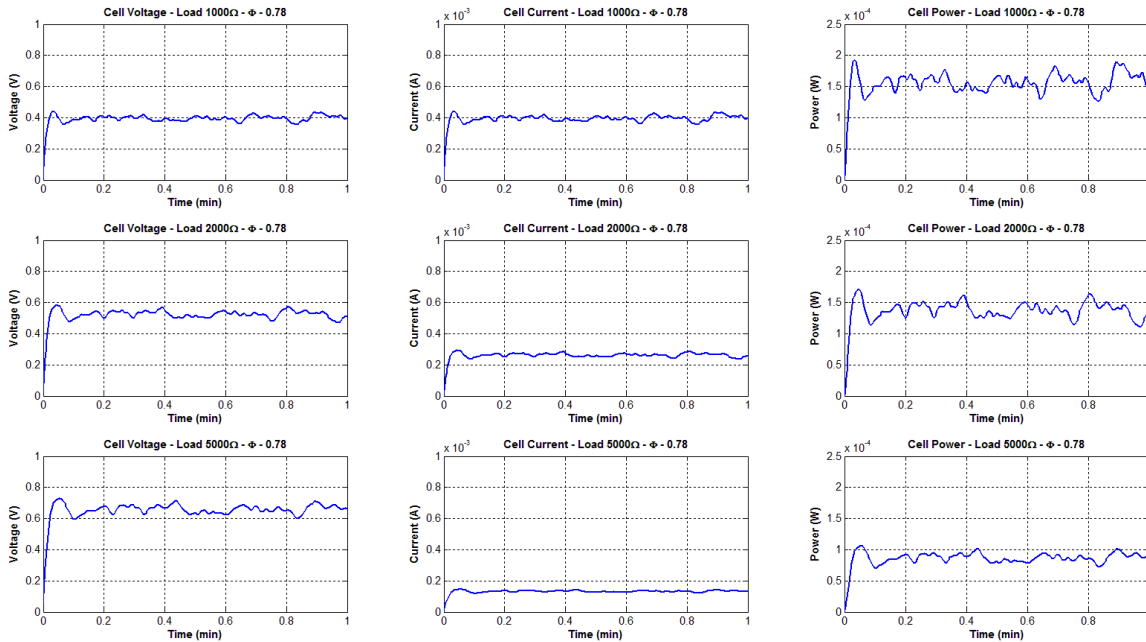
Fig. 4.13b Simulation results of electrical equivalent circuit model of µPSC model under different loading conditions of 1000 Ω, 2000 Ω and 500 Ω
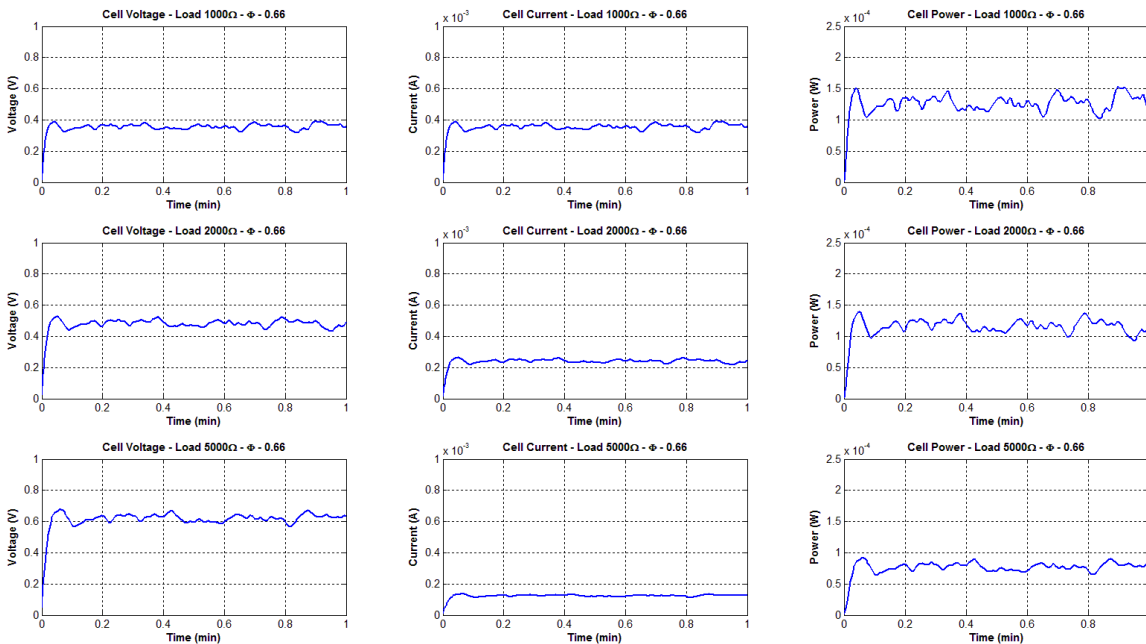
Fig. 4.13c Simulation results of electrical equivalent circuit model of µPSC under different loading conditions of 10 kΩ, 1 MΩ and short sircuit

Figures 4.13 b and c above show the simulation results for a load of 1kΩ, 2kΩ, 5kΩ, 10kΩ, 1MΩ and short circuit condition respectively.

The quantum yield of the cell is varied to 0.66 and the simulations are performed again. Only the results for a load of 1kΩ, 2kΩ, 5kΩ are presented for comparison and to show that the simulation gives appropriate results when the quantum yield is varied. The results are presented in Figure 4.13d below.
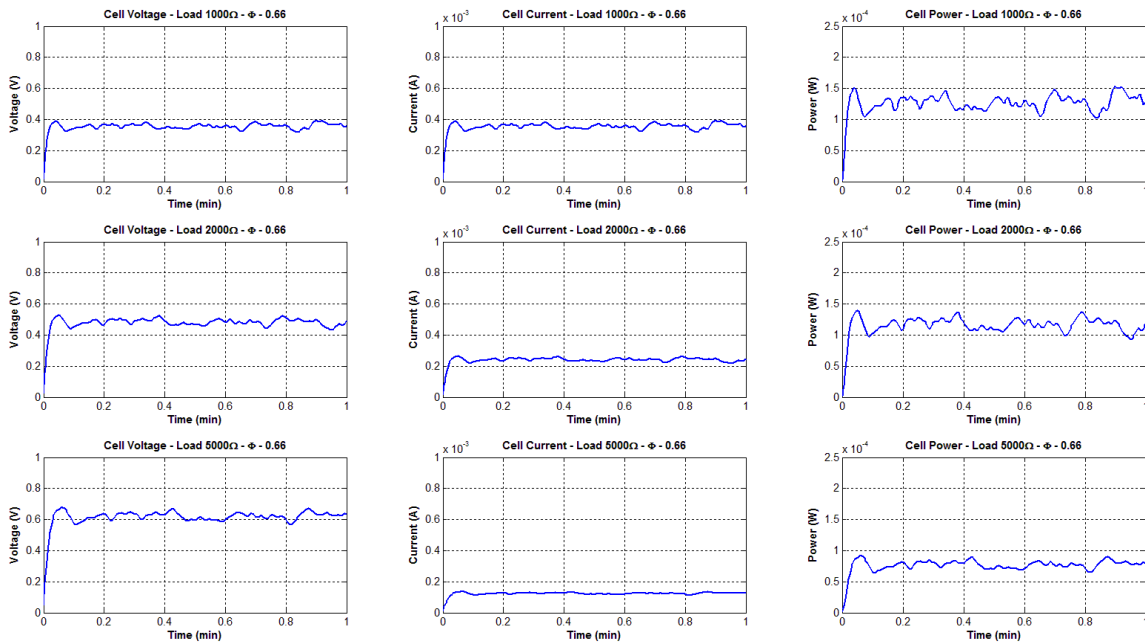
Fig. 4.13d Simulation results with a quantum yield of 0.66 and loads 1k, 2k and 5k Ω

From the results it is evident that the cell characteristics are matched by the simulations and that the simulations can be used to study the behavior of the cell on how it responds to different loads and loading conditions. This section dealt only with simulation results of a single cell μPSC, in the next section the results of cascading of the μPSC is discussed.

4.5　Stacking of µPSC

A single µPSC would not suffice to generate adequate amount of energy that can be harvested. In order to harvest significant amount of energy the cells have to be stacked by connecting them in series and parallel to increase the energy output. It was proven that stacking of MFCs and µPSCs by Aelterman et al., 2006, in their work a six cell configuration were stacked in series and parallel and it was concluded that the desired current or voltage could be obtained by combining the appropriate number of series and parallel connected cells. The cells OCV scaled by an approximate factor of 6 and short circuit current scaled approximately by a factor of 5 [68] [69]. However, electricity production in an algal / microbial process and is influenced by external conditions. Also, the external circuit could have an effect on power generation. Furthermore, different individual cell voltage can cause unwanted current flow between two cells in a stack, which will influence the overall power produced by the cells. This is analogous to the unequal cell voltages in battery pack which causes current flow between two cells and results in losses, as this current cannot be delivered to the load. This problem in batteries is solved by cell balancing circuits. Based on [68] [69], it can thus be assumed that the cells voltage and current could scale proportionally with the number of cells.

Nevertheless, two experiments were performed by stacking two cells in parallel and in series, in order to verify stacking and scalability of µPSC, and to compare with the simulation results of the stacked µPSCs. The stack schematic is show in Figure 4.14 below along with a single cell.
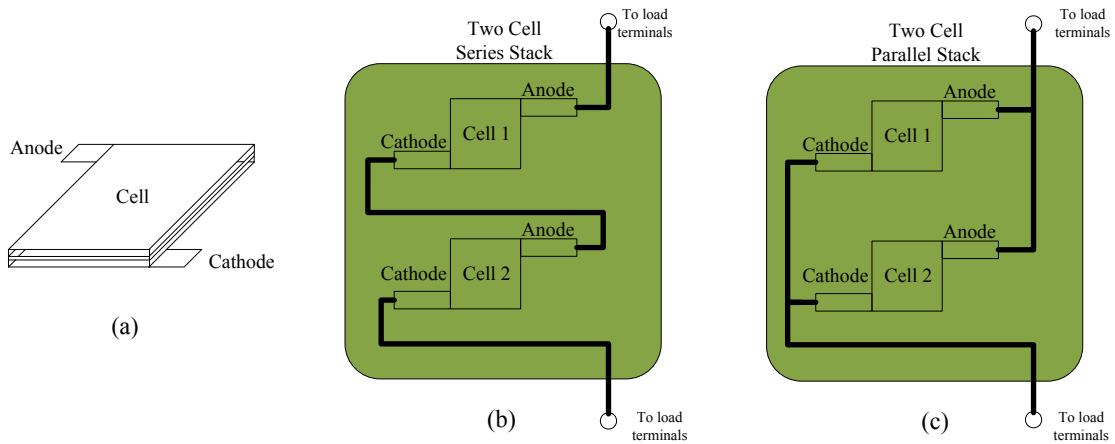
Fig. 4.14 (a) Single cell model, (b) two cell series stack, (c) two cell parallel stack

4.5.1 Experimental results of μPSC stack

Of the two experiments, the first experiment was to test the cells by connecting them in series. Two μPSC were connected in series and tested. In the second, the same two μPSC were connected in parallel and tested. Typically, when two similar sources are connected in series the total voltage will be the sum of the voltages of the individual cells and the same is true for the current when similar sources connected in parallel. The experimental results are show in Figures 4.15, 4.16, 4.17, 4.18 below.
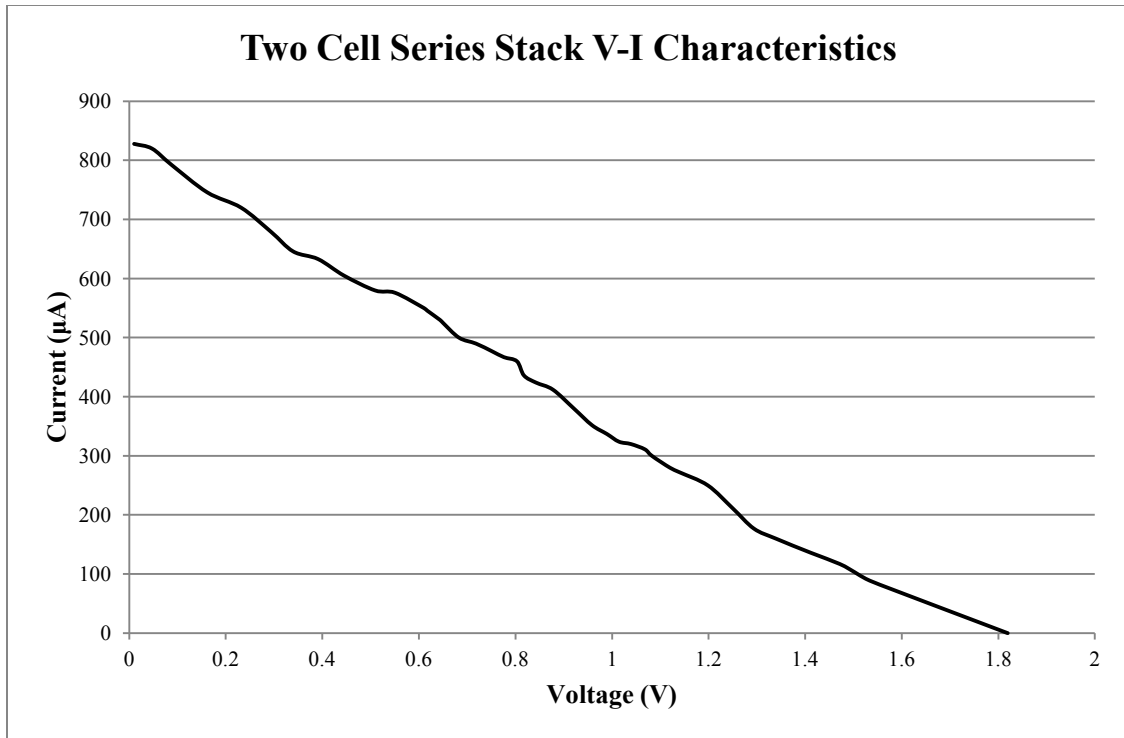
Fig. 4.15 Experimental V-I characteristics of two cell series stack
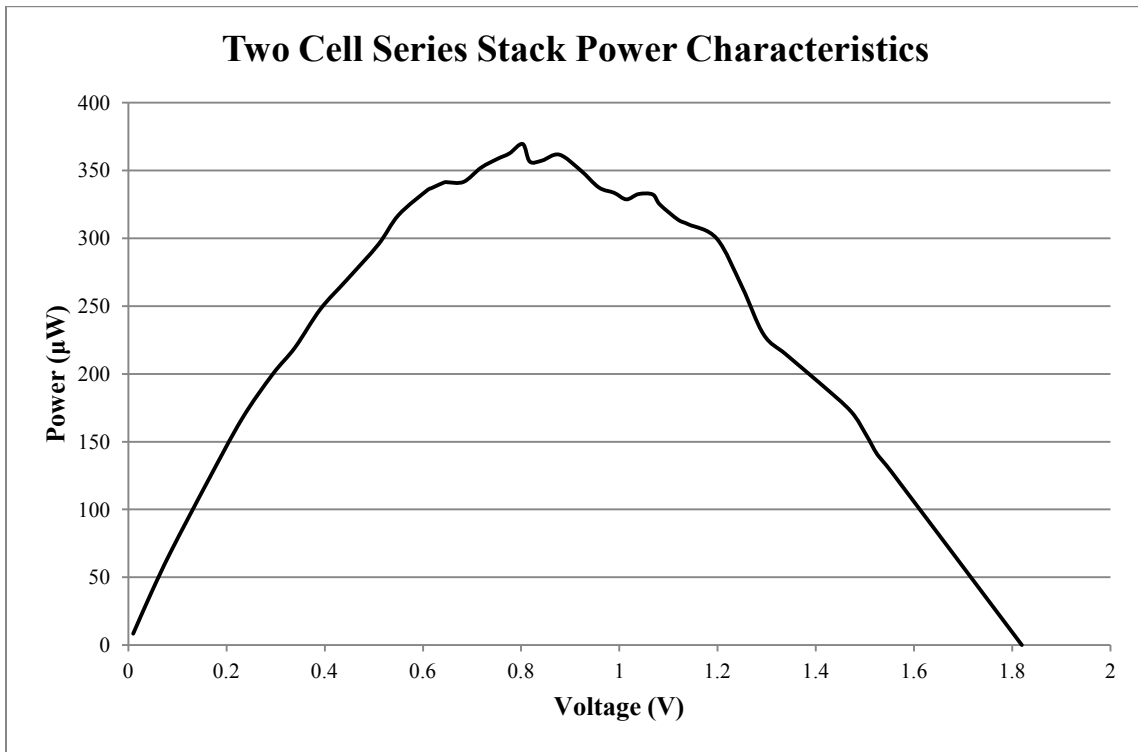
Fig. 4.16 Experimental power characteristics of two cell series stack

Two Cell Parallel Stack V-I Characteristics
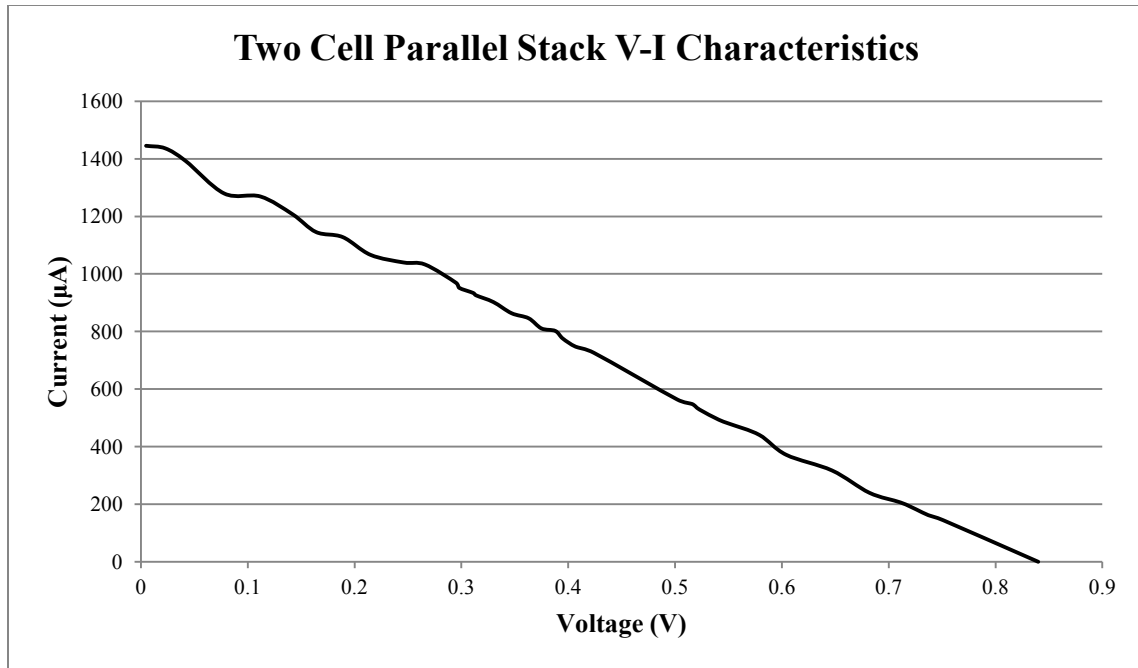
Fig. 4.17 Experimental V-I characteristics of two cell parallel stack

Two Cell Parallel Stack Power Characteristics
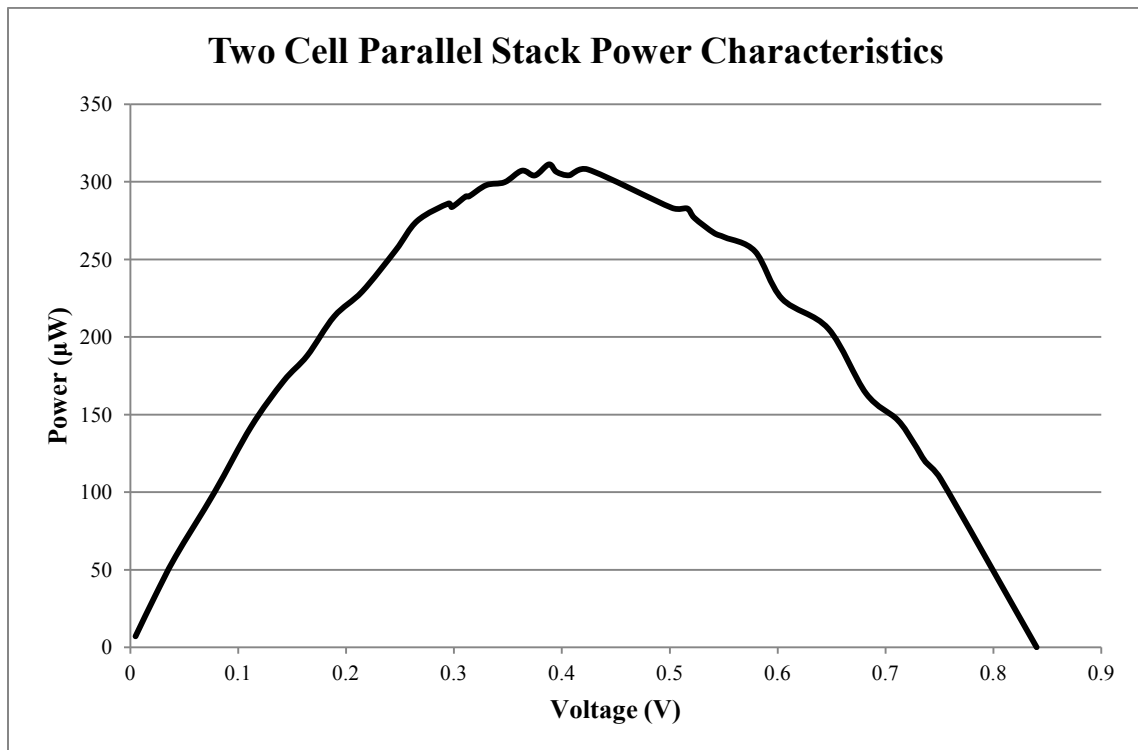
Fig. 4.18 Experimental power characteristics of two cell parallel stack

The experimental results are promising and it can be clearly said that the cells are scalable by stacking them in both series and parallel configurations.

The µPSC cells, when connected in series the voltage scaled by a factor of approximately 2.07 and when connected in parallel the cell current scaled by a factor of approximately 1.77. It should be noted that the stack has more power density when stacked in series as compared to parallel. As the cells are scalable, they can be stacked in big number, and arranged in a panel configuration to generate higher levels of power.

4.5.2   Simulation of stacked µPSC

Including accurate scaling factors in simulations is a very complex process and further investigations have to be done to understand on how the cell parameters scale. Thus, for simplicity, the cells are directly (numerically) scaled in the simulations. The simulation results are shown in Figures 4.19a, b and are compared with the experimental results.
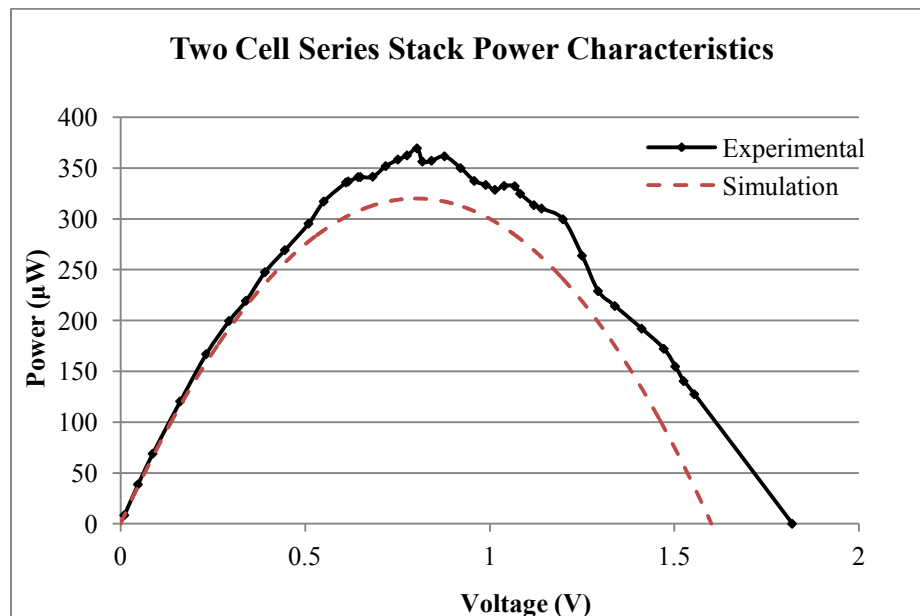
Fig. 4.19a Simulated power characteristics of two cell series stack
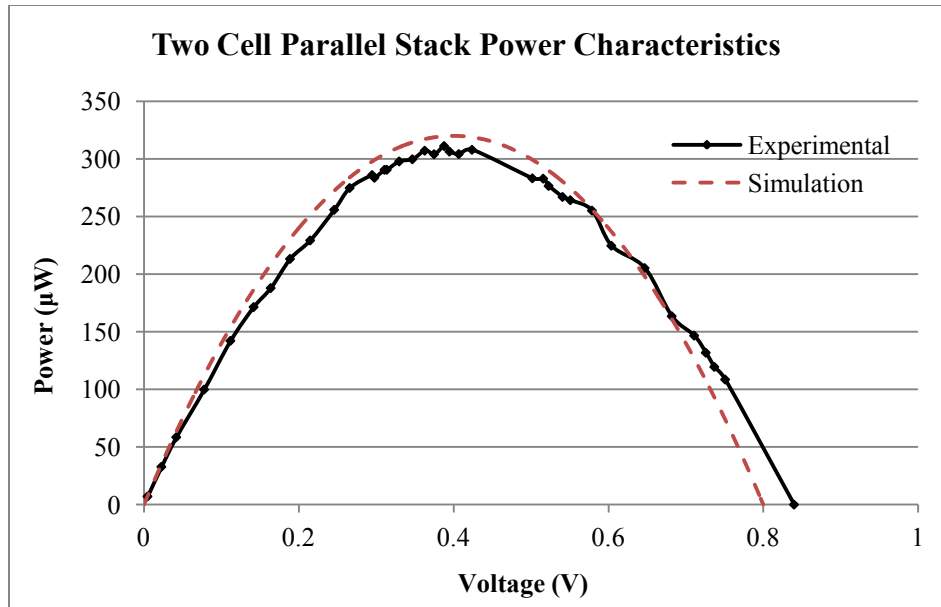
Fig. 4.19b Simulated power characteristics of two cell parallel stack

The μPSC equivalent circuit cell model can be stacked in the needed way and simulated. The results will greatly aid further analysis and can be further used to design, simulate and analyze a suitable power electronic converter for energy harvesting application.

With the help of the model, using stacked μPSC as source, a suitable power electronic energy harvester will be designed and developed to charge a battery.

CHAPTER 5

5 POWER ELECTRONICS AND ENERGY HARVESTING APPLICATION OF THE CELL

All renewable energy and energy harvesting applications require a suitably designed power electronic converter to process the energy from the source and deliver it to an energy storage device or to a load. The design of the power electronic converter depends on various factors such as the load type, power and voltage requirement of the load, etc. If the load requires AC power and if the energy source is a DC source then a suitable inverter should be designed. If the source is AC and the load is DC a rectifier has to be implemented. When both the load and the source are DC and if the load voltage and current requirements are different, a suitable DC − DC converter has to be designed to deliver the processed DC power to the DC load.

Photovoltaic (PV) applications are analogous to the µPSC. They are similar in many ways, both are renewable and DC power sources, the output voltage and current vary depending on the environmental factors, both require power conditioning to deliver the power to a load or to be stored in a energy storage device such as the battery and both require MPPT (maximum power point tracking) to derive the maximum power out of the cell. The goal of this thesis work is to harvest energy using µPSC i.e., store the energy from the µPSC in a battery. This application is similar to photovoltaic energy storage applications. In photovoltaic energy storage applications, the PV solar cell is the DC

source and the energy from it is stored in a suitable battery such a Li-ion or a Li-Po or a lead acid battery using power electronic converter.

In order to identify the suitable power electronic converter topologies, many power electronic energy harvesting applications were studied. The study was not only restricted to solar or microbial fuel cells. Applications such as piezoelectric, thermoelectric energy harvesting and solar energy harvesting wireless sensor network nodes were studied.

5.1 Study of power electronic converters suitable for the application

Since the cell closely resembles a microbial fuel cell and a solar cell, applications pertaining to them were studied first.

Nicolas Degrenne et al., 2011, [70] compared 3 self-starting DC-DC converter topologies for harvesting energy from low-voltage and low-power microbial fuel cells. In their work, they compare other areas in energy harvesting applications and three main converters. The first converter being a boost converter, the second is downsized flyback converter and the third converter is not based on a power electronic converter but on a set up oscillator and a voltage lift circuit with a transformer. The results show that the boost converter suits the application best and has high efficiency, low cost and MPPT.

Cesare Alippi and Cristian Galperti, 2008, [71] device a low-power maximum power point tracker (MPPT) circuit and a power transferring circuit for optimally conveying solar energy into rechargeable batteries using a DC-DC boost converter.

Kim, Sehwan et al., 2011, [72] propose a programmable charge pump driven by a direct digital synthesizer (DDS) to harvest solar energy using a super capacitor to power

90

wireless sensor nodes, with adaptability to add multiple supercapacitors to increase charging.

Yifeng Qiu et al., 2011, [73] develop a MPPT DC-DC boost converter for indoor photo voltaic energy harvesting application with an input power range of 5µW up to 10mW. Ottman et al., 2003, [74] develop a piezoelectric energy harvesting circuit using step-down converter in discontinuous conduction mode. Carlson et al., 2010, [75] present a low input voltage boost converter for thermoelectric energy harvesting. The DC-DC boost converter input range is 20 mV to 250 mV. Lefeuvre, E et al., 2007 [76] develop a DC-DC buck-boost converter for piezoelectric energy harvester.

The usage of DC-DC converter is the most popular in most energy harvesting application with few implementations of switch capacitor based power converters. Based on the literature review, three main power electronic topologies are considered for this energy harvesting application. They are:

- Switched capacitor based charge pump (voltage doubler) with MPPT
- DC-DC boost converter with MPPT
- DC-DC boost and buck-boost cascaded converter, with MPPT and output voltage regulation.

With single stage converters such as the switched capacitor charge pump and the DC-DC boost converter only MPPT can be achieved and is not suitable for a wide range of applications to deliver power to different loads. Most often single stage converters used in renewable energy or energy harvesting serve the purpose of charging a battery or a ultra/super capacitor.

However, the power electronic converter typically used for delivering power to loads are two stage cascaded DC – DC converters. The first DC – DC converter is connected to the renewable source such as the photovoltaic source and its function will be to track the maximum power point (MPP), this is referred to as the MPPT stage. A second DC – DC converter is cascaded with the first converter which provides the regulated voltage and current to the load. In some cases the second converter might have a battery charging algorithm in place to charge the required battery. Both the MPPT algorithm and voltage regulation require control of the duty cycle of the switch, thus making it not possible to achieve both using just a single stage converter. This is makes it unavoidable to have two stages if both MPPT and voltage regulation is required. For this thesis work, DC-DC boost and buck-boost, cascaded approach was considered.

The MPP can be tracked for the μPSC. The MPPT algorithms that are used in solar PV applications are also applicable for the μPSC. The published work "Evaluation of the Main MPPT Techniques for Photovoltaic Applications" [77] and "A New MPPT Method for Low-Power Solar Energy Harvesting" [78]; evaluates the main MPPT techniques that are being implemented in PV and energy harvesting applications. Some of the popular and superior techniques will be simulated with the μPSC, and the best the MPPT technique suitable for μPSC can be selected. MPPT is one of the areas where the developed simulation model of μPSC will be of great help.

5.2   Voltage doubler - Charge pump

Charge pumps are basically switched capacitor converters (SCC). Conventionally, they are used as voltage doubling rectifiers (AC to DC) and are implemented using diodes and

capacitors, with no transistors. DC to DC voltage doublers cannot switch this way; and they require a switching element that has to be controlled directly, such as a transistor/MOSFET instead of relying on the voltage across the switch as in the simple AC to DC case. The switches for the DC-DC charge pump require a driving circuit to control the switching. Figure 5.1 below shows the basic topology of a switch capacitor voltage doubler.
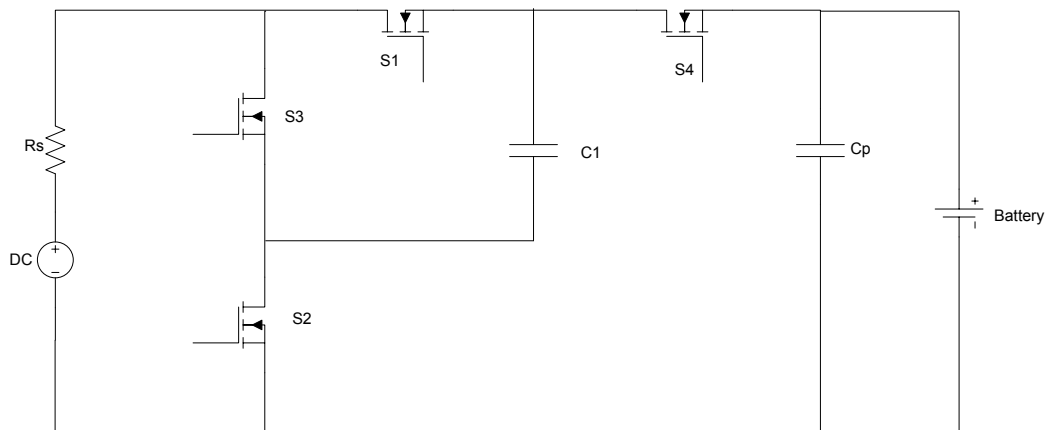
Fig. 5.1 SCC Voltage Doubler Topology

A DC-DC switched capacitor converter (SCC) is a power converter which employs primarily semiconductor switches (generally MOSFETs without anti parallel diodes) and energy transfer capacitors as the energy conversion elements. Due to the absence of inductors, coils and transformers in their configuration, SCCs have become an important field of study among the power converters category because they can be easily embedded in microelectronic circuits, using integrated circuit technology. A voltage doubler is a step-up converter. The output voltage is twice that of the input voltage i.e, by a factor of 2 (ideally). There are many different topologies available for SCC voltage doublers, the one that is chosen is shown in Figure 5.1. It was chosen based on the fact that it is simple and

93

it allows a constant current flow from the input to the load, making it an attractive candidate for PV and μPEC applications.

5.2.1 Voltage doubler charge pump operation

The voltage doubler circuit shown in Figure 5.1 has two stages of operation. The shown charge pump is used a battery charger and Rs represents the source internal resistance, Cp represents the charge pump capacitor and Co represents the output capacitor.

Stage 1

During stage one or the first half cycle, switches S1 and S2 are ON and switches S3 and S4 are OFF. This connects the charge pump capacitor Cp with the voltage source, and is charged to the same voltage level as the source.
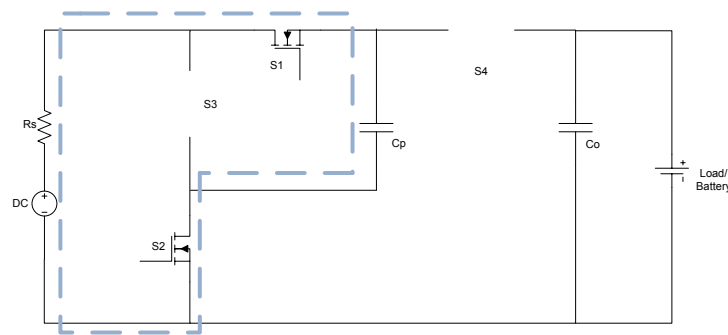
Fig. 5.2 Stage 1 operation SCC Voltage Doubler Topology

Stage 2

During stage two / second half cycle, switches S3 and S4 are ON and switches S1 & S2 are OFF. This connects the voltage source and the charge pump capacitor Cp which is charged to the same voltage as the source in series, and is connected to the output capacitor and the load/battery. Thus the output voltage is the source voltage plus the charge pump capacitor voltage. Since the charge pump is at the same voltage level of the source the output voltage is double that of the source voltage.

94
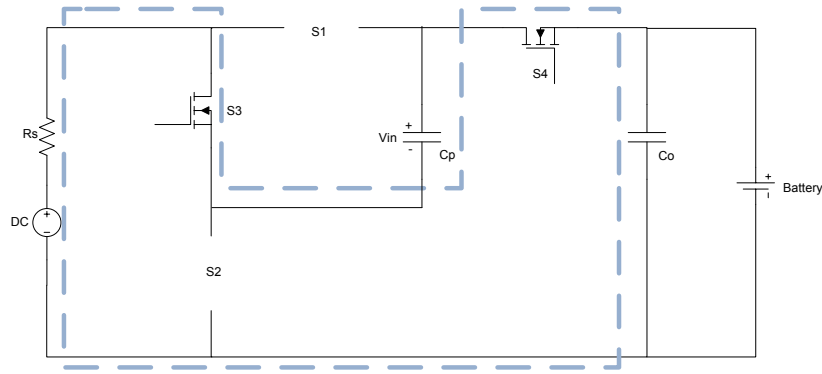
Fig. 5.3 Stage 2 operation SCC Voltage Doubler Topology
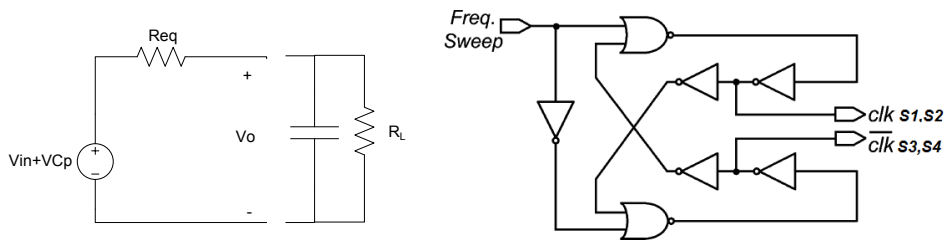
Fig. 5.4 a Equivalent circuit model of charge pump.

Fig .5.4 b Non overlapping clock pulse generator

In addition, the charge pump requires non-overlapping and two-phase clock generator for high-performance operation as shown in Figure 5.5. The implemented non-overlapping clock was adopted from [79].

5.2.2   Efficiency of the Charge Pump

Charge pumps are one of the best choices for powering an application requiring a combination of low power and low cost. The operational principle as explained above, of a charge pump cell is that two input capacitors (Cp & Co) switch between the voltage of the source at the frequency of switching of the switches. A charge pump theoretically produces an output voltage that is twice that of the input, but in reality, it is slightly

lower. The small voltage drop on the output is due to parasitic capacitance, resistive loss, and threshold voltage of switches.

The output voltage is given by the equation

$$Vo = V_{in} + \frac{C_p}{C_p + C_{par}} * Vin - R_{eq} - V_{tt} \tag{5.1}$$

Where

Cp-Charge pump capacitance

Cpar-Parasitic Capacitance

Vtt - threshold voltage of switches.

Using this equation, the voltage drop of the voltage doubler charge pump can be derived.

$$V_{drop} = V_{in}\left(1 + \frac{C_p}{C_p + C_{par}}\right) + \frac{I_o}{2fC_{in}} + V_{tt} \tag{5.2}$$

The percentage voltage drop of the voltage doubler charge pump would be:

$$\eta V_{out} = \frac{V_{out}}{2*Vin} * 100\% = \frac{2*Vin - V_{drop}}{2*Vin} * 100\% \tag{5.3}$$

Power loss in charge pump

To output current of the voltage doubler charge pump depends on the charge transmitted per cycle ΔQ and the frequency f.

$$\Delta Q = 2 * C_{in}(V_{in} - V_{out}) \tag{5.4}$$

$$Iout = f * \Delta Q \tag{5.5}$$

$$P_{loss} = I_{out} * V_{drop} \tag{5.6}$$

96

5.2.3   Design principle

The input / charge pump capacitor value at the power input stage, Cp, affects the efficiency and the ripple magnitude. Operating under maximum power point the current from μPSC is constant, and the charging time of the charge pump capacitor is directly proportional to its capacitance value. Also, this charging time depends on the switching frequency, which in turn affects the efficiency. As the input current from μPSC power increases, the charging time to charge the input capacitor is decreased. In this case, if the chosen switching frequency causes the input capacitor to be charged slower than optimal, then the unutilized current would account for the power loss. On the other hand, if the switching frequency of the charge pump is higher than the time required to charge the capacitor fully, then the charged energy at the input capacitor is transferred to the output capacitor, with a small amount of current. As a result, the charging efficiency decreases.

During the first stage the power supply, is charged to Vin (Fig. 5.2), while the output node capacitor is discharged by the load current I_L , which sinks a charge $Q = I_L T/2$. In the second half period (T/2 to T), the switches change their state (see Fig. 5.3), and now the charge transferred to the output capacitor and load from the source and the charge stored in Cp will be $I_L T/2$. The output voltage at steady state will be:

$$V_{out} = 2V_{in} - \frac{I_L T}{C}$$
(5.7)

Also, the output voltage ripple will be:

$$V_{ripple} = \frac{I_L T}{C_o}$$
(5.8)

Several cycles are needed to reach steady state. The output voltage will steeply increase in the first part of the transient, and will increase in smaller steps to reach the final steady state value.

5.2.4 Design of Voltage doubler charge pump with MPPT for µPSC

For this application a 6x6 µPSCs are stacked in series and parallel. The stack is arranged with 6 cells in series and 6 cells in parallel. The stack will be producing a peak power of 5.8mW.In this application, a voltage doubler charge pump circuit is designed and simulated to operate with the µPSC stack, with MPPT and Li-Ion battery charging. Assuming that the cells having maximum quantum yield of 0.8, the peak power produced will be around 2.4 volts. The voltage doubler charge pump operating at maximum power point will produce 4.8 volts, which is the standard charging for Li-ion cells in many commercial applications such as cell phone battery charger, etc. Figure 5.5 below shows the 6x6 cell simulated stack and Table 5.1 below gives the specifications for voltage doubler charge pump circuit for this application.
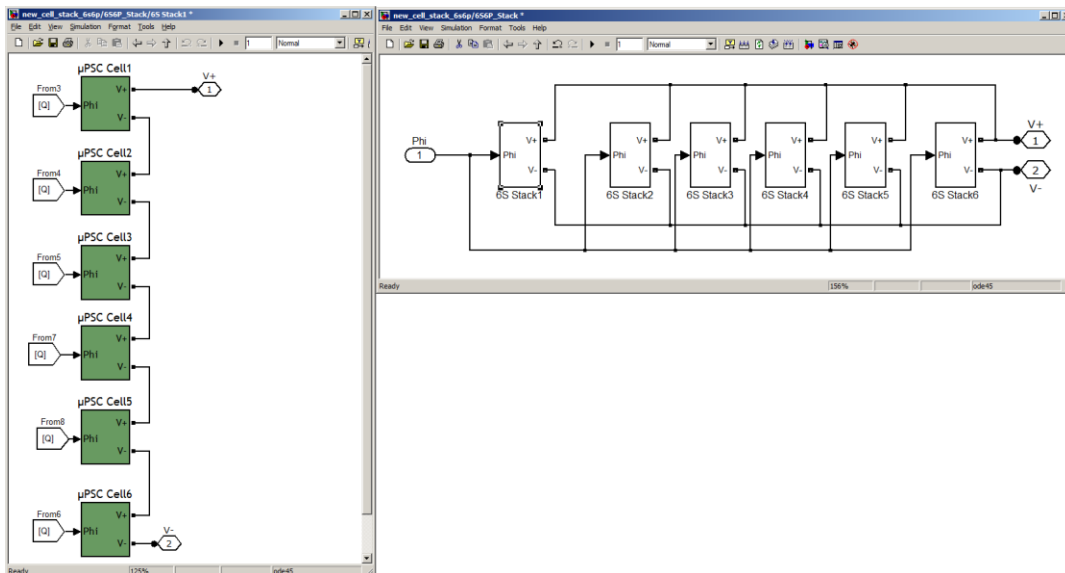
Fig. 5.5 6x6 µPSC Simulation stack

Voltage doubler charge pump Specifications	
Input Voltage	2.4 V
Input Power	5.8 mW
Output Voltage	4.8 V
Cp	540 nF
Co	3.3 uF
Switching frequency	500 Hz to 10 kHz
MOSFET	Picor P15101
MOSFET Rds on	360 $\mu\Omega$
Battery	Li-Ion
Battery Nominal Voltage	3.7 V
Battery Charging Voltage	4.8 V
Battery capacity	1.5 mAh

Table 5.1 Voltage doubler charge pump Specifications

The charge pump capacitor Cp and the output capacitor Co were selected based on the design Equations 5.7 and 5.8. The switching frequency was selected based on a combination of loss minimization, component sizing and commercial availability of components. The loss minimization was achieved by performing frequency sweep with the respective component parameters for that frequency and the 1 kHz was selected based on the performance.

5.2.5   MPPT using Frequency Sweeper

A charge pump can be operated from few kilohertz to tens of megahertz in order to maximize the efficiency for the system. However, most commercially available charge pumps use only one fixed frequency that is optimized for their specific source power and voltage ratings. This fixed frequency operation will be suitable only for stable power sources such as wall outlets, batteries and USB power, etc., but it is not optimized for

variable power sources that depend on the environment, such as the solar cell and μPSC. Basically the frequency of operation of the charge pump makes it adapt to a particular power capacity.

In conventional DC-DC converter, MPPT is achieved by controlling the duty cycle of the converter and this can be implemented using different MPPT algorithms. However, MPPT in a charge pump is achieved by changing the operating frequency of the charge pump, instead of the duty cycle. Similarly, any MPPT algorithm can be used. In order to perform MPPT a high dynamic range oscillator should be used for the charge pump. This oscillator should be able to generate different frequencies from few kilohertz to megahertz. Commercially available oscillators and pulse generator have a maximum tuning range of 100% from a certain center frequency that the oscillator is designed for. In order to achieve with a single analog voltage-controlled oscillator will be very difficult. It is possible to generate this wide range of frequency using multiple analog oscillators, and doing so will increase system complexity and the overall power consumption. To achieve high efficiency using MPTT, the power consumption of the frequency sweeper should be minimized, because the frequency sweeper must always generate a certain frequency to yield maximum power, even when the other subsystems are in sleep mode. A Digital direct synthesizer (DDS) will be the ideal choice (as opposed to a conventional analog oscillator) for controlling the frequency of the charge pump. A Digital direct synthesizer (DDS) is a frequency synthesizer which can create any required arbitrary waveform from a single, fixed-frequency reference clock.

The wide frequency sweeping range of DDS is a crucial function for the MPPT. Once the frequency is tuned to obtain the maximum power point, the tuned frequency should be

generated until the next tracking is required. Typical power consumption of commercial DDS chips consume around 1.5 mW. The frequency from the DDS can be controlled fully by using an MCU with high resolution of frequency steps which would required high speed (clock) MCUs typically around 20MHz [72].

The frequency sweep MPPT method is first tested by operating the charge pump at different frequencies which is connected to a 6x6 cell stack. The simulation results are shown in Figure 5.6 below.
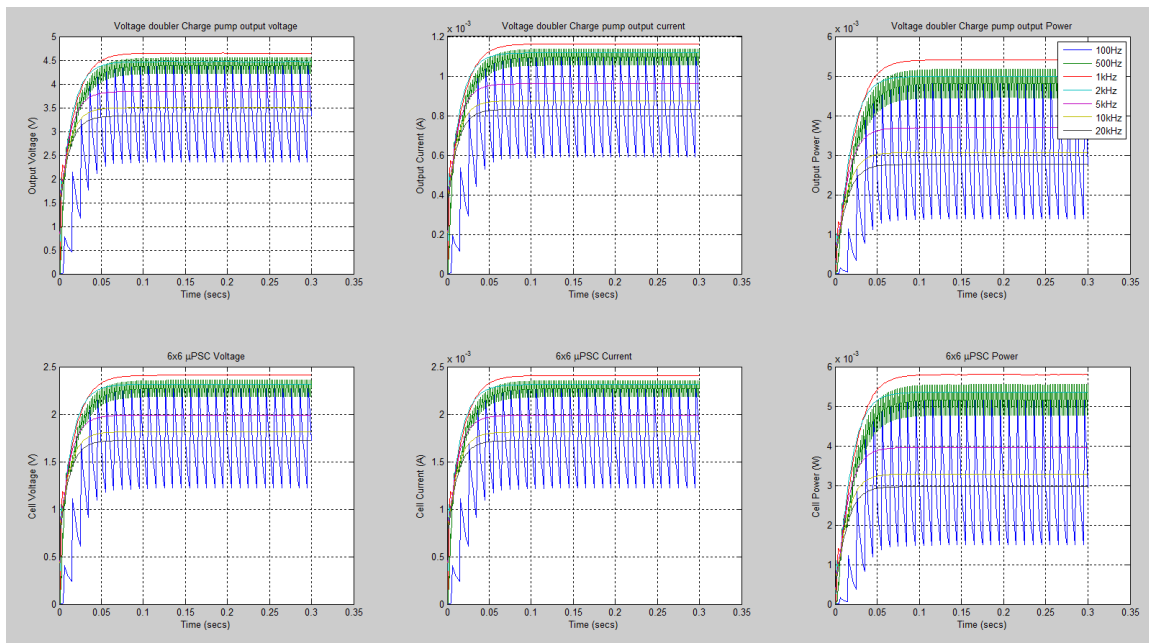
Fig 5.6 Voltage doubler MPPT frequency sweep analysis results

5.2.6   MPPT Algorithm and Li-Ion Battery Charging

As explained in the section above, MPPT is achieved by varying the switching frequency of the charge pump. The most popular MPPT method perturb and observe (P&O) also known as hill climbing technique can be used. In P&O, a initial switching frequency is set in the beginning and the power is obtained with the help of voltage and current

sensors. There are methods to avoid the use of current sensor by estimating the output current with respect to the output voltage. After the initial stage, the frequency is increased by a desired step and the output power is again obtained and is now compared with the power delivered with the previous switching frequency. If the power delivered is higher, the switching frequency is increased until the power delivered increases. However, beyond the maximum power point, increase in the switching frequency decreases the power delivered, at this point the switching frequency is decreased by one step to previous step. After this cycle, the switching frequency is increased and the output power decreases and again it reverts back to the switching frequency that produced the maximum power. This oscillation at the maximum power point is the main disadvantage of the P&O MPPT algorithm. This is relatively acceptable in PV applications as the light irradiance can vary any time causing the power generated to vary by a substantial amount. This is not the case with μPSC. Changes in light intensity does not necessarily cause a substantial change in the power generated as seen in chapter 3 and 4, where the major parameter was quantum yield of the cell. The quantum yield of the cell does not vary often, but does vary over a bigger time interval, relatively. Thus a modified P&O approach was used for the MPPT algorithm for the μPSC. The flow chart in Figure 5.7 outlines the developed MPPT algorithm.
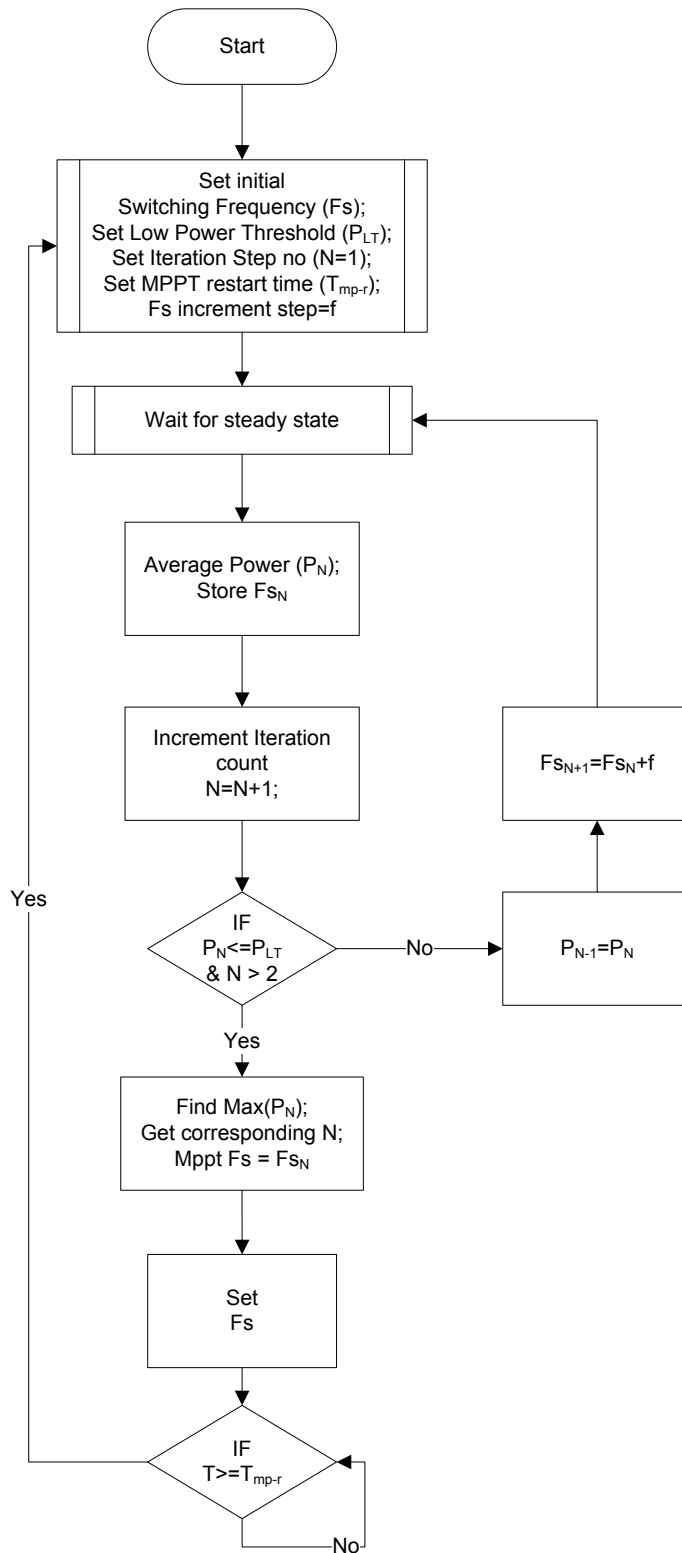
Fig 5.7 MPPT Algorithm

The MPPT is performed by operating the Charge pump by sweeping the switching frequency at specific steps throughout the range of operation of the switching frequency. The power output and the corresponding switching frequency of the charge pump at every step are stored. Once the entire range of switching frequency is swept, the maximum power delivered is found and the corresponding switching frequency is selected and the charge pump is operated at that switching frequency for a particular amount of time called the MPPT restart time. The MPPT restart time can vary from few seconds to few hours. Thus the device can be made to operate at a particular switching frequency for a long period of time. The simulation results are show in Figure 5.8 below.
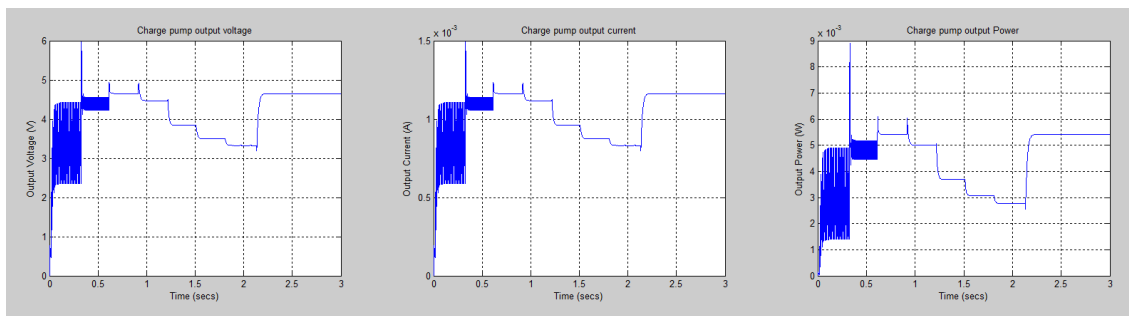
Fig 5.8 Charge pump output with the MPPT Algorithm

Each increment in switching frequency is done after 0.3 seconds. At around 2.1 seconds the best switching frequency is selected and the device operates at that frequency for the remaining period of time.

The Figure 5.9 below show the Li-Ion battery parameters, that the charge pump is charging and the following Figures 5.10 and 5.11 shows the Percentage SOC of the battery.

104
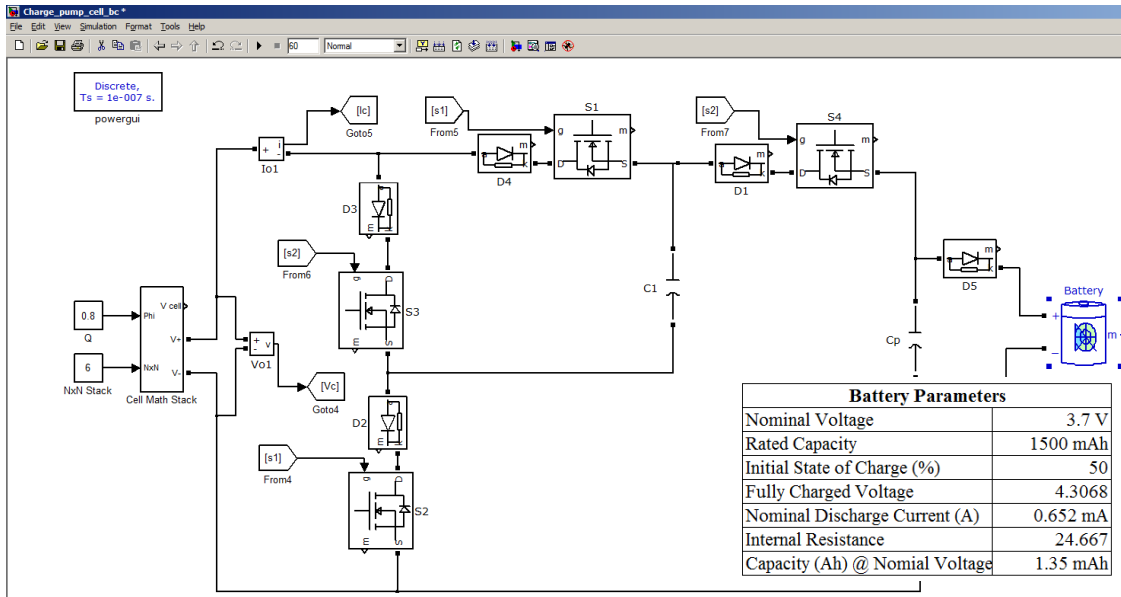
Fig 5.9 Li-Ion battery parameters, charged by the charge pump

The Battery Parameters table shown in the figure:

Battery Parameters	
Nominal Voltage	3.7 V
Rated Capacity	1500 mAh
Initial State of Charge (%)	50
Fully Charged Voltage	4.3068
Nominal Discharge Current (A)	0.652 mA
Internal Resistance	24.667
Capacity (Ah) @ Nomial Voltage	1.35 mAh
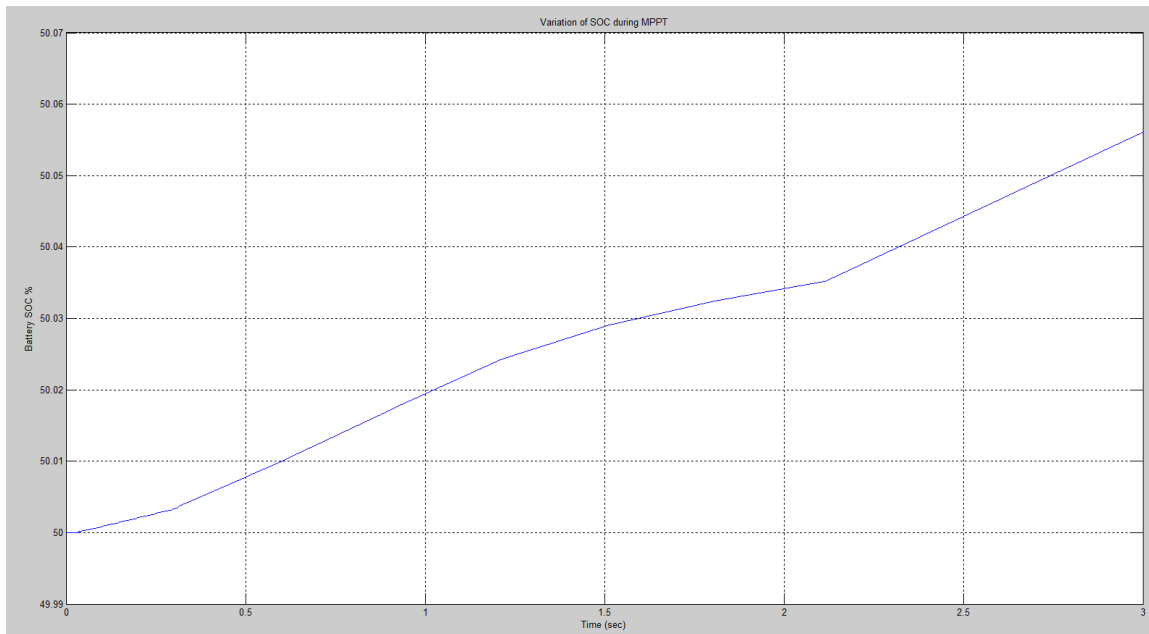
Fig 5.10a SOC % of Li-Ion battery charged by the charge pump with MPPT
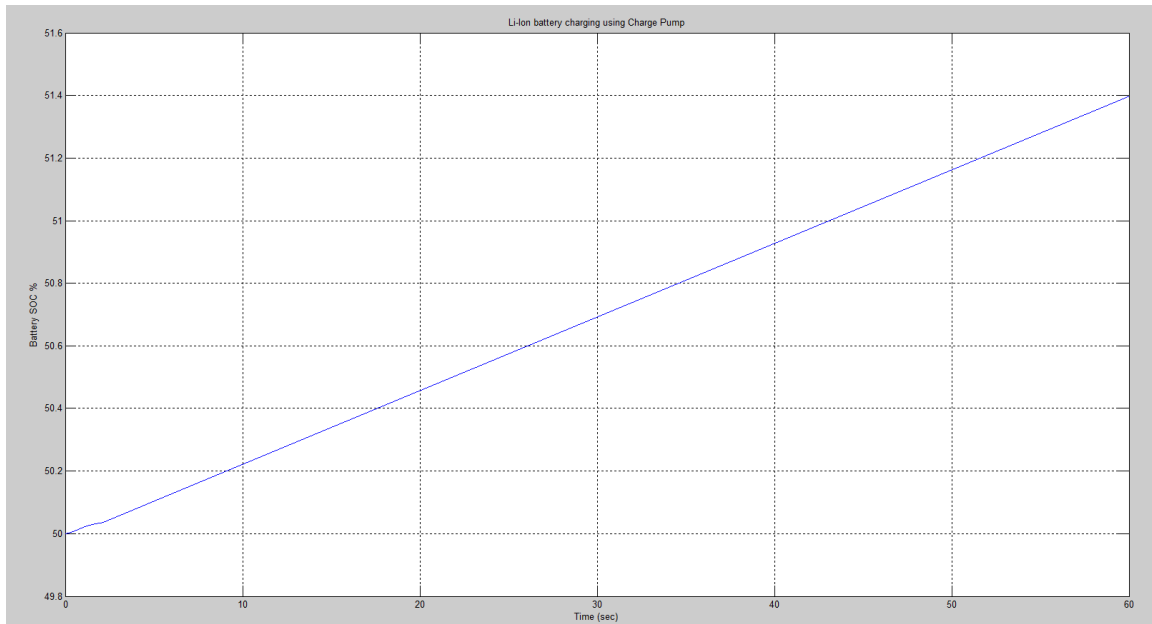
Fig 5.10b SOC % of Li-Ion battery charged for 60 secs (with MPPT)

5.3 Synchronous DC-DC Boost Converter

The DC-DC boost converter is a very popular topology and is widely used in energy harvesting application, PV MPPT applications, renewable energy application and battery chargers. Naturally, the boost converter was chosen for the µPSC energy harvesting application.

The boost converter has many advantages over the voltage doubler charge pump.

- Low cost, as it requires far less switches than voltage doubler charge pump.
- The frequency of the PWM used is constant and only the duty cycle of the converter is controlled to achieve MPPT or output voltage regulation. This method is simple and easier to implement, consumes less power and is low cost

106

over the changing frequency DDS based MPPT implementation in the voltage doubler charge pump.

- Easier control and finer voltage regulation. The output voltage of voltage doubler charge pump is always twice that of the input and cannot be regulated in a finer fashion.

- Better dynamics, when cascaded at the output with other DC-DC converters.

- Most suitable for both MPPT and battery charging applications.

5.3.1 Design of Synchronous DC-DC boost converter for μPSC

The Synchronous DC-DC converter topology is shown is Figure 5.11 below.
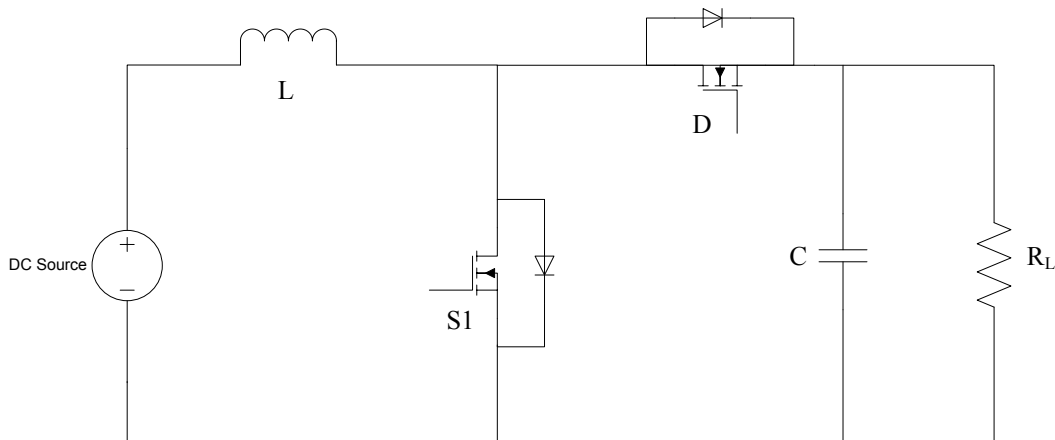
Fig. 5.11 Synchronous DC-DC boost converter

The synchronous DC-DC boost convert uses a transistor based switch such as the MOSFET instead of a diode, shown by D in Figure 5.11. This helps to reduce the voltage drop across the diode, thereby increasing the efficiency of the converter. As the boost converter is popular and used widely, the operating principle is not explained here.

The boost converter can be operated in two modes, CCM – Continuous conduction mode or DCM – Discontinuous conduction mode. Both modes have their own advantages, but the advantages of CCM operation outweigh the DCM mode. DCM produces more ripple, noise, emissions, etc. It is usually against regular design practices to operate in DCM. Also, based on design practices most of the converters are operated in continuous mode for the lowest currents one can imagine for their application. Based on these criterions, the CCM operation was chosen [82].

The design equations for the CCM mode of operation of the boost converter are given by:

$$V_o = \frac{V_{in}}{1-D} \qquad (V_{in}, V_o - \text{Input \& Output voltage of converter}) \qquad (5.9)$$

$$D = \frac{V_o - V_{in}}{V_o} \qquad (D - \text{Duty cycle of operation}) \qquad (5.10)$$

Inductor value at Boundary condition between CCM and DCM

$$L = \frac{I_o \, D \, (1-D)^2}{V_o \, 2 \, f} \qquad (5.11)$$

Output capacitor value for a given output ripple voltage V_{rp}. V_{rp} was chosen as 5 mV.

$$C = \frac{I_o \, D}{V_{rp} \, f} \qquad (5.12)$$

The same 6x6 (6S6P – 6 series, 6 parallel) cell stack used for the voltage doubler charge pump is used as the source for the boost converter application.

Based on these equations, the circuit parameters were derived. The table 5.2 below shows the circuit parameters. The converter was linearized for an output voltage of 4.8 V and maximum current (MPP), which is the most ideal for Li-Ion battery charging

applications. A 6S6P stack produces a peak power of 5.8 mW, thus the boost converter operating at output voltage of 4.8 V would deliver a peak current of 1.2 mA.

Voltage doubler charge pump Specifications	
Input Voltage range	1.8 to 3.6 V
Input Power	5.8 mW
Output Voltage	4.8 V
L-Inductance	25 mF
C-Output Capacitor	800 nF
Switching frequency	100 kHz
MOSFET	Picor P15101
MOSFET R_{ds} on	360 $\mu\Omega$
Battery	Li-Ion
Battery Nominal Voltage	3.7 V
Battery Charging Voltage	4.8 V
Battery capacity	1.5 mAh

Table 5.2 Synchronous boost converter specifications

The switching frequency was purposefully selected to be high (100 kHz) and lower switching frequencies were yielding higher inductor values.

5.3.2   MPPT Algorithm - MPP Exploration technique

Similar to the MPPT implemented in voltage doubler charge pump, two different MPPT algorithms are implemented in the boost converter too. The first is the conventional P&O /hill climbing algorithm, which is popular and is widely used. The algorithm is represented using a flow chart in Figure 5.12b.

The second method is the MPP Exploration technique developed specific for µPSC energy harvesting application. The algorithm is loosely based on P&O but is modified heavily. It is devised in such a way that is more stable and is made to suit the needs of the µPSC energy harvesting.

In this method:

- The converter is operated under the entire range of the duty cycles that the converter is designed to operate for.

- After this exploration, the duty cycle which produced the maximum power is selected and the converter is made to operate at that duty cycle for a longer duration of a time. This time (T_{bop} – base operating point time) is configurable and can be made shorter or longer.

- After this the reference voltage (V_{ref}) that is used to generate the duty cycle is perturbed positively and the change in power gradient is observed if the gradient is positive, V_{ref} is increased positively. If the gradient is negative, V_{ref} is decreased.

- After a prolonged period if operation (To), the whole cycle is repeated. To is made configurable.

This method ensures that there are no oscillations around the peak power. It is more advantageous because, the power produced by μPSC varies by a negligible amount due changes in light and other environmental conditions. The power produced mainly depends on the quantum yield of the cells, which varies much slowly and is a bulk quantity. The modified MPPT algorithm is show in Figure 5.12a. Since the algorithm explores for the maximum power point (MPP), it was chosen to be called the 'MPP Exploration technique'.
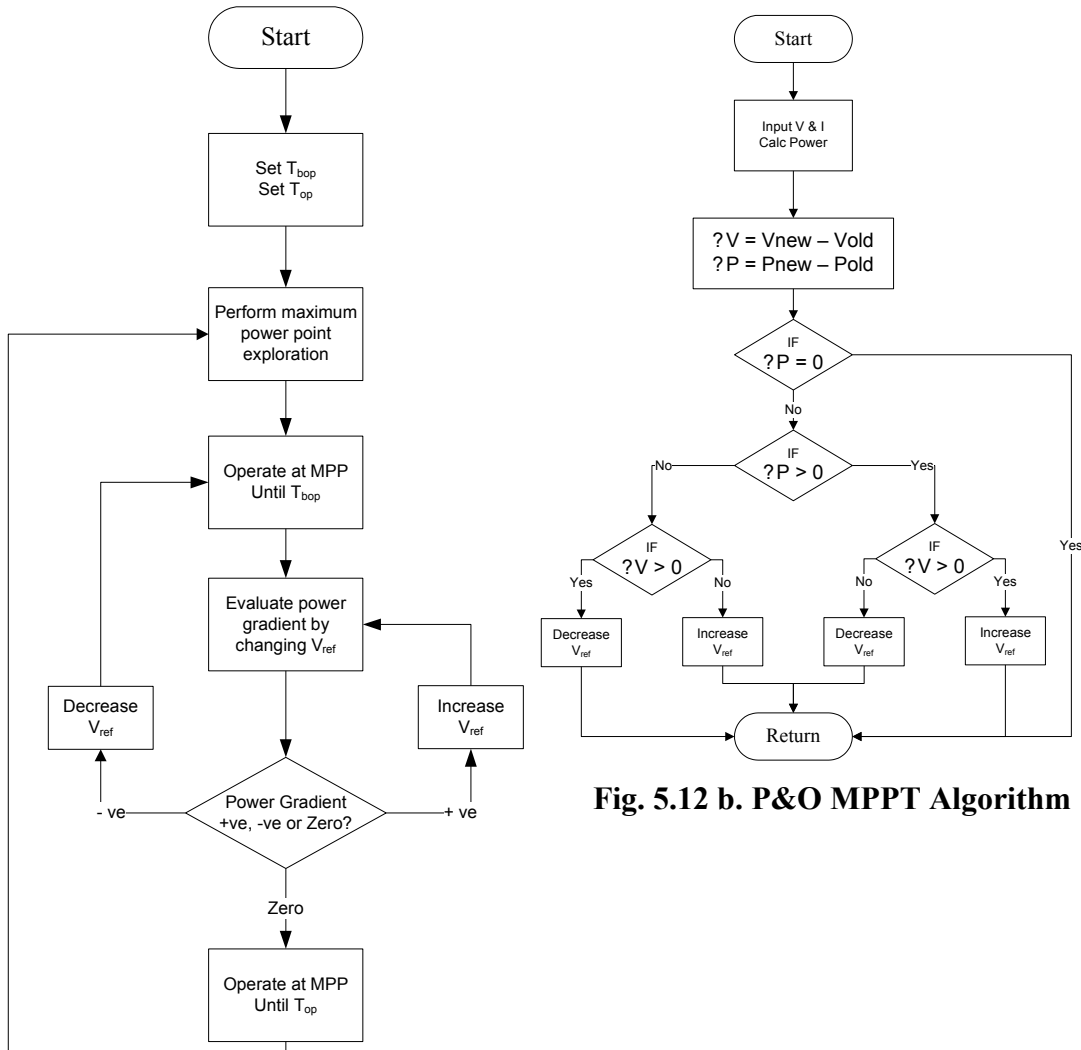
Fig. 5.12 b. P&O MPPT Algorithm

Fig. 5.12 a MPP Exploration Technique – Algorithm

5.3.3 Robust and Stable operation of the boost converter

Since the boost converter is used for MPPT, it does not have a feedback loop and therefore it does not have controller that can control the converter to make it stable, robust and fast. Thus, a different analysis approach was used to achieve stability, robustness and fast response.

111

Deriving the small signal transfer function of the DC-DC boost converter will yield the converters poles and zeros. Using the poles and zeros, the open loop behavior of the plant can be easily determined.

From state space averaging, the small signal transfer function of the boost converter is derived and is given by the equation 5.13.

$$G(s) = \frac{\widetilde{v_o}}{\widetilde{d}} = \frac{V_{in}}{(1-D)^2} \cdot \frac{\left(1+\frac{s}{\omega_z}\right)\left(1+\frac{s}{\omega_{rz}}\right)}{1+\frac{s}{\omega_o Q}+\frac{s^2}{\omega_o^2}} \qquad (5.13)$$

$$\omega_z = \frac{1}{r_c C} \qquad (5.14)$$

$$\omega_{rz} = \frac{I_o V_{in}^2}{L\,V_o} \qquad (5.15)$$

$$\omega_o = \frac{V_{in}}{\sqrt{L\,C}\,V_o} \qquad (5.16)$$
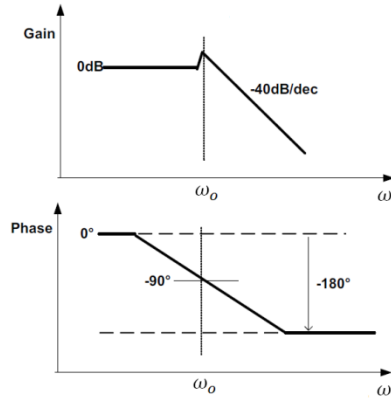
Fig 5.13a Bode plot of double pole in G(S)

From the transfer function it can understood that the system has a left hand plane zero ω_z, a right hand plane zero ω_{rz}, and a double pole. Since the left hand pole does not cause any problems, it need not be analyzed in depth.

Shown in Figure 5.13a is the bode plot of the double pole. The double pole frequency ω_o is dependent on Vin, Vo, L and C. Thus, choosing
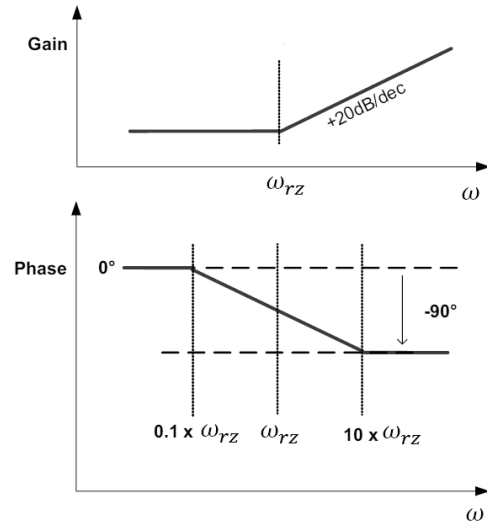
Fig 5.13b Bode plot of RHP Zero in G(S)

of these parameters is very important; any random selection of these parameters will not help the plant. Figure 5.13b shows the bode plot of the right hand plane zero. The right

hand plane zero frequency is ω_{rz}, and the RHP-zero depends on the inductance (L), input voltage (Vin), output current Io, and output voltage (Vo). This affects the loop gain stabilization, and this is because of the fact that while the RHP-zero phase begins to drop at 10% of ω_{rz}, the gain increases at 20 dB/dec from ω_{rz}. Even though the addition of the RHP-zero is at a higher frequency than the converter double pole, the RHP-zero phase drop starts a decade earlier, and therefore negatively impacts the potential phase margin of the converter's control loop. This is the nature of instability of a boost converter running in CCM.

In order to maintain stability for boost converters with control schemes, the following are the criterions that must be met [82]:

1. The RHP-zero must be at a higher frequency than ω_o (by a ratio $\omega_{rz}/\omega_o >= 15$) in order to prevent the RHP-zero's phase drop from affecting the power stage's double-pole.

2. The crossover frequency (ω_{bw}) must be set at or lower than the frequency of the maximum phase-boost effect generated by feed-forward compensation network with zero set at ω_z. If ω_{bw} is set higher than the frequency of the maximum phase boost, the phase-boost effect becomes small while gain increases, reducing the stability margin.

Now for the feedforward compensation lets, assume the maximum frequency for phase boost from the feed-forward network is $2 \times f_z$.

$$f_{bw} \leq 2 \cdot f_z \cong f_o 10^{\frac{G_o}{30}} \qquad\qquad (5.17)$$

From the equation and the parameters given in table 5.2, the open loop bode plot of the plant is plotted and is shown in Figure 5.14 below.
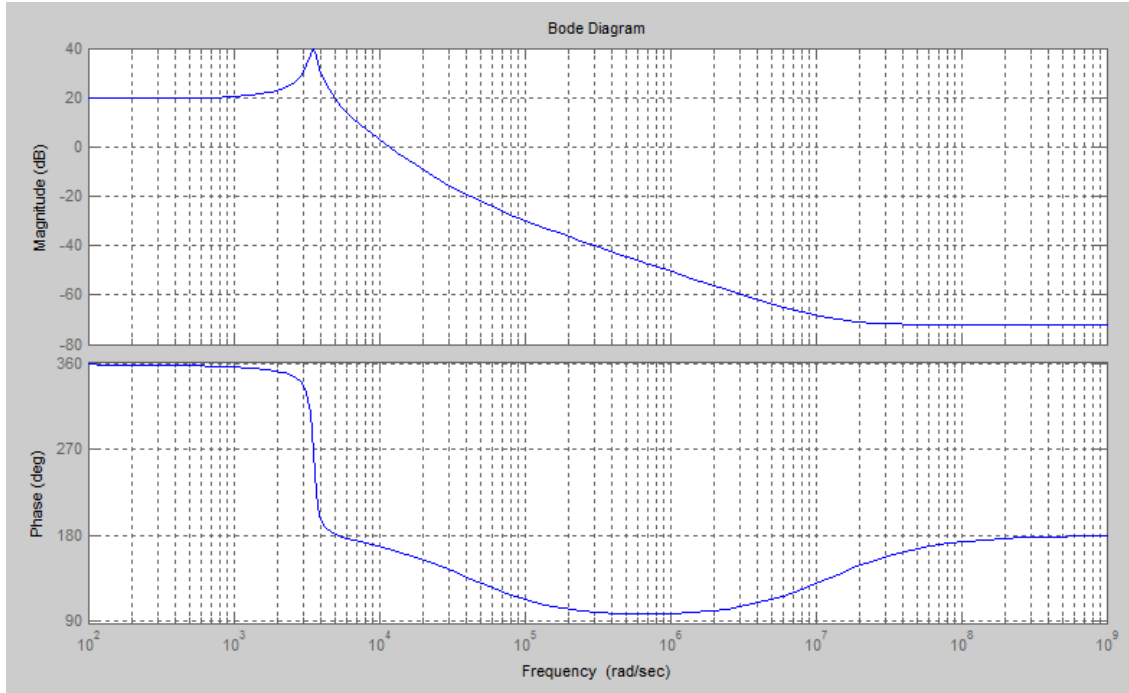
Fig. 5.14a Boost Converter open loop Bode plot

From the bode plot, it can said that the system is unstable. The crossover frequency of the system is 1.17×10^4 rad/sec, gain margin of -18.6 dB and phase margin of -14.5 deg.

Based on standard design procedures [82], the bandwidth of the converter is chosen as 10 % of the switching frequency and the phase margin of the system was chosen as 45° and a suitable feedforward compensator was designed. The bode plot and the step response of the compensated system is shown in Figure 5.14b below. The designed compensator makes the system completely stable. The compensated system has a cross over frequency of 1.11×10^3 rad/sec, which is 7% of the switching frequency with a phase margin of 45.5°. The system now reaches steady state in approximately 6ms.
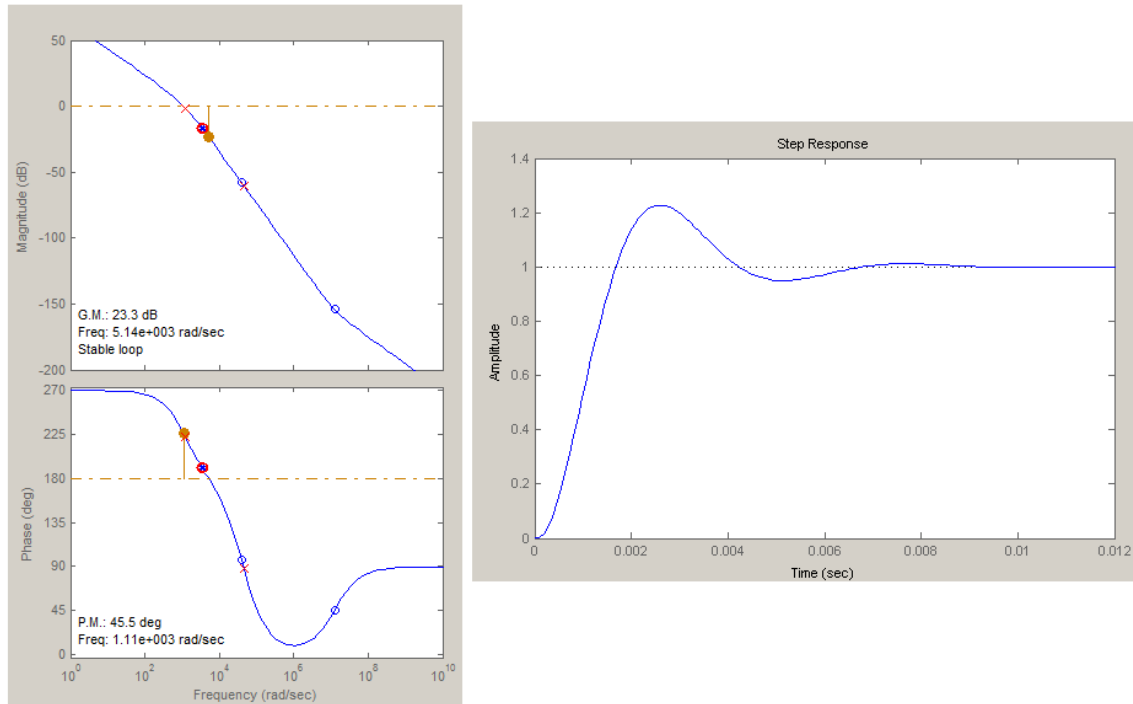
Fig. 5.14b Compensated Boost Converter Bode plot and step response

The section below shows the simulation results of the DC-DC boost converter with MPPT and feedforward compensation with µPSC as the source.

5.3.4 Synchronous DC-DC boost converter simulation results

The DC-DC boost converter was designed with feedforward compensation. The converter is used to simulate both the MPPT algorithms discussed in Section 5.3.2 with a 6x6 µPSC stack as the source. The DC-DC boost converter was used to charge a Li-Ion battery. It has to be noted that, the if the output voltage of the boost converter is less that the battery voltage the current will flow in the reverse direction, in order to avoid this a forward blocking diode is used. This voltage is usually the battery nominal voltage. For this application, since it is a Li-Ion battery, the nominal voltage is 3.7. If the output voltage of the boost converter is less than or equal to 3.7 then there will be no charging current. Thus the converter initiation has to be handled; this is done by setting the initial

115

duty cycle of the converter such that the output voltage is greater than that of the battery nominal voltage. It can be observed in the simulation results; that even during the start up the output voltage of the boost converter is higher than 3.7 volts. Figures 5.15 to 5.17 show the simulation results with P&O MPPT algorithm and MPP Exploration algorithm.
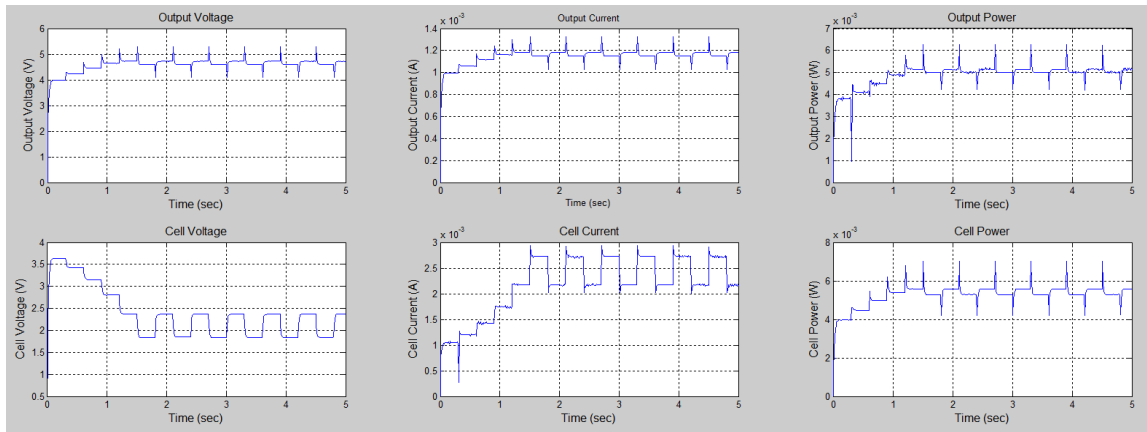
Fig 5.15 Boost converter output using P&O MPPT Algorithm
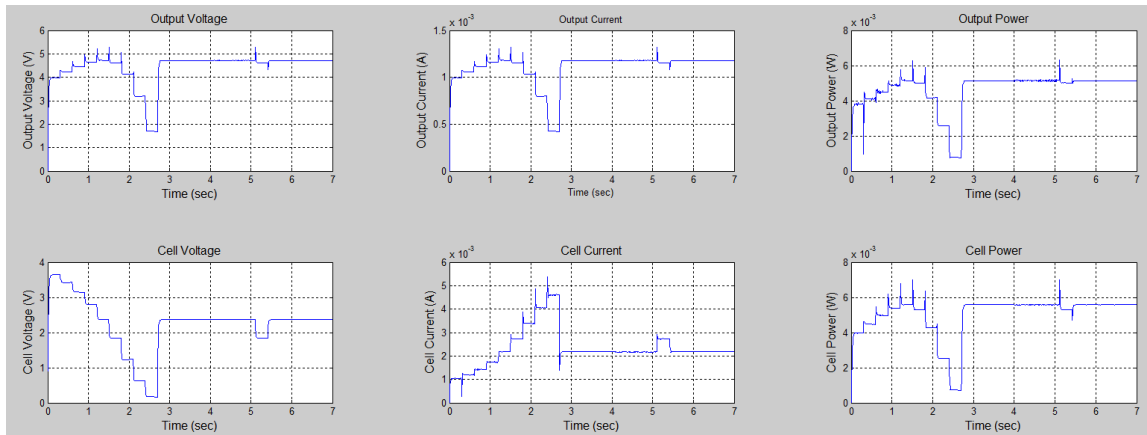
Fig 5.16 Boost converter output using MPP Exploration Algorithm

The above simulations were run for a time period of 5 seconds and 7 seconds respectively. However, this small time period was not enough to see a substantial change in the SOC of the Li-Ion battery. Hence, the simulations were run for a long period of time. Figure 5.17 illustrate the battery SOC% that is being charged.

116
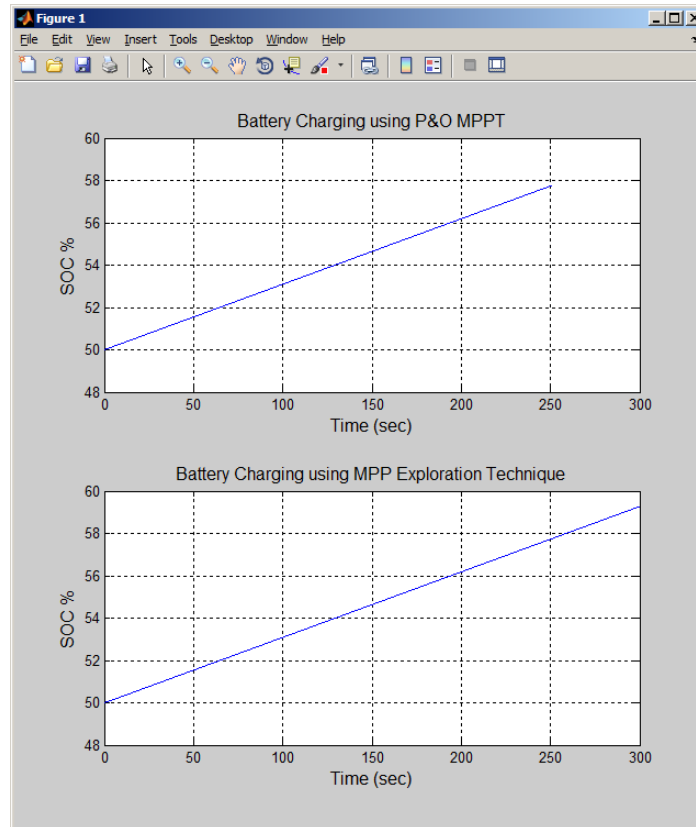
Fig 5.17 Battery charging using boost converter with P&O and MPP Exploration

The graph does not bring out the minute difference between the different MPPT techniques. From the data, after 250 seconds of charging the battery from a initial 50% SOC reached 57.67 % using P&O MPPT algorithm and 57.73 % using MPPT exploration technique. Though this is not a significant difference, it will eventually become significant at larger durations. Thus, it can be said that the MPP exploration technique is slightly better than the P&O algorithm.

5.4   Cascaded Converter - Boost & Buck-Boost

The converters in the above two sections can only perform MPPT, but not output voltage regulation; this is acceptable if the application is limited. However that is not the scenario; largely many applications in the real world require output voltage regulation for

proper operation, and at the same time it is important to perform MPPT. The only way of achieving both MPPT and output voltage regulation is with the help of two cascaded converters, where the first converter performs MPPT and the second converter is used for output voltage regulation. Cascaded converters are typically not used in very low power applications. Since the future goal of the energy harvesting from μPSC is to be able to produce higher levels of power and be able to configure them in a panel fashion. Thus for this application, the scenario of many μPSC cascaded together was considered.

Based on current standard solar panel size, it was calculated that the same area will hold 6400 μPSCs and would produce 1.28 W. Figure 5.18 below shows the cascaded converter. The MPPT stage is accomplished using a boost converter and the output stage using a buck-boost converter.
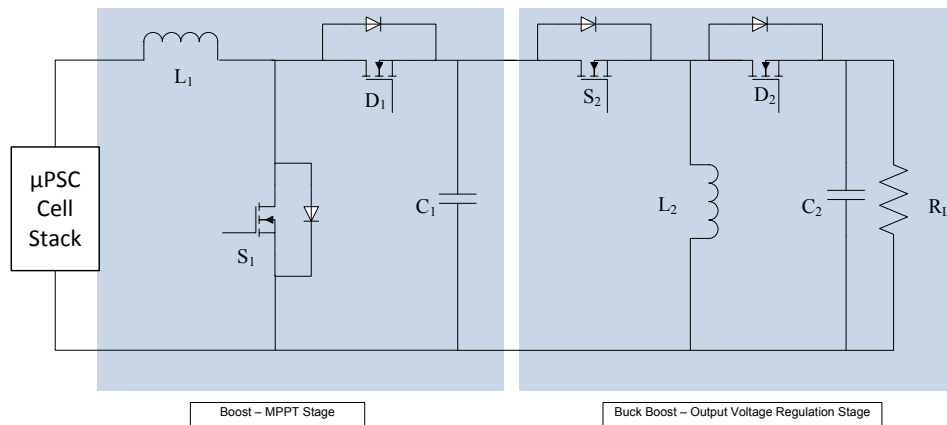
Fig 5.18 Cascaded Boost and Buck-Boost Converter

The boost converter was chosen based on its performance observed in the Section 5.3 above. As for the output stage, the buck-boost converter was chosen because depending on any application, the output voltage can be made extremely low as 4.8 V to charge a Li-Ion battery or as high as 120 V so as to feed an inverter and then send the power back

118

to the grid. Design a buck-boost converter for that wide operation is very challenging. The table 5.3 below gives the design considerations for the cascaded operation.

Design Considerations	
No. of μPSCs	6400 (80S 80p)
Input Power	1.28 W
Input Voltage @ MPP	32
Output voltage range	4.8 to 120 V

Table 5.3 Design considerations for cascaded converter

Based on the design equations for the boost converter as explained in the Section 5.3.1 above, the circuit parameters for the boost converter to operate in CCM were obtained, and are given in table 5.4 below.

MPPT Boost Converter parameters	
Inductance L	1.6 nH
Output Capacitor	220 μF
Output Voltage range	32 to 64 V
Maximum Output Current	50 mA
Maximum power output	2W
Switching Frequency	10 kHz

Table 5.4 Cascaded Boost stage converter parameters

The switching frequency 10 kHz is notable lower than the switching frequencies used for the earlier, this is because of the increased voltage and current the same high bandwidth is very difficult to achieve.

5.4.1 Design of Buck-Boost converter

Similar to the design of the boost converter, the buck-boost converter was also decided to be operated in CCM. The design equations for the CCM mode of operation of the buck-boost converter are given by:

$$V_o = \frac{D}{1-D} V_{in} \quad (V_{in}, V_o - \text{Input \& Output voltage of converter}) \tag{5.18}$$

$$D = \frac{V_o}{V_o + V_{in}} \quad (D - \text{Duty cycle of operation}) \tag{5.19}$$

Inductor value at Boundary condition between CCM and DCM

$$L = \frac{V_o \ (1-D)^2}{I_o \ 2 \ f} \tag{5.20}$$

Output capacitor value for a given output ripple voltage $V_{rp.}$ V_{rp} was chosen as 5 mV.

$$C = \frac{I_o \ D}{V_{rp} \ f} \tag{5.21}$$

Based on these equations and the transfer function of the converter, the parameter for the buck-boost converter was chosen, the parameters are given in table 5.5 below.

Buck-Boost Converter parameters	
Inductance L	62 mH
Output Capacitor	1 µF
Output Voltage range	4.8 to 120 V
Maximum Output Current	0.5 A
Maximum power output	2W
Switching Frequency	10 kHz

Table 5.5 Buck-Boost converter parameters

The switching frequency 10 kHz is notable lower than the switching frequencies used for the single stage boost MPPT converter in the previous section.

5.4.2   Control of buck-boost converter

Current mode control was chosen over the voltage mode control. In current mode control, the output element considered is the current, and the control element is the duty cycle of

the converter. Using state space averaging, the converter transfer function is derived and is given by:

$$G(s) = \frac{\tilde{i_o}}{\tilde{d}} = \frac{(V_{in}+V_o)}{R\,(1-D)} \cdot \frac{\left(1-\frac{s\,L\,D}{R(1-D)^2}\right)(1+s\,r_c)}{1+\frac{s\,L}{R(1-D)^2}+\frac{s^2 L\,C}{(1-D)^2}} \qquad (5.22)$$

$$\omega_n = \sqrt{\frac{(1-D)}{L\,C}} \qquad (5.23)$$

$$Q = R\sqrt{\frac{(1-D)C}{L}} \qquad (5.24)$$

Based on the circuit parameters and choosing 20% of the switching frequency as the bandwidth with a phase margin of $65°$, Type III converter was chosen.

The Type III controller transfer function is

$$C(s) = \frac{\widetilde{v_{con}}}{\tilde{i_o}} \qquad (5.25)$$

In order to achieve the desired Phase margin, equation 5.26 is used.

$$K = \sqrt{tan^2\left(\frac{PM-\beta-90°}{4} + 45°\right)} \qquad (5.26)$$

K represents the intensity of frequency compensation. PM is the desired phase margin of the system, and β is the phase value of the open loop plant at cross over frequency.

Figure 5.19 below shows the open loop Bode plot of the buck-boost converter. From the Bode plot the open loop system's crossover frequency is 4.05×10^4 rad/sec with a gain margin of -42.1 dB and a phase margin of $-50.4°$, which is an unstable system.
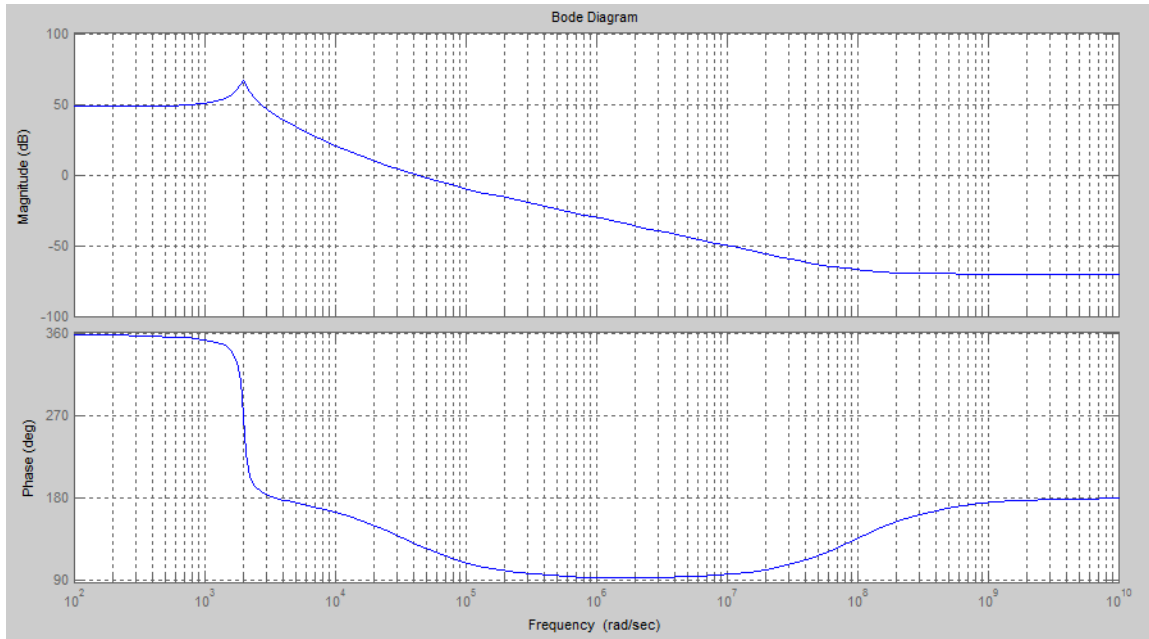
Fig 5.19a Buck-Boost open loop Bode plot
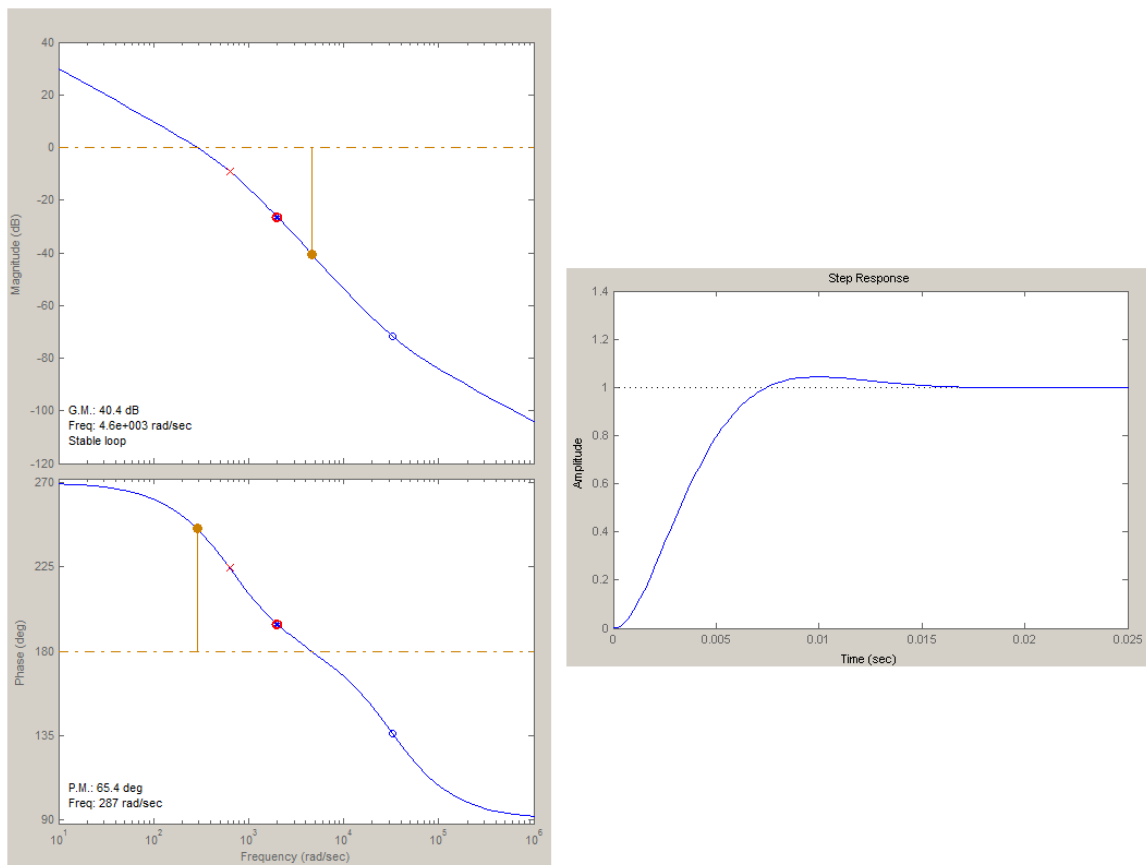
Fig 5.19b Compensated Buck-Boost converter Bode plot and step response

122

With the designed Type III compensator, a crossover frequency of 287 rad/sec (18% of switching frequency) was achieved with a phase margin of 65.4^o, and this provides a robust system with relatively fast response. The bode plot of the compensated system and its step response is shown in Figure 5.19b.

5.4.3   Simulation results of Cascaded boost Converter

The block/topology diagram of the cascaded converter application for μPSC was shown in Figure 5.18. The μPSC stack is connected to the boost converter which performs the MPPT and the boost converter in turn is connected to a buck-boost converter, which delivers power to the load. The various simulation results for this application are show in Figures 5.20 to 5.23 below. For the cascaded converter, only the MPP Exploration technique was used (P&O was ignored for the cascaded converter application).
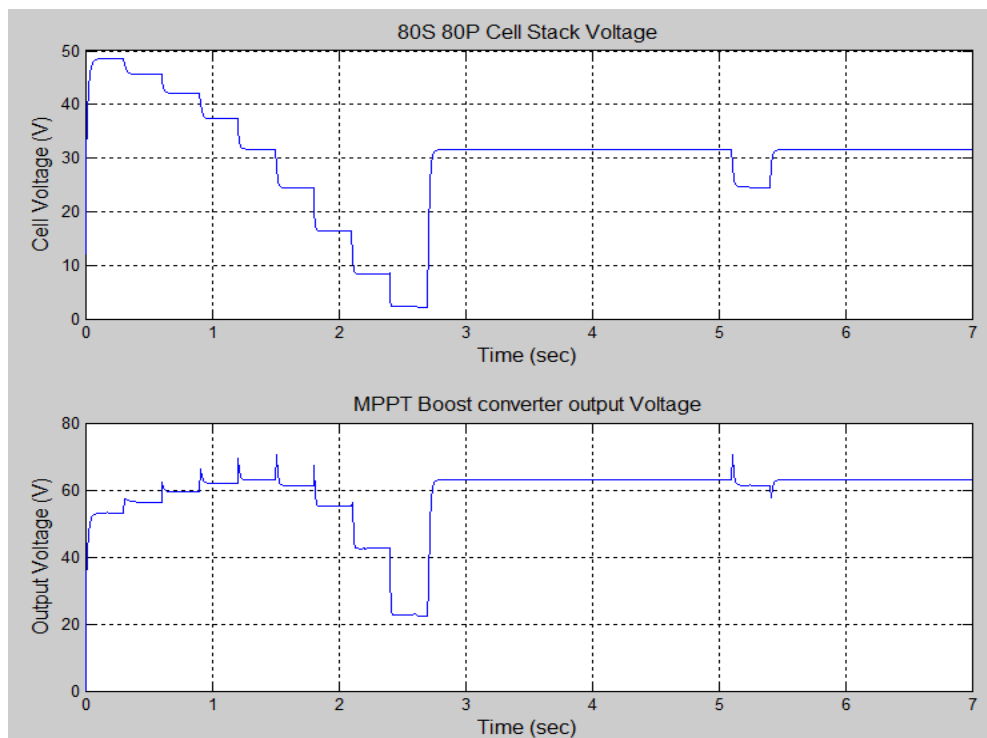
Fig 5.20 MPPT Boost converter and μPSC Stack output results

The MPP Exploration lasts until 2.7 seconds from start. After 2.7 seconds it operates at MPP, and check for new MPP every two seconds, this can be observed in Figure 5.20. The corresponding µPSC stack and the boost converter output voltages are shown.

The buck boost converter was designed to operate from 4.8 to 120 V, and was linerazied to operate at an input voltage of 64 V from the boost converter. Since, the range was very wide, the controller of the buck-boost converter saturated when the duty cycle of the MPPT boost converter was higher than %86. Thus the upper saturation limit for the MPPT boost converter for the cascaded operation was set at 80% duty cycle. Hence the MPP exploration lasts till 2.4 seconds instead of 2.7 seconds. Operating at the boundary, at 80% duty cycle of operation of the boost converter, the buck-boost converter output voltage had a ripple of 2.8%, whereas the converter was designed for an output ripple of 0.08% (5 mV). However, this condition was only during 80% duty cycle of the MPPT boost converter. The simulation results are shown in Figure 5.21 and 5.22.
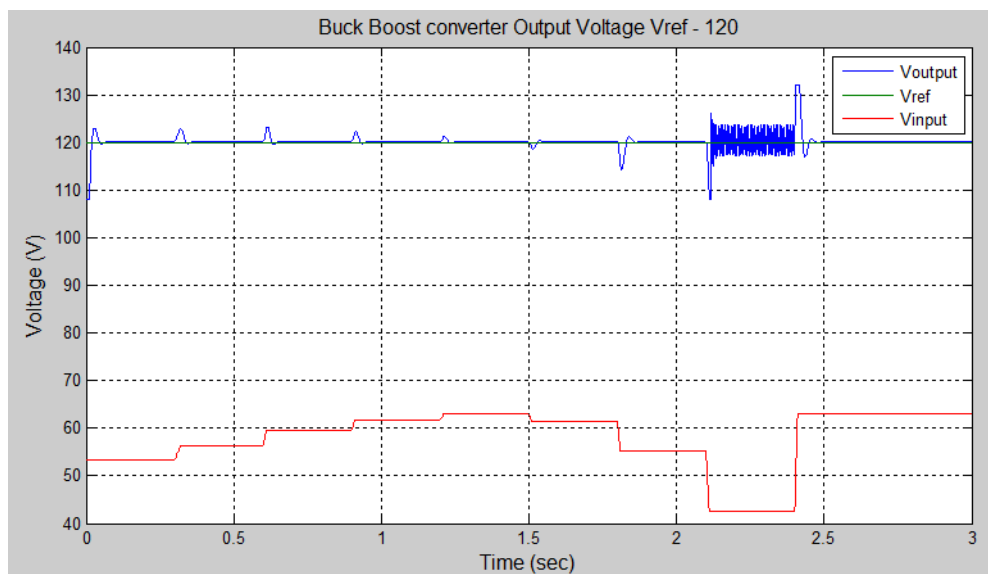
Fig 5.21 Buck-Boost converter output voltage (Vo = 120 V)

124

Figure 5.21 illustrates the simulation results of the buck-boost converter, which was set to produce an output voltage of 120 V; the input was from the MPPT boost converter.
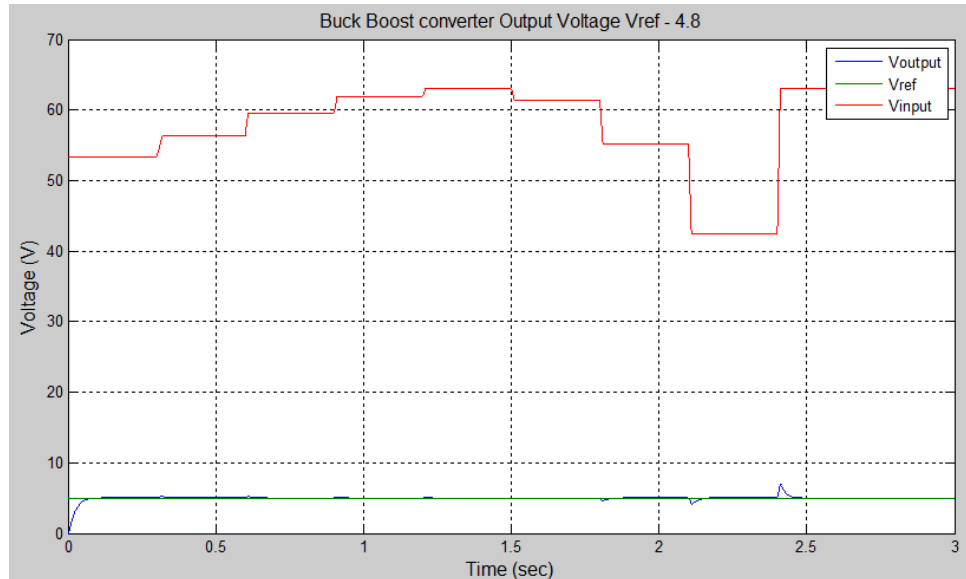
Fig 5.22 Buck-Boost converter output voltage (Vo = 4.8 V)

Figure 5.22 illustrates the simulation results of the buck-boost converter, which was set to produce an output voltage of 4.8 V; the input was from the MPPT boost converter. These results show the designed MPPT Boost converter produced very good results, and the buck-boost converter performs really well under wide range of operation.
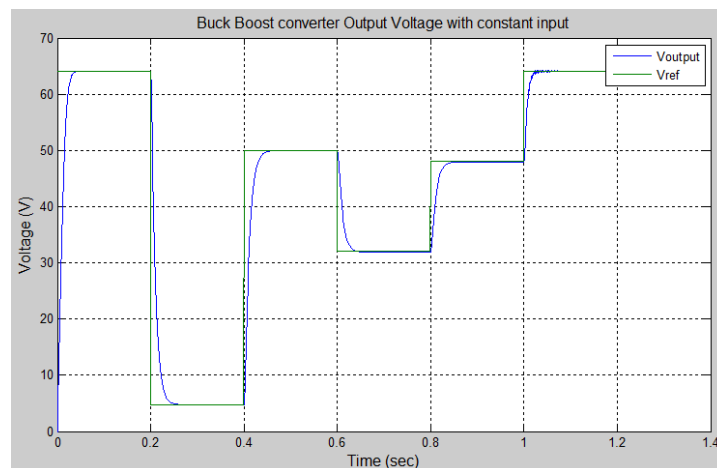
Fig 5.23 Buck-Boost converter output voltage at different levels

125

Just to illustrate the buck-boost converter operation dynamics it was operated at many different output voltage levels, which is some of the commonly used DC voltage operations of 4.8 V, 32 V, 48 V, 50V and 64 V. Figure 5.23 above, shows the converter performance and the results are very satisfying. The buck-boost converter will be able to satisfy many applications, from low voltage battery charging to high voltage outputs. This wide operation was mainly achieved used a classical control designs. This also proves that, this application does not require modern control techniques and will help keep the costs low. It can be observed that the system damping is very good, this type of damping are most preferred for battery charging applications.

5.5   Converters Summary

The developed electrical equivalent model of the μPSC helped in design and simulation of three different converters. The three converters, voltage doubler charge pump, boost converter, and the cascaded boost & buck-boost converter were identified, analyzed designed and simulated for the μPSC energy harvesting application. The simulation results prove that all the three identified converters are suitable for energy harvesting. These converters are very versatile and are applicable to low power low voltage battery charging to stacked or scaled high voltage applications applications. The power converters also, helped in finding out the fact the common MPPT techniques as well as custom MPPT techniques can be used for energy harvesting application using the μPSC and MFCs. Therby, which a custom MPPT algorithm was developed to suit the needs of μPSC, which can also be used to for MFCs.

The voltage doubler charge pump, an inductor less switched capacitor based converter was able to accommodate the custom developed MPPT algorithm and be used for Li-Ion battery charging. The boost converter was more versatile than the voltage double charge pump in delivering the same results. This will help any user to identify the suitable converter for a particular application, be it restricted by cost or ease of implementation for fast development, etc. The cascaded converter proved to be the most versatile and can accommodate varied applications when μPSCs are stacked or scaled; from low voltage applications such as a 4.8 or 5 volt battery charger to feeding a 120 V inverter. It also showcases the potential of the μPSCs, though the latter needing improvements in power density.

CHAPTER 6

6 CONCLUSION & FUTURE WORK

6.1   Summary

The work presented in this thesis, proves and contributes important findings for harvesting energy from unconventional energy sources, using μPSCs. Through this work, the μPSC working principle is understood, and is applied to achieve an electrical equivalent model. In order to achieve this, the cell's mathematical model was first developed based on experimental results. Experimental data based modeling is very popular and one of the most common methods. The mathematical model of the μPSC can also be modeled based on the understanding of chemical reactions and processes involved in production of the electrons. The chemical model might be more advantageous in understanding the cell and improving the cell's performance, but modeling it the chemical way would be involving electrochemistry, which is not the area of focus for this thesis work. Although this shouldn't be neglected, it will form an important part of the future work and future directions for improving the cell's performance.

The main objectives and the respective contributions are discussed first followed by added contributions.

Design and Performance:

- It was proven that energy harvesting is feasible using the PSCs. A test, in which the cell was operated for two weeks continuously produced power constantly and

consistently, and other tests such as load testing, testing with different electrolytes to verify the power produced the cell were all conclusive in proving that the cell was capable of producing power consistently under various scenarios.

- The tests also proved that the cell can be operated continuously when constructed robustly.

- The cells were stacked by connecting them in series and in parallel and tested. The test results proved that the cells can be stacked and thereby scaled accordingly based on the power requirements for an application.

Electrical Modeling and Power Converters:

- Experiments were conducted and it was discovered that quantum yield of algae was the most influential parameter, rather than light irradiance as it was imagined to be.

- A mathematical model of the cell was developed based on quantum yield, cell voltage and current.

- An electrical equivalent model was deduced from the mathematical model, incorporating other cell behaviours. This developed electrical equivalent cell model was simulated and the simulation results converged with the experimental results of the cell.

- Three power electronic converters were studied for energy harvesting application and it was concluded that the suitable power electronic converter should be chosen based on the application.

- It was verified that MPPT would be required for the energy harvesting application.

- Developed a custom MPPT algorithm based on perturb and observe method, which can be used for both switched capacitor converters (inductor less) or more conventional inductor based topologies.

- Designed three different power electronic converters for both low and large power energy harvesting applications.

Fabrication:

- The fabrication output was doubled. 6 electrode assemblies were fabricated from a 10cm x 10cm Nafion membrane compared to 3 earlier.

- Assembling the device by enclosing the cells using a custom built enclosure. This process reduced the cost, assembling time was reduced by a considerable amount of time, and the device was now more robust over the complex, time consuming and expensive process of plasma bonding which was used earlier.

- Reduced the time required for gold sputtering of Nafion by storing it in a vacuum chamber prior to sputtering.

Apart from these achievements and contributions, it was found out that the electron transfer chain in photosynthetic is analogous to that of the solar cell. Also, the developed model can be easily modified to match other microbial fuel cell (MFC) characteristics and help build suitable harvesting power converters.

The work presented here would certainly enhance the research ecosystem of MFCs and PSCs, and would pave way for the technology and research. This will lead to much improved and sophisticated model development as well as accurate cell behavior emulation methodologies. Such improved models will enable designing and building

highly efficient and optimal power electronic converters for MFCs and PSCs. Thus, moving forward, a strong conclusive case can be made for the maturity of PSCs, in general, which can lead to the development of a fairly cheap and sustainable energy resource.

6.2   Future work

Curiosity, ability to question, the desire to explore are the traits that differentiate our species to that of all other known species on our planet. Exploration of the μPSC will continue to yield better results. Some of the directions for future research work for μPSC based on the work done in this thesis work would be:

- Develop and integrate chemical reactions and process based models to the simulation model.
- Investigate methods and ways to improve efficiency.
- Collaborate with biologists to extract the electron donor from the cell and develop a biological life independent system.
- Improve the fabrication processes to reduce cost.
- Investigate alternatives to Nafion, again to reduce cost.
- Identify methods to increase power density of the device.
- Incorporate circulation of electrolytes using self sustainable micro pumps.
- Scaling up to produce high level of power by stacking the cells.
- Test different physical combinations to stack the cells in order to achieve higher power densities.
- Building the proposed converter topologies and harvest energy.

- Develop an emulator to aid in design and development of power electronic converter.

Although a niche and tough area to research on, fellow researches and competitors in µPSC field are stepping up the game and have unveiled the World's first algae-powered building in Hamburg Germany (March 2013) [83].

Publications:

This work was presented / published in the following conferences and journals:

Journals:

[1] Ramanan, A.V.; Pakirisamy, M.; Williamson, S.S., "Advanced Fabrication, Modeling, and Testing of a Micro-Photosynthetic Electrochemical Cell for Energy Harvesting Applications", (TPEL-Reg-2013-02-0151) *IEEE Transactions on Power Electronics* (Accepted Apr,2013).

Conferences:

[1] Ramanan, A.V.; Pakirisamy, M.; Williamson, S.S., "Photosynthetic electrochemical cell charging infrastructure versus photovoltaic cell charging infrastructure for future electric vehicles," *Vehicle Power and Propulsion Conference (VPPC), 2011 IEEE* , vol., no., pp.1,5, 6-9 Sept. 2011

[2] Energy Harvesting, Characterization and Modeling of Photosynthetic Electrochemical Cell, Packarisamy M; Ramanan A. V.; Williamson S.S, *RESEARCH & INNOVATION FOR TRANSPORT SYSTEMS OF THE FUTURE, Paris, Ministère de l'Enseignement Supérieur et de la Recherche*, November 12-15, 2012

[3] Ramanan, A.V.; Pakirisamy, M.; Williamson, S.S., "Analysis of three different converters with MPPT for energy harvesting from photosynthetic power cell," *IECON 2013 - 39th Annual Conference of the IEEE Industrial Electronics Society*, 10 Nov - 13 Nov 2013 (Submitted).

REFERENCES

[1] Energy – Consumption'A1 "Consumption by fuel, 1965–2008" (XLS). Statistical Review of World Energy 2009. Retrieved 24 October 2009.

[2] "Jiuquan wind power base completes first stage". Retrieved, 4-Oct2010. http://www.chinadaily.com.cn/bizchina/2010-11/04/content_11502951.htm

[3] "Excellence in Renewable Energy Awards Winners: Project of the Year and Readers' Choice". Renewable Energy World. 17 February 012. http://www.renewableenergyworld.com/rea/news/article/2012/02/excellence-in-renewable-energy-awards-winners-project-of-the-year-and-readers-choice?cmpid=WNL-Wednesday-February22-2012

[4]"India's Gujarat bares 500-MW solar park to businessmen". ecoseed.org. 2011-01-03. Retrieved 2011-01-14. http://www.ecoseed.org/business-article-list/article/1-business/8741-india%E2%80%99s-gujarat-bares-500-mw-solar-park-to-businessmen

[5]Khaligh, A.; Peng Zeng; Cong Zheng; , "Kinetic Energy Harvesting Using Piezoelectric and Electromagnetic Technologies—State of the Art," Industrial Electronics, IEEE Transactions on , vol.57, no.3, pp.850-860, March 2010

[6]R. Amirtharajah and A. P. Chandrakasan, "Self-powered signal processing using vibration-based power generation," IEEE J. Solid State Circuits, vol. 33, no. 5, pp. 687–695, May 1998

[7] N. S. Shenck, "A demonstration of useful electric energy generation from piezoceramics in a shoe," M.S. thesis, MIT, Cambridge, MA, 1999.

134

[8] Peng Zeng; Hao Chen; Zhi Yang; Khaligh, A.; , "Unconventional wearable energy harvesting from human horizontal foot motion," Applied Power Electronics Conference and Exposition (APEC), 2011 Twenty-Sixth Annual IEEE , vol., no., pp.258-264, 6-11 March 2011

[9] http://www.bnl.gov/magnets/staff/gupta/cryogenic-data-handbook/Section13.pdf

[10] http://www.micropelt.com/products/thermogenerator.php

[11] Arias-Thode, Y.M.; Richter, K.; Wotawa-Bergen, A.; Chadwick, D.B.; Jinjun Kan; Nealson, K.; , "Development of microbial fuel cell prototypes for examination of the temporal and spatial response of anodic bacterial communities in marine sediments," OCEANS, 2011 IEEE - Spain , vol., no., pp.1-5, 6-9 June 2011

[12] M.C. Potter, "Electrical effects accompanying the decomposition of organic compounds," Royal Society (Formerly Proceedings of the Royal Society) B, vol. 84, pp. 260-276, 1911.

[13] I. Karube, T. Matasunga, S. Suzuki and S. Tsuru, "Biochemical cells utilizing immobilized cells of Clostridium butyricum," Biotechnology and Bioengineering, vol.19, pp. 1727–1733, 1977.

[14] David P.B.T.B. Strik, Ruud A. Timmers, Marjolein Helder, Kirsten J.J. Steinbusch, Hubertus V.M. Hamelers, Cees J.N. Buisman, Microbial solar cells: applying photosynthetic and electrochemically active organisms, Trends in Biotechnology, Volume 29, Issue 1, January 2011, Pages 41-49, ISSN 0167-7799

[15] Voyager - The Interstellar Mission, http://voyager.jpl.nasa.gov/

[16] Nealson KH, Conrad PG (December 1999). "Life: past, present and future". Philos. Trans. R. Soc. Lond., B, Biol. Sci. 354 (1392): 1923–39. doi:10.1098/rstb.1999.0532. PMC 1692713. PMID 10670014.

[17] Whitmarsh J, Govindjee (1999). "The photosynthetic process". In Singhal GS, Renger G, Sopory SK, Irrgang KD, Govindjee. Concepts in photobiology: photosynthesis and photomorphogenesis. Boston: Kluwer Academic Publishers. pp. 11–51. ISBN 0-7923-5519-9. "100 x 1015 grams of carbon/year fixed by photosynthetic organisms which is equivalent to 4 x 1018 kJ/yr = 4 x 1021J/yr of free energy stored as reduced carbon; (4 x 1018 kJ/yr) / (31,556,900 sec/yr) = 1.27 x 1014 J/yr; (1.27 x 1014 J/yr) / (1012 J/sec / TW) = 127 TW."

[18] World Consumption of Primary Energy by Energy Type and Selected Country Groups, 1980–2004" (XLS). Energy Information Administration. July 31, 2006. Retrieved 2007-01-20. http://www.eia.doe.gov/pub/international/iealf/table18.xls

[19] W. R. Grove, "On voltaic series and combination of gases by platinum", Philosophical magazine, Vol. 14, 1839, pp. 127 – 130

[20] B. C. Steel and A. Heinzel, "Materials for fuel cell technologies", Nature, 414, 2001, pp. 345 – 352

[21] http://cronodon.com/BioTech/Chlamydomonas.html

[22] Charging lithium ion batteries;

http://batteryuniversity.com/learn/article/charging_lithium_ion_batteries, October,2012

[23] Battery Management Systems: Design by Modelling by H.J. Bergveld, W.S. Kruijt and P.H.L Notten (Sep 30 2002)

[24] Lam, K.B.; Johnson, E.; Lin, L.; , "A bio-solar cell powered by sub-cellular plant photosystems," Micro Electro Mechanical Systems, 2004. 17th IEEE International Conference on. (MEMS) , vol., no., pp. 220- 223, 2004

[25] Chiao, Mu, Kien B. Lam, and Liwei Lin. "Micromachined microbial and photosynthetic fuel cells." Journal of Micromechanics and Microengineering 16.12 (2006): 2547.

[26] Potter, Michael C. "Electrical effects accompanying the decomposition of organic compounds." Proceedings of the Royal Society of London. Series B, Containing Papers of a Biological Character 84.571 (1911): 260-276.

[27] I. Ieropoulos, J. Greenman, C. Melhish and J. Hart, "Comparative study of three types of microbial fuel cell", Enzyme and microbial technology, Vol. 37, 2005, pp. 238 – 245

[28] R. M. Allen and H. P. Bennetto, "Microbial fuel cells: electricity production from carbohydrates", Applied Biochemistry Biotechnology, Vol. 39, Issue 40, 1993, pp. 27-40

[29] M. Allen and A. Crane, "Null Potential Voltammetry – An approach to the study of the plant photo system", Bioelectrochemistry and Bioenergetics, Vol. 3, 1976, pp. 84 – 91.

[30] D. Park and J. Zeikus, "Electricity generation in microbial fuel cells using neutral red as electronophore", Applied and Environmental Microbiology, Vol. 66,Issue 4, 2000, pp. 1292 - 1297

[31] D. L. Nelson and M. M. Cox, "Lehninger Principles of Biochemistry", 3rd edition, 2000, pp. 691 – 714

[32] M. Aizawa, M. Hirano and S. Suzuki, "Photoelectrochemical energy conversion system modeled on the photosynthetic process", Electrochimica Acta, Vol. 23, 1978, pp. 1185 – 1190 156

[33] L. A. Drachev, A. A. Kondrashin, V. D. Samuilov, and V. P. Skulachev, "Generation of electric potential by reaction center complexes from Rhodospirillum rubrum", FEBS Letters, Vol. 50, 1975, pp. 219 – 222

[34] L. A. Drachev, A. A. Jasaitis, A. D. Kaulen, A. A. Kondrashin, L. V. Chu, A. Y. Semenov, I. I. Severina and V. P. Skulachev, "Reconstitution of biological molecular generators of electric current: Cytochrome oxidase", Journal of Biological Chemistry, Vol.251, 1976, pp. 7072 – 7076

[35] N. K. Packham, D. M. Tiede, P. Mueller and P. L. Dutton, "Construction of a flash – activated cyclic electron transport system by using bacterial reaction centers and the ubiquinone-cytochrome b-c1/c segment of mitochondria", Proceedings of the National Academy of Science,Vol. 77, 1980, pp. 6339 - 6343

[36] N. K. Packham, C. Packham, P. Mueller, D. M. Tiede and P. L. Dutton, "Reconstitution of photochemically active reaction centers in planar phospholipid membranes", FEBS Letters, Vol. 110, 1980, pp. 101 – 106

[37] A. F. Janzen, "Photoelectrochemical conversion using reaction-center electrodes", Nature, Vol. 286, 1980, pp. 584 – 585

[38] K. Tanaka, R. Tamamushi and T. Ogawa, "Bioelectrochemical fuel cells operated by cyanobacterium anabaena variabilis", Journal of Chemical Technology & Biotechnology, Vol. 35, 1985, pp. 191 – 197

[39] K. Tanaka, N. Kashiwagi and T. Ogawa, "Effects of light on the electrical output of bioelectrochemical fuel-cells containing anabaena variabilis M-2 mechanisms of the post-illumination burst", Biotechnology, Vol. 42, 1988, pp. 235 – 240

[40] T. Yagishita, S. Sawayama, K. Tsukahara and T. Ogi, "Photosynthetic bio-fuel cell using cyanobacteria", Renewable Energy, Vol.9, 1996, pp. 958 – 961

[41] T. Yagishita, T. Horigome and K. Tanaka, "Effect of light, CO2 and inhibitors on the current output of bio-fuel cells containing the photosynthetic organism synechococcus sp. ", Journal of Chemical Technology & Biotechnology, Vol. 56, 1993, pp. 393 – 399

[42] T. Yagishita, T. Horigome and K. Tanaka, "Bio-fuel cells containing photosynthetic microorganisms", Journal of the electrochemical society, Vol. 61, 1993, pp. 687 – 688

[43] T. Yagishita, S. Sawayama, K. Tsukahara and T. Ogi, "Effects of intensity of incident light and concentration of synechococcus sp. and 2-hydoxy-1,4-naphthoquinone

on the current output of photosynthetic electrochemical cell ", Solar Energy, Vol. 61, 1997, pp. 347 – 353 157

[44] T. Yagishita, S. Sawayama, K. Tsukahara and T. Ogi, "Effects of glucose addition and light on current outputs in photosynthetic electrochemical cell using synechocystis sp. Pcc40.", Journal of bioscience and bioengineering, Vol. 99, 1999, pp. 210 – 214

[45] R. Bhardwaj, R. Pan and E. Gross, "Solar energy conversion by chloroplast photochemical cells", Nature, Vol. 289, 1981, pp. 396 – 398

[46] W. Haehnel and H. Hockheimer, "On the current generated by a galvanic cell driven by photosynthetic electron transport", Bioelectrochem. Bioeng. ,Vol. 6, 1979, pp. 563 – 574

[47] Tree Identification - Parts of a Tree www.butler.edu/herbarium/treeid/treeparts.html

[48] Plant photosynthesis schools.look4.net.nz/science/biology/plant/photosynthesis

[49] Plant Cells, Chloroplasts, and Cell Walls
http://www.nature.com/scitable/topicpage/plant-cells-chloroplasts-and-cell-walls-14053956

[50] Wikipedia, Photosynthesis http://en.wikipedia.org/wiki/Photosynthesis, October,2012

[51] M. Shahparnia, "Polymer Micro Photosynthetic Power Cell: Design, Fabrication, Parametric Study and Testing", A Thesis In The Department Of Mechanical and Industrial Engineering at Concordia University, Montreal, Quebec, Canada, July 2011

[52] Rate of photosynthesis limiting factors, RSC-Advancing the chemical sciences, retrieved October 2012

[53] Ku, Sun-Ben, Gerald E. Edwards, and Champ B. Tanner. "Effects of light, carbon dioxide, and temperature on photosynthesis, oxygen inhibition of photosynthesis, and transpiration in Solanum tuberosum." Plant Physiology 59.5 (1977): 868-872.

[54] Measurement of sunshine duration, CIMO Guide, World Meteorological Organization, 2008

[55] G. Rechtsteiner and J. Ganske, "Using natural and artificial light sources to illustrate quantum mechanical concepts", The chemical educator, Springer Berlin, Vol. 3, No. 4, pp. 1-12, 1998

[56] Kobza, John, Ernest G. Uribe, and George J. Williams III. "Temperature dependence of photosynthesis in Agropyron smithii Rydb. III. Responses of protoplasts and intact chloroplasts." Plant physiology 75.2 (1984): 378-381.

[57] J. P. Decker, "Effect of temperature on photosynthesis and respiration in red and loblolly pines", Plant Physiology, Vol. 4, pp. 679 – 688, 1944

[58] Plant Physiology, Fifth edition, Lincoln Taiz, Eduardo Zeiger

[59] http://en.wikipedia.org/wiki/Daylight

[60] Bender, E.A. [1978] (2000). An Introduction to Mathematical Modeling, New York : Dover. ISBN 0-486-41180-X

[61] Qing Wen, Ying Wu, Dianxue Cao, Lixin Zhao, Qian Sun, Electricity generation and modeling of microbial fuel cell from continuous beer brewery wastewater, Bioresource Technology, Volume 100, Issue 18, September 2009, Pages 4171-4175, ISSN 0960-8524, 10.1016/j.biortech.2009.02.058.

[62] C. Picioreanua, I.M. Head, K.P. Katuri, M.C.M. Van Loosdrecht, K. Scott. A computational model for biofilm-based microbial fuel cells. Water Research, 41 (2007), pp. 2921–2940

[63] C. Picioreanua, K.P. Katuri, I.M. Head, M.C.M. Van Loosdrecht, K. Scott. Mathematical model for microbial fuel cells with anodic biofilms and anaerobic digestion. Water Science and Technology, 57 (7) (2008), pp. 965–971

[64] K. Rabaey, G. Lissens, S.D. Siciliano, W. Verstraete. A microbial biofuel cell capable of converting glucose to electricity at high rate and efficiency. Journal of Biotechnology, 25 (2003), pp. 1531–1535

[65] Markvart, T.; Landsberg, P.T.; , "Solar cell model for electron transport in photosynthesis," Photovoltaic Specialists Conference, 2002. Conference Record of the Twenty-Ninth IEEE, vol., no., pp. 1348- 1351, 19-24 May 2002. doi: 10.1109/PVSC.2002.1190859

[66] Theory of solar cells, http://en.wikipedia.org/, October 2012.

[67] Correa, J.M.; Farret, F.A.; Popov, V.A.; Simoes, M.G.; , "Sensitivity analysis of the modeling parameters used in Simulation of proton exchange membrane fuel cells," Energy Conversion, IEEE Transactions on , vol.20, no.1, pp. 211- 218, March 2005.

[68] Aelterman et al., 2006, P. Aelterman, K. Rabaey, H.T. Pham, N. Boon, W. Verstraete; Continuous electricity generation at high voltages and currents using stacked microbial fuel cells, Environ Sci Technol, 40 (2006), pp. 3388–3394

[69] Zhuwei Du, Haoran Li, Tingyue Gu, A state of the art review on microbial fuel cells: A promising technology for wastewater treatment and bioenergy, Biotechnology Advances, Volume 25, Issue 5, September–October 2007, Pages 464-482, ISSN 0734-9750, 10.1016/j.biotechadv.2007.05.004.

[70] Degrenne, N.; Allard, B.; Buret, F.; Morel, F.; Adami, S.-E.; Labrousse, D., "Comparison of 3 self-starting step-up DC:DC converter topologies for harvesting energy from low-voltage and low-power microbial fuel cells," *Power Electronics and Applications (EPE 2011), Proceedings of the 2011-14th European Conference on* , vol., no., pp.1,10, Aug. 30 2011-Sept. 1 2011.

[71] Alippi, C.; Galperti, C., "An Adaptive System for Optimal Solar Energy Harvesting in Wireless Sensor Network Nodes," *Circuits and Systems I: Regular Papers, IEEE Transactions on* , vol.55, no.6, pp.1742,1750, July 2008 doi: 10.1109/TCSI.2008.922023

[72] Sehwan Kim; Keun-Sik No; Chou, P.H., "Design and Performance Analysis of Supercapacitor Charging Circuits for Wireless Sensor Nodes," *Emerging and Selected Topics in Circuits and Systems, IEEE Journal on* , vol.1, no.3, pp.391,402, Sept. 2011 doi: 10.1109/JETCAS.2011.2167274

[73] Yifeng Qiu; Van Liempd, C.; Op het Veld, B.; Blanken, P.G.; Van Hoof, C., "5µW-to-10mW input power range inductive boost converter for indoor photovoltaic energy harvesting with integrated maximum power point tracking algorithm," *Solid-State*

Circuits Conference Digest of Technical Papers (ISSCC), 2011 IEEE International , vol., no., pp.118,120, 20-24 Feb. 2011 doi: 10.1109/ISSCC.2011.5746245

[74] Ottman, G.K.; Hofmann, H.F.; Lesieutre, G.A., "Optimized piezoelectric energy harvesting circuit using step-down converter in discontinuous conduction mode," *Power Electronics, IEEE Transactions on* , vol.18, no.2, pp.696,703, Mar 2003 doi: 10.1109/TPEL.2003.809379

[75] Carlson, E.J.; Strunz, K.; Otis, B.P., "A 20 mV Input Boost Converter With Efficient Digital Control for Thermoelectric Energy Harvesting," *Solid-State Circuits, IEEE Journal of* , vol.45, no.4, pp.741,750, April 2010. doi: 10.1109/JSSC.2010.2042251

[76] Lefeuvre, E.; Audigier, D.; Richard, C.; Guyomar, D., "Buck-Boost Converter for Sensorless Power Optimization of Piezoelectric Energy Harvester," *Power Electronics, IEEE Transactions on* , vol.22, no.5, pp.2018,2025, Sept. 2007. doi: 10.1109/TPEL.2007.904230

[77] De Brito, M.A.G.; Galotto, L.; Sampaio, L.P.; de Azevedo e Melo, G.; Canesin, C.A., "Evaluation of the Main MPPT Techniques for Photovoltaic Applications," *Industrial Electronics, IEEE Transactions on* , vol.60, no.3, pp.1156,1167, March 2013 doi: 10.1109/TIE.2012.2198036

[78] Lopez-Lapena, O.; Penella, M.T.; Gasulla, M., "A New MPPT Method for Low-Power Solar Energy Harvesting," *Industrial Electronics, IEEE Transactions on* , vol.57, no.9, pp.3129,3138, Sept. 2010. doi: 10.1109/TIE.2009.2037653

[79] K. Martin and A. Sedra, "Switched-capacitor building blocks for adaptive systems," in I*EEE Trans. Circuits Syst.*, Jun. 1981, vol. 28, no. 6, pp. 567–584.

[80] Palumbo, G.; Pappalardo, D., "Charge Pump Circuits: An Overview on Design Strategies and Topologies," *Circuits and Systems Magazine, IEEE* , vol.10, no.1, pp.31,45, First Quarter 2010. doi: 10.1109/MCAS.2009.935695

[81] Pricor PI5101 MOSFET datasheet. Retrieved Sep, 2011. http://cdn.vicorpower.com/documents/datasheets/Picor/ds_PI5101.pdf

[82] Abraham Pressman, Keith Billings, Taylor Morey. "Switching Power Supply Design." *McGraw-Hill Professional, 3 edition*, Mar 26 2009.

[83] Retrieved March, 2013. http://inhabitat.com/splitterwerk-architects-design-worlds-first-algae-powered-building-for-germany

[84] Retrieved October, 2012. http://www.tutorpace.com/science/biology